**Fakultät für Medizin**

**Institut für Zellbiologie des Nervensystems**

# Plasticity of the *vsx1*$^{+}$ progenitor lineage during zebrafish retinogenesis

**Peter Engerer**

Vollständiger Abdruck der von der Fakultät für Medizin der Technischen Universität München zur Erlangung des akademischen Grades eines

**Doctor of Philosophy (Ph.D.)**

genehmigten Dissertation.

**Vorsitzender:** Univ.-Prof. Dr. Arthur Konnerth

**Betreuer:** Univ.-Prof. Dr. Thomas Misgeld

**Prüfer der Dissertation:**

1. apl. Prof. Dr. Helmuth Adelsberger

2. Prof. Dr. Herwig Baier

Die Dissertation wurde am 17.06.2016 bei der Fakultät für Medizin der Technischen Universität München eingereicht und durch die Fakultät für Medizin am 17.08.2016 angenommen.

# ACKNOWLEDGEMENTS

I would like to thank my supervisors Dr. Leanne Godinho and Prof. Dr. Thomas Misgeld for constant support, encouragement, and guidance during my PhD work, as well as providing me with the opportunity to inhale science at places like Woods Hole and Janelia Farm. I feel lucky that I had a desk next to Dr. Philip Williams who constantly mentored me regarding science, foosball, chicken, and life. I would like to thank Prof. Dr. Helmuth Adelsberger and Prof. Dr. Herwig Baier for being members of my thesis advisory committee and providing critical feedback. I am grateful to have experienced the generosity of Prof. Dr. Rachel Wong who has supported my research in (almost) all possible aspects. In the same breath, I want to express gratitude to my collaborators Dr. Prisca Chapouton, Nancy Obeng, Prof. Dr. Benjamin Odermatt, Dr. Sachihiro Suzuki and Dr. Takeshi Yoshimatsu for their valuable contributions. Furthermore, I want to thank Kristina Wullimann (for taking excellent care of the fish husbandry) and Yvonne Hufnagel (for help with cloning). It is needless to say that I am very happy to have worked with numerous great colleagues at Biederstein Campus - so many thanks go to Alex(es), Andy, Barbara, Bogdan, Caro, Carsten, Christian, Christoph, Dietmar, Doug, Franz, Franzi, Gabi, Grace, Laura, Marion, Marina. Michael, Mike, Minh, Monika(s), Natalia, Nic, Petar, Rachel, Sarah, Selin, Tatjana, Tim, Tobi, Toni and Vlad. Also special thanks to my mitochondria, which valiantly provided energy and kept me going. Lastly, the biggest thanks go to my family, my girlfriend Bubu and all my friends for unconditional support and inspiration.

# ABSTRACT

As most studies on the development of the central nervous system (CNS) in vertebrates were done in fixed preparations and/or *in vitro*, our knowledge about the plasticity of progenitor cells and newly-born neurons *in vivo* is limited. Using the terminally-dividing *vsx1*$^{+}$ progenitor lineage of the zebrafish retina as an *in vivo* model for vertebrate CNS development, I could directly observe the ontogenetic events neurogenesis, neuronal migration and neuronal differentiation. In contrast to the widely-accepted view, I found that a stereotypical and fixed sequence of neurodevelopmental events does not necessarily occur *in vivo*. Using various markers to determine the relative timing of mitosis and neuronal differentiation, I discovered that *vsx1*$^{+}$ progenitors undergo terminal mitosis at markedly disparate stages of differentiation. Intriguingly, the state of differentiation of *vsx1*$^{+}$ progenitors at mitosis is not arbitrary, but matches that of the post-mitotic *vsx1*$^{+}$ bipolar cells in their vicinity. Moreover, following the fate of the two daughter cells, I could also reveal a terminal, asymmetric mode of *vsx1*$^{+}$ division yielding a bipolar cell and an amacrine cell. These terminal, asymmetric *vsx1*$^{+}$ divisions challenge the invariant nature of the 'committed' *vsx1* lineage and suggest that neuronal identity can be re-specified during CNS development. Probing the molecular mechanisms underlying the asymmetric divisions, I revealed a dual role for Notch in nascent post-mitotic *vsx1*$^{+}$ cells: First, conferring a degree of plasticity that permits changes in fate and differentiation status and second activating a signaling cascade involving Ptf1a to instruct amacrine cell fate. I directly tested the degree to which Notch confers plasticity to newly-born neurons by over-expressing Notch together with Atoh7, and found the emergence of *vsx1*$^{+}$ cells with a phenotype similar to retinal ganglion cells. Taken together, instead of a stereotypic, linear progression of developmental events, I found a surprising degree of plasticity in progenitors and newly-born neurons during CNS development *in vivo*.

# ZUSAMMENFASSUNG

Da die meisten Studien zur Entwicklung des zentralen Nervensystems (ZNS) in fixierten Präparaten und/oder unter *in vitro* Bedingungen durchgeführt wurden, ist unser Wissen über die Plastizität von Progenitorzellen sowie neu-geborenen Nervenzellen unter *in vivo* Bedingungen sehr beschränkt. Mithilfe des Modelsystems von sich terminal-teilenden *vsx1*$^{+}$-Progenitorzellen der Zebrafisch-Retina konnten im Rahmen dieser Doktorarbeit die ontogenetischen Vorgänge Neurogenese, neuronale Migration und neuronale Differenzierung in einem Vertebraten *in vivo* untersucht werden. Entgegen der weitverbreiteten Meinung wurde festgestellt, dass die Hauptschritte der neuronalen Entwicklung *in vivo* nicht notwendigerweise in einer fixen, stereotypischen Sequenz ablaufen. Mithilfe von verschiedenen Markern konnte bestimmt werden, dass sich *vsx1*$^{+}$-Progenitorzellen in sehr unterschiedlichen Stadien der neuronalen Differenzierung teilen und nicht zu einem bestimmten, stereotypischen Zeitpunkt ihres Differenzierungsprozesses. Interessanterweise ist das Differenzierungsstadium der *vsx1*$^{+}$-Progenitorzellen zum Zeitpunkt der Mitose nicht willkürlich, sondern dem der post-mitotischen *vsx1*$^{+}$-Bipolarzellen in unmittelbarer Nachbarschaft ähnlich. Außerdem wurde das Schicksal der Tochterzellen von sich terminal-teilenden *vsx1*$^{+}$-Progenitorzellen untersucht. Hierbei konnte festgestellt werden, dass sich *vsx1*$^{+}$-Progenitorzellen auch terminal-asymmetrisch teilen können, und dabei eine Bipolar- und eine Amakrinzelle generieren. Diese terminalen-aysmmetrischen *vsx1*$^{+}$-Zellteilungen stellen die Invarianz von ‘determinierten’ Progenitorzellen in Frage und implizieren eine Respezifikation von neuronaler Identität während der Entwicklung des ZNS. Als die molekularen Mechanismen der asymmetrischen Zellteilungen analysiert wurden, konnte eine zweifache Rolle von Notch für sich entwickelnde, post-mitotische *vsx1*$^{+}$-Zellen gezeigt werden: Zum einen verleiht Notch ein gewisses Ausmaß von Plastizität, welche Änderungen im

Zellschicksal und Differenzierungsstatus ermöglichen; zum anderen aktiviert Notch durch eine Signalkaskade Ptf1a um das Zellschicksal einer Amakrinzelle zu instruieren. Als das Ausmaß der Notch-induzierten Plastizität in neu-geborenen Neuronen durch Überexpression von Notch und Atoh7 direkt getestet wurde, konnte in *vsx1*$^{+}$-Zellen der Phänotyp von retinalen Ganglionzellen induziert werden. Insgesamt wurde in dieser Doktorarbeit eine überraschende Plastizität von Progenitorzellen und neu-geborenen Neuronen während der Entstehung des ZNS *in vivo* vorgefunden und nicht, wie eigentlich erwartet, ein stereotypischer, linearer Fortgang von Entwicklungsschritten.

# TABLE OF CONTENTS

# 1. INTRODUCTION

"*Omnis cellula e cellula*[1]" (Robert Virchow, 1855)

Robert Virchow is widely credited for adding the third tenet to cell theory (Virchow, 1855). However, it was originally the embryologist Robert Remak, who discovered that new cells are generated by mitotic divisions of pre-existing cells (Remak, 1852). Tremendous progress has been made since these early days of modern developmental biology; e.g. the entire early embryogenesis of a vertebrate was recently described on a cellular level in the form of a 'digital embryo' (Keller et al., 2008) highlighting the persisting importance and innovative mind of the field. Nevertheless, developmental biology still harbors numerous enigmatic questions. This assessment is particularly true for the development of the nervous system. The main reason for our limited knowledge on neural development is the unmatched, complicated structure of the nervous system: it contains a large number of different neuronal cell types, of which each has a highly complex morphology and synapses with numerous partners (Kasthuri et al., 2015). How these features are established during neural development is largely unknown.

On the one hand, a better anatomical and physiological understanding of the nervous system will be crucial to fully appreciate neural development (obviously, we need to know which cell types exist in order to study how they develop). On the other hand, studies on the development of the nervous system can directly lead to functional insight and thus research on both, neural development and function, could propel and advance each other (Krishnaswamy et al., 2015; Li et al., 2012a).

[1] *All cells come from cells*

For my graduate work, I focused on basic principles of how interneurons are derived from the *vsx1*$^{+}$ (*visual system homeobox 1*) progenitor lineage, using the zebrafish retina as an *in vivo* vertebrate model. Therefore, I will describe in the introduction (1) the anatomy of the vertebrate retina, (2) basics of retinal development in vertebrates and (3) zebrafish as a model organism for neural development. Finally, I will introduce (4) the *vsx1*$^{+}$ progenitor lineage and the specific questions I addressed, namely (I) the uncoupling of mitosis and differentiation and (II) the re-specification of neuronal identity during retinal development.

I would like to emphasize that sections in all parts of the thesis (Introduction, Materials and Methods, Results and Discussion) are based on several first-author manuscripts: *"Imaging Subcellular Structures in the Living Zebrafish Embryo"* (Engerer et al., 2016), *"Uncoupling of neurogenesis and neuronal differentiation during CNS development"* (Engerer et al, in revision) and *"Re-specification of neuronal identity during CNS development"* (Engerer et al, in preparation).

## 1.1. The anatomy of the vertebrate retina

The retina is a thin, laminated structure of neural tissue at the back of the eye. It belongs to the central nervous system (CNS) and has the main function to provide the animal with visual information from the outside world. In contrast to many other parts of the CNS, retinal anatomy is comparably simple and well understood (**Figure 1.1**). As a result, the retina is a popular model for studies on neural development and function (Dowling, 2012; Hoon et al., 2014).

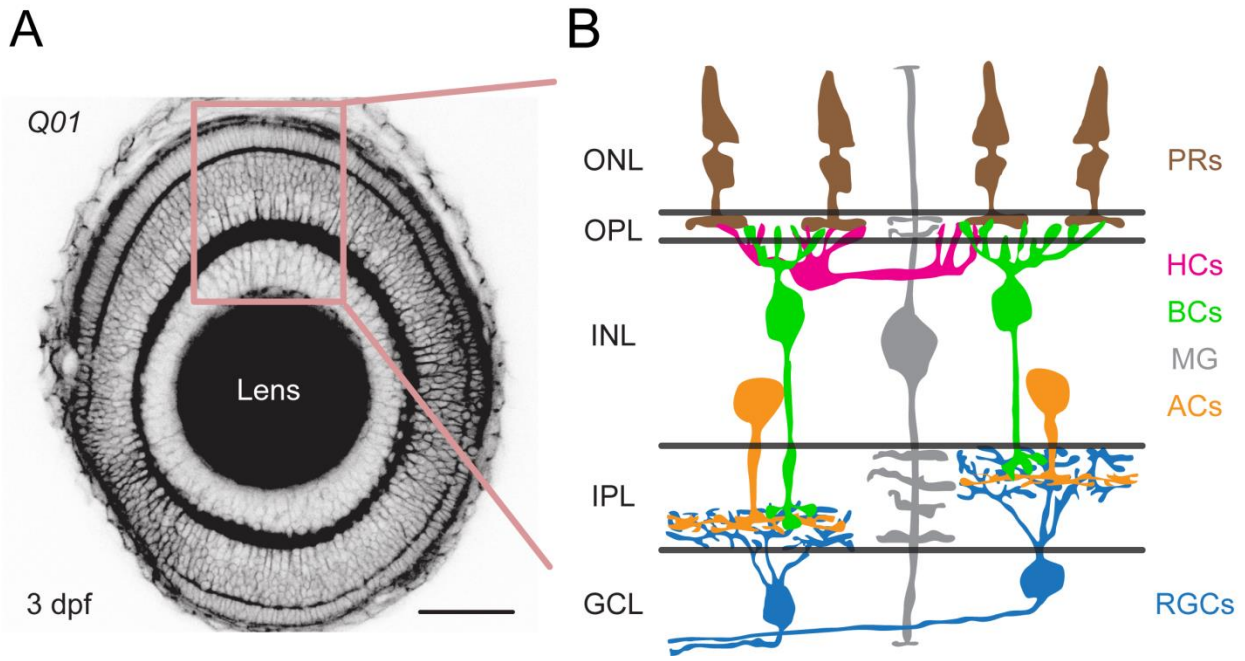


**Figure 1.1 - The anatomy of the vertebrate retina.**

(A) Contrast-inverted image from an eye of a *Q01* larval zebrafish 3 days post fertilization (dpf), in which all cellular membranes are labelled with the genetically-encoded fluorescence protein CFP. The lamination of the retina has already been established at 3 dpf. Scale bar: 50 µm. Image courtesy of Dr. Leanne Godinho. (B) Schematic representation of the vertebrate retina. Cell bodies of neurons and glia show specific morphologies and are invariably located in the three nuclear layers (ONL, INL and GCL). Synaptic connections are confined to the plexiform layers (OPL and IPL). Abbreviations: outer nuclear layer (ONL), outer plexiform layer (OPL), inner nuclear layer (INL), inner plexiform layer (IPL), ganglion cell layer (GCL), photoreceptors (PRs), horizontal cells (HCs), bipolar cells (BCs), Müller glia (MG), amacrine cells (ACs) and retinal ganglion cells (RGCs).

The retina is structured in three cellular layers [outer nuclear layer (ONL), inner nuclear layer (INL) and ganglion cell layer (GCL)] and two synaptic layers [outer plexiform layer (OPL) and inner plexiform layer (IPL)] (**Figure 1.1**). While the somata of all retinal neurons and glia are arranged in the cellular layers, the entirety of synaptic connections is confined in the two plexiform layers. In addition to its laminated structure, the retina has the advantage of only harboring five major neuronal types and one glial cell type. With some minor exceptions, each cell type is invariably located in a specific cellular layer and has a stereotypic morphology.

*Photoreceptors (PRs)*

PRs are located in the ONL and are the principal sensory cells of the retina (**Figure 1.1**). They can absorb photons with the help of visual pigments and thus eventually convert light into a change in neurotransmitter release. Counterintuitively, PRs hyperpolarize upon light stimulation and release less of the neurotransmitter glutamate. PRs synapse in the OPL onto bipolar cells (BCs) and horizontal cells (HCs). Like all other neurons of the retina, PRs can be further classified into subtypes, rods and cones. Rods are PRs with rhodopsin as a photosensitive pigment and are engaged in scotopic (night) vision. Cones are PRs with opsins as a photosensitive pigment and are engaged in photopic (color) vision. In contrast to a single subtype of rod PRs, multiple subtypes of cone PRs exist, each having a distinct opsin to absorb photons of a specific spectrum of wavelengths, e.g. the UV-, blue-, green- and red-cones in zebrafish[2] (Vihtelic et al., 1999).

[2] As I exclusively did experiments in the retina of zebrafish during my PhD thesis, I will mainly refer to examples in the zebrafish retina.

*Bipolar cells (BCs)*

BCs are (mostly) glutamatergic interneurons that reside in the INL. As their name suggests, BCs have a 'textbook' bipolar morphology (**Figure 1.1**): on their apical side, BCs elaborate a dendrite tree to the OPL to receive synaptic inputs from PRs and HCs; on their basal side, BCs send an axon to the IPL to synapse with retinal ganglion cells (RGCs) and amacrine cells (ACs). Given their circuitry, BCs are considered as relay neurons that convey information (directly or indirectly) from PRs to RGCs. In very simple terms, BCs can be subdivided into ON- and OFF-BCs depending on whether they are activated by the onset of a light stimulus (ON-BCs) or by the termination of a light stimulus (OFF-BCs). Remarkably, ON- and OFF-BCs can be readily distinguished by their morphology as the axonal boutons of ON-BCs stratify in the lower half of the IPL (**Figure 1.1, left BC**), whereas the boutons of OFF-BCs stratify in the upper half of the IPL (**Figure 1.1, right BC**). However, based on axonal and dendritic morphology, ON- and OFF-BCs have been classified in further categories leading to a large number of BC subtypes, e.g. up to 18 BC subtypes have been described in the zebrafish retina (Connaughton, 2011; Li et al., 2012b).

*Retinal ganglion cells (RGCs)*

RGCs reside in the GCL and are highly polarized, glutamatergic projection neurons (**Figure 1.1**): on their apical side, RGCs extend a dendritic tree into the IPL to receive inputs from BCs and ACs; on their basal side, RGCs send axonal projections that leave the retina via the optic nerve to synapse in different brain areas, particularly in the lateral geniculate nucleus of the thalamus (in mammals) or the tectum (in teleosts). Mainly based on the stratification of their dendrites in the IPL, numerous subtypes of RGCs have been classified, e.g. more than 50 subtypes have been

proposed in the zebrafish retina (Robles et al., 2014). For some RGC subtypes, responses to a very specific stimulation have been observed and, in exceptional cases, even a link to behavior proposed, e.g. RGCs important for prey recognition (Semmelhack et al., 2014) and looming-evoked escape (Temizer et al., 2015). Moreover, there are special subtypes of non-image forming, light-sensitive RGCs, which are important for the circadian rhythm (Berson et al., 2002; Matos-Cruz et al., 2011) and pupillary reflex (Chen et al., 2011; Gamlin et al., 2007).

*Horizontal cells (HCs)*

HCs are inhibitory interneurons in the outer part of the INL. They have a multipolar morphology which is established by multiple dendrites (and, additionally, in some subtypes by a single axon) (**Figure 1.1**). HCs receive glutamatergic inputs from photoreceptors and release the neurotransmitter GABA to synapses that feedback on PRs. This feedback between PRs and HCs is the first station of lateral processing in the retina and important for accommodation to changing light levels. Relatively low numbers of HC subtypes (H1, H2 and H3) have been described in the zebrafish retina so far (Song et al., 2008).

*Amacrine cells (ACs)*

ACs are inhibitory interneurons which are mainly located in the inner part of the INL (however, so-called 'displaced ACs' reside in the GCL). ACs have a unipolar morphology with their sole dendrite projecting to the IPL to contact BCs and RGCs (**Figure 1.1**). ACs are important for lateral processing, e.g. to modulate or integrate visual information. To our current knowledge, ACs are the most diverse neuronal type in the vertebrate retina (Seung and Sumbul, 2014) and 28

subtypes have been described in zebrafish so far (Jusuf and Harris, 2009). ACs are mostly classified based on three criteria: (1) width of the dendritic tree (e.g. narrow-field), (2) in which strata of the IPL the dendritic tree stratifies (e.g. bistratified with a beaded morphology), and (3) which neurotransmitter they use (e.g. glycine). The AC subtype just described is known as an AII AC and is essential for information flow from rod BCs onto RGCs (Demb and Singer, 2012). Another well studied AC subtype is the cholinergic starburst AC, which is important for the emergence of direction selectivity (Yoshida et al., 2001). Nevertheless, the function of most ACs remain poorly understood and thus ACs are currently the most enigmatic cell type of the retina (Masland, 2012).

*Müller glia (MG)*

MG are the principal glial cell type of the retina. They have a relatively large soma which resides in the middle of the INL and span with their processes the entire thickness of the retina (**Figure 1.1**). Like other glial cells, their function is to support neurons, e.g. by uptake of neurotransmitters, ionic homeostasis of the extracellular milieu, or forming a mechanical support structure (MacDonald et al., 2015). As MGs are non-myelinating glia, all neurons within the retina proper are not myelinated. In lower vertebrates (like zebrafish), MGs maintain the potential, even in adulthood, to undergo mitosis as they can dedifferentiate after injury and divide to replenish lost neurons (Goldman, 2014).

## 1.2. The development of the vertebrate retina

As my work exclusively addressed mechanisms during late(r) stages of retinal development, I only refer to excellent reviews and book chapters for early stages of retinal development (Chow and Lang, 2001; Schmitt and Dowling, 1994; Wong, 2012; Zuber and Harris, 2012), and start to illustrate retinal development at the stage of a pseudostratified neuroepithelium (**Figure 1.2**).

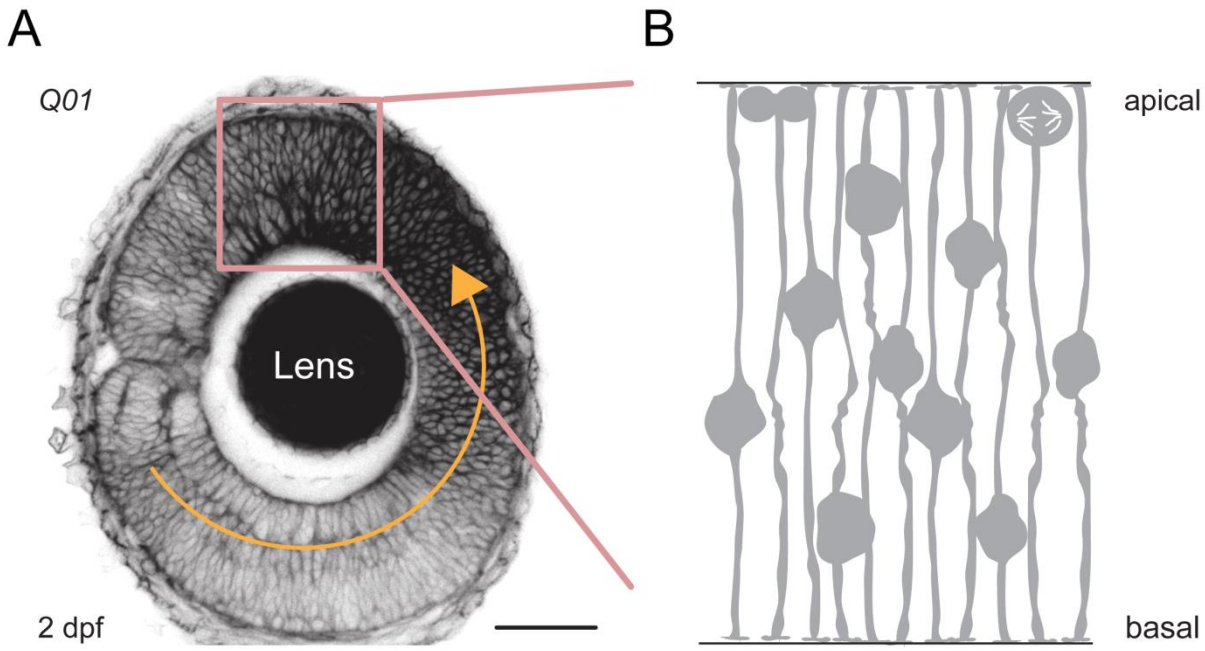


**Figure 1.2 - Morphology of a pseudostratified neuroepithelium.**

(A) Contrast-inverted image from an eye of a *Q01* larval zebrafish 2 days post fertilization (dpf), in which all cellular membranes are labelled with the genetically-encoded fluorescence protein CFP. The lamination of the mature retina has not been established at 2 dpf. In the boxed region, the retina appears to be constituted by several layers of undifferentiated cells. The orange arrow indicates the retinal gradient. Neuronal development commences in the ventro-nasal patch (starting point of the orange arrow) and subsequently advances to the nasal, dorsal and temporal parts of the retina. Scale bar: 50 µm. Image courtesy of Dr. Leanne Godinho. (B) Schematic representation of the retinal neuroepithelium. At the developmental stage of a pseudostratified neuroepithelium, the retina consists of progenitor cells which span with their processes the entire thickness of the retina. As the cell bodies of progenitor cells are arranged at different depths of the apico-basal axis, the retina appears to be constituted by multiple strata (layers) and thus is referred to as a pseudostratified neuroepithelium.

During late(r) stages of retinal development, the unstructured neuroepithelium (**Figure 1.2**) transforms to a functional retina (**Figure 1.1**). This transformation requires three major ontogenetic events to occur, starting with neurogenesis, followed by neuronal migration and concluding with neuronal differentiation (**Figure 1.3**). In the following paragraphs, I will describe our current knowledge about each ontogenetic event in greater detail.

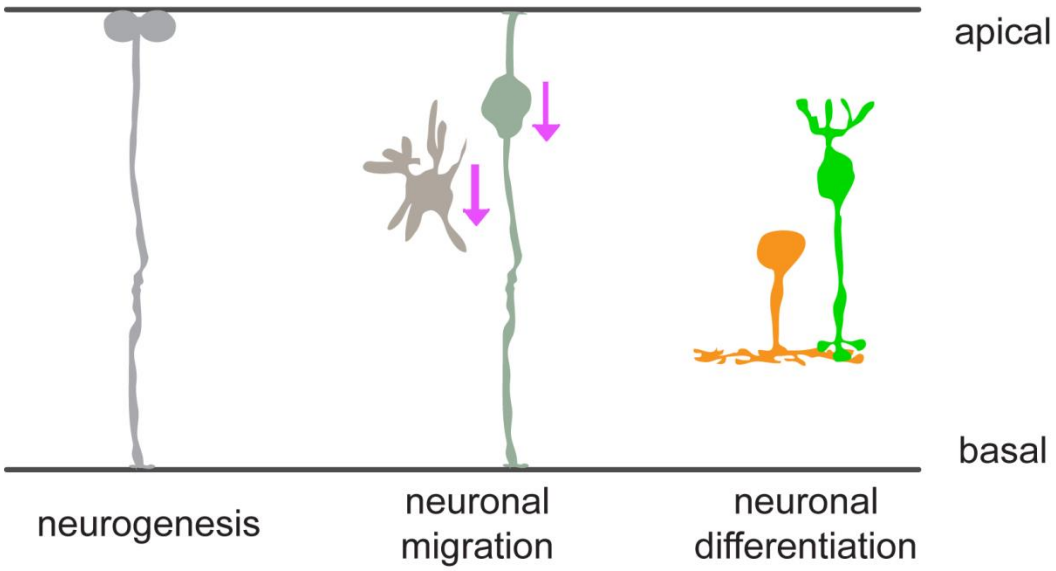


**Figure 1.3 – Neurogenesis, neuronal migration and neuronal differentiation.**

Schematic representation of the three major ontogenetic events during late(r) stages of retinal development: (1) neurogenesis, the birth of neurons by progenitor cell mitosis; (2) neuronal migration, the re-positioning of post-mitotic neurons from proliferative zones to the proper laminar position; and (3) neuronal differentiation, the acquisition of a neuronal morphology and gene expression profile to allow for circuit integration.

### 1.2.1. Neurogenesis

Initially, progenitor divisions of the pseudostratified neuroepithelium (**Figure 1.2**) are symmetric, proliferative divisions, i.e. each progenitor division produces another two progenitors (Gotz and Huttner, 2005) (**Figure 1.4**). However, as development proceeds, the progenitor mitoses shift to cell-divisions that could be described as (1) a stem-cell mode of division in which a progenitor and a post-mitotic cell are generated (asymmetric division) and (2) a terminal-mode of division in which two post-mitotic cells are generated (terminal division). If at least one of the post-mitotic daughter cells is a neuron, the division can also be referred to as a neurogenic division (**Figure 1.4**); if at least one of the post-mitotic daughter cells is a Müller glial cell, the division can also be referred to as a gliogenic division.

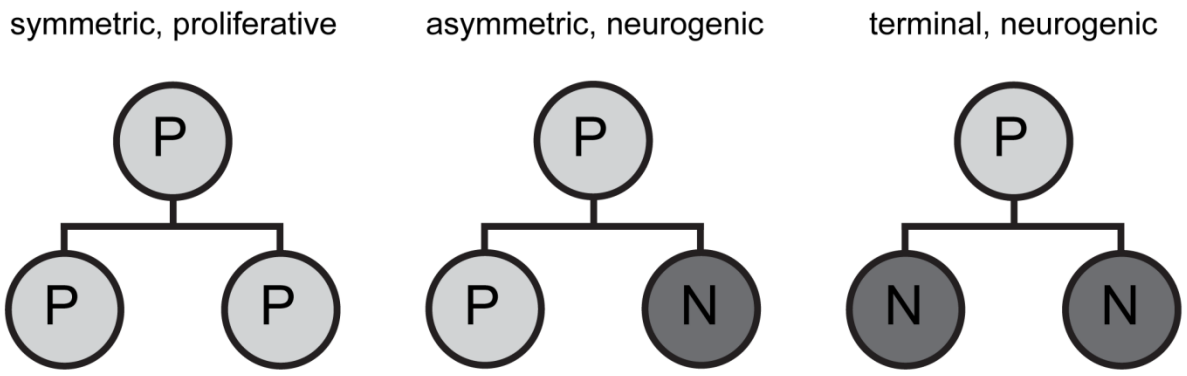


**Figure 1.4 - Modes of cell division during retinal neurogenesis.**

In principle three different modes of cell division can be distinguished during retinal neurogenesis: (1) symmetric, proliferative divisions in which each progenitor generates another two progenitors; (2) asymmetric, neurogenic divisions in which each progenitor generates a progenitor and a neuron; (3) terminal, neurogenic divisions in which each progenitor generates two neurons[3]. Abbreviations: progenitor cell (P) and neuron (N).

[3] Terminal divisions can even be further subdivided into (1) terminal, symmetric divisions (both daughter cells are the same post-mitotic cell type, e.g. two BCs) and (2) terminal, asymmetric divisions (daughter cells are distinct post-mitotic cell types, e.g. an AC and a BC).

The developmental process of neuron production by progenitor cell mitoses is referred to as 'neurogenesis'. Our knowledge on how the appropriate numbers and types of retinal neurons are generated is still limited. However, certain principles have emerged that help to accomplish this complex task.

*Birth dating of retinal cell types*

It is generally accepted that progenitors (at least at the early stages of neurogenesis) are multipotent, i.e. a progenitor lineage can produce post-mitotic cells with multiple distinct cellular fates (He et al., 2012; Holt et al., 1988; Turner and Cepko, 1987; Turner et al., 1990; Wetts and Fraser, 1988) (see also **Figure 1.6**). However, a progenitor lineage is not able to produce all cellular fates at a single time-point of retinogenesis. Several birth dating studies have shown (He et al., 2012; Hu and Easter, 1999; La Vail et al., 1991; Rapaport and Stone, 1983; Rapaport et al., 2004; Wong and Rapaport, 2009; Young, 1985a, b) that progenitors generate distinct neuronal types at different developmental stages, e.g. RGCs are the first cell type to be born in all vertebrate retinae (**Figure 1.5**). As retinogenesis proceeds, in addition to RGCs, other retinal cell types are born. The birth order of distinct cell types can show variations amongst different species, e.g. HCs are born late in zebrafish, while they are born early in rodents (Godinho et al., 2007; He et al., 2012; Hu and Easter, 1999; Rapaport et al., 2004; Young, 1985a). Furthermore, it is important to note that multiple distinct cell types (e.g. ACs and BCs) can be generated concurrently (**Figure 1.5**).

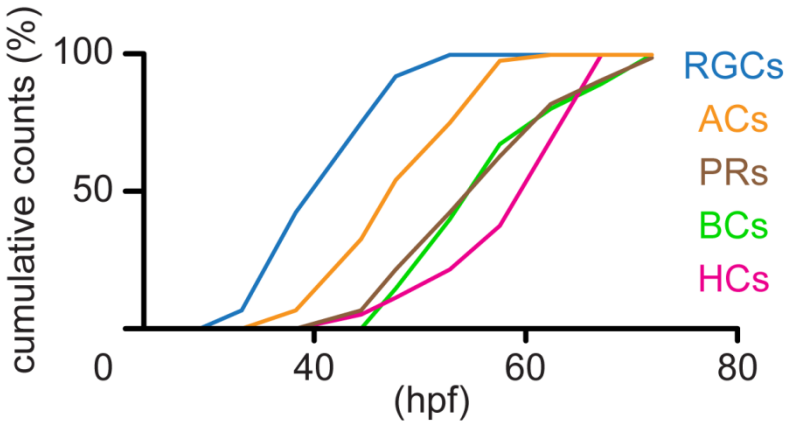


**Figure 1.5 – Birth dating of neurons in the zebrafish retina.**

Birth dating of neurons in the zebrafish retina shows that RGCs are the first cell type to be born, and that the genesis of retinal neurons is broadly overlapping. Abbreviations: photoreceptors (PRs), horizontal cells (HCs), bipolar cells (BCs), amacrine cells (ACs) and retinal ganglion cells (RGCs). Adapted from (He et al., 2012)

*Temporal competence model*

Especially for repetitive rounds of asymmetric, neurogenic divisions of a progenitor lineage (which produce one neuron and one progenitor cell following mitosis), a temporal competence model has been conceptualized (**Figure 1.6**). In this model, a progenitor lineage undergoes a developmental program, which is defined by the sequential action of transcription factors, leading to the competence of producing a certain cell type at a given stage of development (e.g. an RGC when neurogenesis commences). As retinogenesis proceeds, the transcriptional landscape of the progenitor lineage changes leading to the production of another, later-born cell type (e.g. an AC). Importantly, the model implies a one-way road, i.e. once a progenitor lineage has passed a certain competence stage, it cannot go back to produce an earlier-born cell type (Cepko, 2014; Kohwi and Doe, 2013).

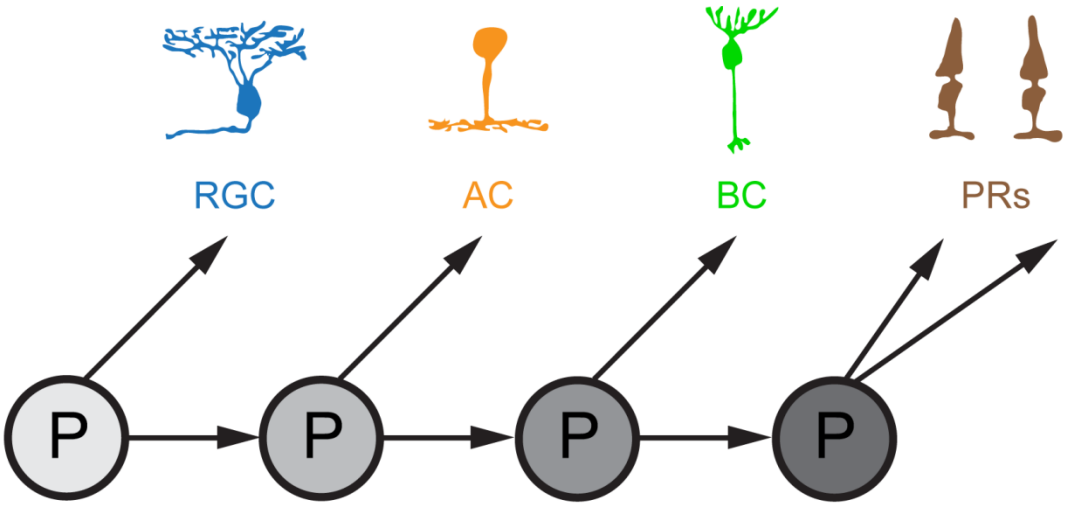


**Figure 1.6 - Lineage tree of a multipotent progenitor lineage according to the temporal competence model.**

A scheme of a progenitor lineage illustrates the capacity of a multipotent progenitor to produce several distinct neuronal cell types. While the early-dividing progenitor (light gray) undergoes an asymmetric, neurogenic division to generate a progenitor and an RGC, the late-dividing progenitor (dark grey) undergoes a terminal, symmetric division to generate two PRs. The changing hue saturation of progenitor cells indicates the shift in transcription factor expression during neurogenesis and their altered potential to produce distinct neuronal cell types. Abbreviations: progenitor cell (P), retinal ganglion cell (RGC), amacrine cell (AC), bipolar cell (BC) and photoreceptors (PRs).

*Deterministic vs stochastic model*

To date, it is clear that there is not a single progenitor lineage, i.e. even if two retinal progenitors are labeled at the very same time-point of development, their lineages will be variable with regards to number and type of produced neurons and glia (He et al., 2012; Holt et al., 1988; Turner and Cepko, 1987; Turner et al., 1990; Wetts and Fraser, 1988). Consistently, a large variety of molecularly distinct progenitors have been found (Blackshaw et al., 2004; Livesey et al., 2004; Trimarchi et al., 2008). How these variable progenitors produce an invariant retina is unclear (He et al., 2012). Two models are in principle conceivable:

On the one hand, a deterministic model has been proposed. In this model, multiple different progenitors exist, each having a specific, hardwired lineage. Some support for this model came

from studies of *trβ2*$^{+}$ progenitors in the zebrafish retina, which undergo multiple rounds of divisions and exclusively produce RGCs, HCs and red cones (Suzuki et al., 2013). Moreover, for the development of the mammalian cortex, a model with a deterministic component has been proposed (Gao et al., 2014).

On the other hand, studies in the retina have suggested that fate choices and lineage trees are stochastic; this means for example that the fate choice of an earlier division does not influence the fate choice of later divisions (Boije et al., 2015; Gomes et al., 2011; He et al., 2012). As the finding of committed *trβ2*$^{+}$ progenitors and an entirely stochastic model are mutually exclusive, future work will be needed to gauge the extent of deterministic and stochastic mechanisms during neurogenesis in the retina and other parts of the nervous system.

*Extrinsic vs intrinsic determinants*

Irrespective of a deterministic or stochastic model, it has been shown that both intrinsic and extrinsic factors could influence retinal development. Intrinsic factors are genetic programs of progenitors. Accordingly, over-expression or deletion of transcription factors and signaling pathways (e.g. *Ascl1*, *Atoh7*, *Notch* or *trβ2*$^{+}$) can profoundly change the lineage of progenitors (Brzezinski et al., 2011; Jadhav et al., 2006b; Mizeracka et al., 2013; Suzuki et al., 2013; Yang et al., 2003). Extrinsic factors are the environment of a progenitor, e.g. surrounding neurons. Likewise, a change in the composition of the surrounding cells can profoundly influence progenitor lineages (Belliveau and Cepko, 1999; Jusuf et al., 2011; Kay et al., 2005). Importantly, intrinsic and extrinsic factors are not mutually exclusive and could act cooperatively (Neumann and Nuesslein-Volhard, 2000).

*Terminally-dividing progenitors*

Over the past few years, it has become clear that some retinal neurons (especially late-born cell types) are generated predominantly or exclusively by terminally-dividing progenitors (He et al., 2012). It has been suggested that some of these progenitors are 'committed progenitors' (Emerson et al., 2013; Godinho et al., 2007; Suzuki et al., 2013). A committed progenitor is molecularly-defined and invariably produces a distinct cell type(s). Examples of committed progenitors in the zebrafish retina are HC and cone progenitors (Godinho et al., 2007; Suzuki et al., 2013).

In some instances, committed progenitors even show signs of 'precocious neuronal differentiation'. The term 'precocious neuronal differentiation' is (so far) not widely used in the literature but I would like to define it as the observation that certain neuronal progenitors are already expressing 'neuronal' genes [these 'neuronal' genes are conventionally thought to be only expressed in post-mitotic neurons and thus are used as markers thereof, e.g. TuJ1 (Memberg and Hall, 1995)]. Such 'differentiating' progenitors are not restricted to the zebrafish retina but are also present in other species and in other parts of the CNS, including the rodent cortex (Attardo et al., 2008; Haubensak et al., 2004; Miyata et al., 2004; Noctor et al., 2004). However, the most compelling evidence for precocious neuronal differentiation in neuronal progenitors can be observed in the peripheral nervous system (PNS) (DiCicco-Bloom et al., 1990; Rohrer and Thoenen, 1987; Rothman et al., 1980) where progenitors of sympathetic ganglia were reported to express the *bona fide* neuronal marker tyrosine hydroxylase (an enzyme important for the synthesis of catecholamines).

*Apically and non-apically dividing progenitors*

Conventionally, all retinal neurons are thought to be generated by retina spanning progenitors which have their somata scattered along different depth of the neuroepithelium and undergo mitosis at the apical surface (see also **Figure 1.2**). This means that every progenitor has to move its soma to the apical surface in order to divide (**Figure 1.7 A**), leading to characteristic oscillatory nuclear movements prior to mitosis (Sauer, 1935), a phenomenon termed 'interkinetic nuclear migration' (IKNM). Recently, the direction and driving forces of IKNM have been linked to specific phases of the cell cycle (Baye and Link, 2007; Kosodo et al., 2011; Leung et al., 2011). It was proposed that passive forces (generated by surrounding cells) push progenitor somata during $G_1$ phase away from the apical surface. During S-phase, progenitors are located in the basal parts of the retina and undergo only little, undirected movement. However, in $G_2$-phase, progenitors show microtubule and/or actin-myosin driven directed movement toward the apical surface to undergo mitosis at this location (Del Bene et al., 2008; Norden et al., 2009).

About a decade ago, studies in the rodent cortex reported that neuronal progenitors can also undergo mitosis in non-apical locations (Haubensak et al., 2004; Miyata et al., 2004; Noctor et al., 2004) (**Figure 1.7 B**). These progenitors were named 'basal progenitors', 'intermediate progenitors' or 'non-apical progenitors'. Subsequently, non-apically dividing progenitors have also been described in the zebrafish retina (Godinho et al., 2007; Weber et al., 2014). The migration of these non-apical progenitors is less understood, e.g. it is unclear whether non-apically dividing progenitors undergo IKNM. So far, it has been suggested that mechanical constraints could prevent apical movement and force progenitors to divide non-apically (Weber et al., 2014).

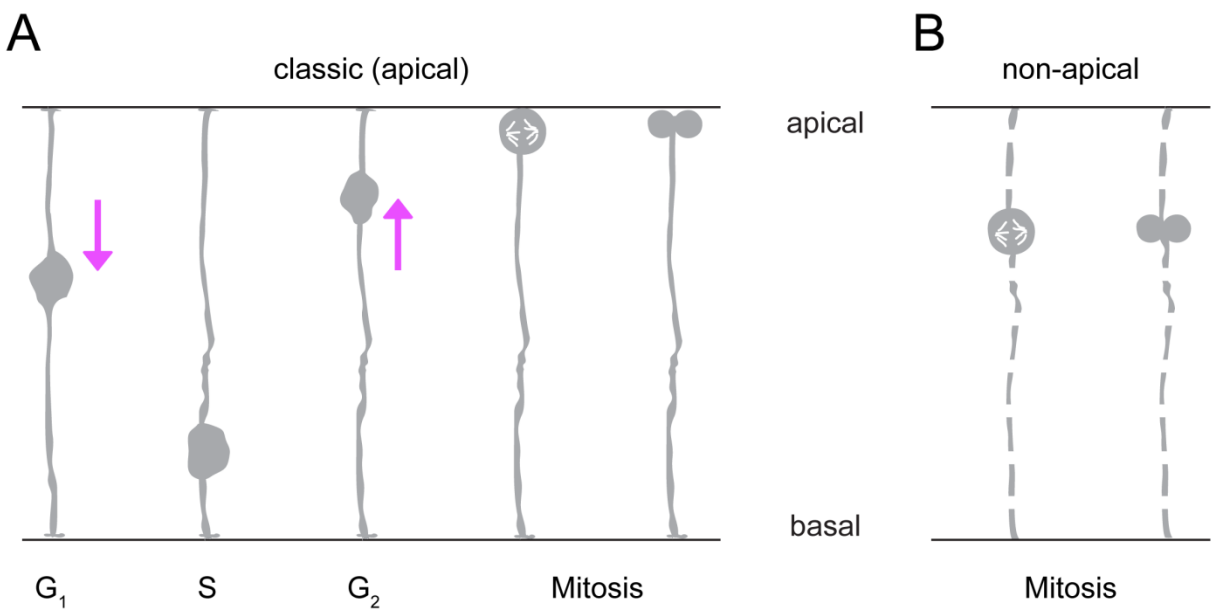


**Figure 1.7 - Apically and non-apically dividing progenitors.**

(A) An apically dividing retinal progenitor undergoing IKNM and mitosis at the apical surface. The scheme illustrates the somal movement of the progenitor during the cell cycle. The soma moves basally during $G_1$ phase, shows little movement during the S phase, and moves apically during $G_2$ phase. At the beginning of mitosis, the progenitor has reached the apical surface to undergo cell division. (B) A non-apically dividing progenitor undergoing mitosis at a non-apical location. For non-apically dividing progenitors, it is unknown whether they undergo IKNM. The morphology of non-apically dividing progenitors is less studied and potentially variable (indicated by dashed processes).

### 1.2.2. Neuronal migration

After being generated by neurogenic mitosis, the nuclei of the daughter cells migrate to place their cell bodies in the appropriate layer (**Figure 1.3**). During neuronal migration, two distinct morphologies have been observed for retinal neurons: On the one hand, nuclear translocation reminiscent of progenitor cell IKNM has been described for immature RGCs and BCs (Quesada et al., 1981; Zolessi et al., 2006). On the other hand, an amoeboid-like migration has been described for ACs and HCs (Deans et al., 2011; Godinho et al., 2005; Godinho et al., 2007; Hinds and Hinds, 1978, 1983; Quesada et al., 1981) (**Figure 1.3**). Additionally, a recent publication suggests that inhibitory cells could undergo distinct phases of migration involving both somal translocation and amoeboid-like migration (Chow et al., 2015). While the radial displacement of post-mitotic cells to the appropriate layer is necessary for neuronal development, it is not sufficient to form the retinal mosaic with regularly distributed cell types. Accordingly, several studies have shown that some retinal neurons can undergo tangential dispersion to contribute to retinal mosaic formation (Reese and Galli-Resta, 2002).

Unlike interneurons of the neocortex (Anderson et al., 1997), all retinal cells are born within the retina and thus the migration distances for newly-born neurons are short. This is especially true for non-apically dividing progenitors as they can undergo mitosis in their daughter cells' future layer (e.g. HC progenitors divide in the INL, the layer in which HCs reside). It has been speculated that these *in situ* divisions minimize the need for post-mitotic neuronal migration and could thus speed up neuronal development (Godinho et al., 2007). Intriguingly, exactly these non-apically dividing progenitors show signs of precocious neuronal differentiation.

### 1.2.3. Neuronal differentiation

Neurons are highly specialized cells, which can receive, integrate and convey information. To this end, neurons display a sophisticated, highly-polarized morphology (Cajal, 1899) which enables them to interact very precisely. Neuronal morphologies are cell type specific and hence can be vastly heterogeneous (**Figure 1.1**). In most cases, neurons extend a single axon and a variable number of dendrites. Neurosciences have begun to understand some of the cellular, subcellular and molecular processes of how axons and dendrites form (Lewis et al., 2013; Whitford et al., 2002). While much work has been done *in vitro* (Bradke and Dotti, 2000), some studies have addressed these questions *in vivo* (Godinho et al., 2005; Mumm et al., 2005; Zolessi et al., 2006). For example, time-lapse recordings have revealed the dynamics of axonal and dendritic development of BCs. It has been proposed that BCs initially have retinal spanning processes which are then pruned to restrict the neurites to the IPL and OPL (Randlett et al., 2013). In addition, studies have looked at subcellular organelles, e.g. the centrosome and its role in establishing the axon (Distel et al., 2010; Randlett et al., 2011). Finally, some of the molecular players that promote axon or dendrite formation have been cloned (Barnes et al., 2007; Shelly et al., 2007; Shelly et al., 2011).

A correct morphology is necessary to bring the processes of different neurons in close proximity and enable them to potentially interact. For functional circuits, however, neurons must be excitable and establish synapses. To this end, neurons show a unique gene expression profile including genes for specific ion channels, neurotransmitter synthesis and the pre- and postsynaptic machinery. Accordingly, as neuronal differentiation proceeds, post-mitotic neurons commence neuron-specific gene expression to allow for neuronal excitability and connectivity (Cahoy et al., 2008).

## 1.3. Zebrafish as an *in vivo* model of neural development

The teleost zebrafish (*Danio rerio*) is a popular vertebrate model organism for multiple reasons. Since the early days of zebrafish research, the potential to conduct large-scale genetic screens in a vertebrate has been appreciated (Nusslein-Volhard, 2012). Later, after new labeling and imaging methods came of age, zebrafish embryos emerged also as a popular model for *in vivo* imaging (Beis and Stainier, 2006; Engerer et al., 2016; Keller, 2013). Zebrafish embryos are conducive for intravital microscopy for a number of reasons: (1) Zebrafish embryos develop rapidly and externally, while at the same time being transparent. (2) Zebrafish embryos can be easily prepared for (repeated) microscopic observation without the need for any surgical procedure. (3) Zebrafish offer a large variety of tools for fluorescence labeling, including the bi-partite *Gal4*/*UAS* system, which allows for amplified and flexible expression of (multiple) transgenes (Brand and Perrimon, 1993; Distel et al., 2010; Koster and Fraser, 2001; Scheer and Campos-Ortega, 1999).

The convenience of imaging zebrafish embryos *in vivo* is particularly valuable to study neural development. I want to illustrate this by highlighting two major hurdles in mice, the prime model system for neural development in mammals: (1) Since neural development in rodents occurs largely *in utero* within an opaque embryo, direct optical access to the intact developing nervous system is precluded and surgical procedures are involved [e.g. slice preparations and whole explants (Gahwiler et al., 1997; Kerschensteiner et al., 2008)]. (2) Neural development in rodents takes significantly longer, rendering it difficult to study certain events in a single preparation [e.g. synapse elimination; but see also (Walsh and Lichtman, 2003)].

On the contrary, it is important to realize that the organization of the zebrafish nervous system is in some parts profoundly different from mammals, e.g. zebrafish do not have a six-layered

cerebral cortex (Mueller and Wullimann, 2015). Thus certain aspects of mammalian neural development cannot be addressed in zebrafish. On that note, it is not surprising that the retina has for a number of reasons drawn more attention than any other structure for studies on neural development in zebrafish: (1) The retina of zebrafish shares the same principle organization of all vertebrate retinae. Thus zebrafish researchers cannot only benefit from work in other species but also produce insight potentially relevant for mammals. (2) Zebrafish are visual animals and thus the entire visual system occupies large areas of their nervous system. In addition, several behavioral assays to probe vision have been established. (3) The retina is on the surface of the zebrafish head and as such an 'accessible part of the brain'.

*In vivo* studies of the zebrafish retina have been reported more than a decade ago, covering diverse questions of neural development, such as the modes of cell division during neurogenesis (Das et al., 2003), the lineage of progenitors (He et al., 2012; Poggi et al., 2005; Suzuki et al., 2013; Vitorino et al., 2009), interkinetic nuclear migration of progenitors (Baye and Link, 2007; Del Bene et al., 2008; Leung et al., 2011; Norden et al., 2009), the migration and polarization of post-mitotic neurons (Chow et al., 2015; Godinho et al., 2005; Mumm et al., 2005; Randlett et al., 2011; Zolessi et al., 2006), the selectivity of neuronal connectivity (Randlett et al., 2013; Yoshimatsu et al., 2016; Yoshimatsu et al., 2014) or the role of Müller glia (MacDonald et al., 2015; Williams et al., 2010).

## 1.4. The plasticity of the *vsx1*$^{+}$ lineage during zebrafish retinogenesis

Taking advantage of the genetic and optical accessibility of zebrafish embryos, I aimed to investigate how interneurons are born *in vivo* by a molecularly-defined progenitor cell population. To this end, I studied the *vsx1*$^{+}$ progenitor lineage of the retina.

Previous studies have suggested that *vsx1*$^{+}$ progenitors of the zebrafish retina undergo terminal, symmetric division to yield two BCs (He et al., 2012; Weber et al., 2014) and thereby generate the vast majority of BCs (> 95% of all mature BCs are *vsx1*$^{+}$) (Vitorino et al., 2009). In addition, expression of *vsx1* has also been observed in a heterogeneous, small subset of mature ACs (< 5% of all mature ACs are *vsx1*$^{+}$) (Vitorino et al., 2009). However, the expression of *vsx1* in ACs is enigmatic as the homeobox transcription factor *vsx1* has previously only been implicated in the specification and maintenance of BCs (Chow et al., 2001; Passini et al., 1997; Shi et al., 2011).

By following terminally-dividing *vsx1*$^{+}$ progenitors and their daughter cells with single cell precision, I could directly observe the plasticity of progenitors and newly-born post-mitotic neurons *in vivo*. In the first project, focusing on the plasticity of progenitors, I addressed the stereotypy of the developmental program in the molecularly-defined *vsx1*$^{+}$ progenitor population. Or in other words, I explored the relative timing of neurogenesis, neuronal migration and neuronal differentiation in this molecularly-defined progenitor population of the CNS. In contrast to the canonical view, which suggests that neurogenesis, neuronal migration and neuronal differentiation occur in a fixed sequence (**Figure 1.3**), I found an uncoupling of these ontogenetic events in *vsx1*$^{+}$ progenitors. In the second project, focusing on the plasticity of newly-born post-mitotic daughter cells, I found that *vsx1*$^{+}$ progenitors can also generate ACs and investigated the molecular mechanisms underlying the production of *vsx1*$^{+}$ ACs. To this end, I found evidence for Notch-mediated re-specification of neuronal identity during CNS development.

# 2. MATERIALS AND METHODS

## 2.1. Cloning

***pCH-14xUAS*:memTagRFP-T**: TagRFP-T was subcloned from *5xUAS*:TagRFP-T (gift from Dr. M. Meyer, King's College, London, GB) into a *14xUAS*:mYFP vector (Mumm et al., 2006) using XmaI/NotI. Subsequently, *14xUAS*:memTagRFP-T was cloned via PCR (f-primer: 5'-GGA AAA GCT AGC CCT ATG GAA AAA CGC CAG CAA CGC-3', r-primer: 5'-CGC CTT AAG ATA CAT TGA-3') into a pColdHeart Tol2 vector (gift from Dr. M. Nonet, Washington University, St. Louis, USA) using NheI/ClaI.

***pCH-14xUAS*:centrin4-YFP,*14xUAS*:MA-Cerulean**: Centrin4-YFP was isolated from *5xUAS*:Centrin4-YFP using EcoRI/ApaI and ligated into the NotI restriction site of *14xUAS*:memCerulean (gift from Drs. S.C. Suzuki and T. Yoshimatsu, University of Washington, Seattle, USA). Subsequently, a *14xUAS* sequence was cloned in front of the Centrin4-YFP using the XhoI restriction site. Finally, the *14xUAS*:centrin4-YFP,*14xUAS*:MA-Cerulean sequence was subcloned into the pColdHeart Tol2 vector using ApaLI/DraIII.

***pCH-5xUAS*:Atoh7**: The coding sequence of zebrafish *atoh7* (*atonal bHLH transcription factor 7*) was cloned via PCR (f-primer: 5'- GGA AAA GAA TTC ATG AAG CCC CGC AGG CCG AG -3', r-primer: 5'- GGG CCC GCGGCCGC TCA GAG GCT TTC GTA GTG GT -3') from a plasmid containing full-length *athoh7* cDNA (I.M.A.G.E Clone IRBVp5006D093D, Source Bioscience) into the *5xUAS*:TagRFP-T vector using EcoRI/NotI. Subsequently, *5xUAS*:Atoh7 was excised with AseI/AflII and ligated into the pColdHeart Tol2 vector using blunted NheI/ClaI restriction sites. (Cloning was done by Dr. Leanne Godinho and Yvonne Hufnagel).

***pCH-5xUAS*:Ptf1a**: The coding sequence of zebrafish *ptf1a* (*pancreas-specific transcription factor, 1a*) was cloned via PCR (f-primer: 5'- GGA AAA GCG GCC GCC CCG GGA TGG ACA CTG TGT TGG ATC CAT TCA and r-primer: 5'- GGA AAA GCG GCC GCC CCG GGT TAG GAA ATG AAA TTA AAG GG) from zebrafish cDNA (obtained by reverse transcription, Omniscript RT kit, Qiagen) into the *5xUAS*:TagRFP-T vector using XmaI/NotI. Subsequently, *5xUAS*:Ptf1a was released with AseI/AflII and ligated into the pColdHeart Tol2 vector using blunted NheI/ClaI restriction sites. (Cloning was done by Dr. Leanne Godinho).

***pGH-Vsx1:*Gal4**: The entry clones *p5E-Vsx1* (Randlett et al., 2013), *pME*-Gal4VP16 and *p3E*-pA were recombined into the *pTol2CG2* vector (Kwan et al., 2007) using the GATEWAY system (Invitrogen). (Cloning was done by Drs. S.C. Suzuki and T. Yoshimatsu, University of Washington, Seattle, USA).

***pCS2* mOrange2-PCNA**: mOrange2-PCNA was PCR amplified (f-primer: 5'-GGA AAA CTC GAG ATG GAT CCA AAA AAG AAG AGA-3', r-primer: 5'-GGG CCC TCT AGA CTA AGA TCC TTC TTC ATC CTC-3') from mOrange2-PCNA-19-SV40NLS-4 (plasmid # 57971, Addgene) and cloned into the *pCS2+* vector using XhoI/XbaI.

***pCS2* Centrin4-YFP**: Centrin4-YFP was subcloned from *5xUAS*:Centrin4-YFP (Distel et al., 2010) into the *pCS2+* vector using EcoRI/ApaI. (Cloning was done in collaboration with Nancy Obeng).

***pGEM-T* Easy *ribeye a***: The first exon of *ribeye a* was cloned via PCR (f-primer: 5'-TCC AGT AAG CAG TTG CCG AT-3', r-primer: 5'-TCC GGA TGC ATG ACC ATA CC-3') from a plasmid containing full length *ribeye a* (gift from Dr. T. Nicolson, Vollum Institue, Portland, USA) into the *pGem-T* Easy vector. This vector was used as a template to generate a digoxigenin-labeled riboprobe.

## 2.2. Animals

All experiments were performed according to local regulations as approved by the local regulatory bodies. Zebrafish were maintained, mated, and raised as described (Mullins et al., 1994). Embryos were kept in 0.3x Danieau's solution (for recipe see section **2.13**) at 28.5°C and staged as previously described (Kimmel et al., 1995). Fish were in AB wild-type, Tuebingen Long Fin (TLN) or *roy orbison* (Ren et al., 2002) background. The transgenic lines used are listed in **Table 2.1**. I generated Tg(14x*UAS*:memTagRFP-T), Tg(*UAS*:cetn4-YFP,*UAS*:MA-Cerulean)tum1, Tg(5x*UAS*:Ptf1a) and Tg(5x*UAS*:Atoh7) by Tol2 mediated insertion (Kawakami, 2004).

**TABLE 2.1 - Transgenic lines**

| Transgenic Line | Referred to as | Reference |
|---|---|---|
| Tg(*vsx1*:GFP)nns5 | *vsx1*:GFP | (Kimura et al., 2008; Vitorino et al., 2009) |
| Tg(*vsx2*:GFP)nns1 | *vsx2*:GFP | (Kimura et al., 2006; Vitorino et al., 2009) |
| Tg(ptf1a:eGFP)jh1 | *ptf1a*:GFP | (Godinho et al., 2005) |
| Tg(*pax6-DF4*:gap43-CFP)q01 | *Q01* | (Godinho et al., 2005) |
| Tg(*gfap*:GFP)mi2001 | *GFAP*:GFP | (Bernardos and Raymond, 2006) |
| Tg(v*sx1:*MCerulean)q19 | *Q19* | (Randlett et al., 2013) |
| Tg(14x*UAS*:MYFP) | *UAS*:memYFP | (Williams et al., 2010) |
| Tg(crx:MA-CFP)q20 | *crx*:mCFP | (Suzuki et al., 2013) |
| Tg(-1.8ctbp2:gap43-EGFP)lmb1 | *ctbp2*:mEGFP | (Odermatt et al., 2012) |
| Tg(*UAS*:myc-notch-intra) | *UAS*:nicd | (Scheer and Campos-Ortega, 1999) |
| Tg(T2KTp1bglob:hmgb1-mCherry)jh11 | Notch:reporter | (Parsons et al., 2009) |
| Et(e1b:GAL4)s1101t | s1101 | (Mason et al., 2009) |
| Tg (*UAS*:Kaede)s1999t | *UAS*:Kaede | (Scott et al., 2007) |
| Tg(*vsx1*:Gal4)q26 | *Q26* | Unpublished (Provided by Suzuki and Yoshimatsu) |
| Tg(*UAS*:cetn4-YFP,*UAS*:MA-Cerulean)tum1 | *CentrinFish* | Generated (Engerer et al., 2014) |
| Tg(14x*UAS*:memTagRFP-T) | *UAS*:memTagRFP-T | Generated |
| Tg(5x*UAS*:Atoh7) | *UAS*:Atoh7 | Generated |
| Tg(5x*UAS*:Ptf1a) | *UAS*:Ptf1a | Generated |

## 2.3. Genotyping of *Q26* crosses

*Q26* NICD

The presence of *UAS*:NICD was initially determined by immunostaining for the myc-tag (99.1 ± 0.6% of *UAS*:mYFP$^+$ cells immunostained for the myc-tag; 428 *Q26 UAS*:mYFP$^+$ cells, 3 fish). Subsequently, as the expression of *UAS:*NICD correlated in all fish (12/12) with the exuberant growth of BC axonal arbors and the loss of IPL lamination, the *Q26* NICD genotype was determined by the lamination of the IPL (see also **Figure 3.23** and compare the structure of the IPL in control and *UAS*:NICD).

*Q26* Ptf1a

The presence of *UAS*:Ptf1a was determined by the expression of the 'ColdHeart' marker (cyan fluorescence of the heart).

*Q26* NICD Ptf1a

The presence of *UAS:*NICD and *UAS*:Ptf1a was determined for each transgene as described above.

*Q26* NICD Atoh7

The presence of *UAS:*NICD was determined as described above. The presence of UAS:Atoh7 was determined by the expression of the 'ColdHeart' marker.

## 2.4. mRNA synthesis and injection

Plasmids were linearized (PCNA: NotI, centrin4: ApaI). Capped mRNA was produced using the Ambion mMESSAGE mMACHINE kit (Applied Biosystems) according to the manufacturer's instructions. mRNA was injected at 100 ng/µl into one or two-cell stage embryos.

## 2.5. Morpholino injection

*Ptf1a* (0.5 to 1.0 mM, Gene tools) and *p53* (0.02 to 1.0 mM, Gene tools) morpholinos were injected with a picospritzer into the yolk of one or two-cell stage embryos.

## 2.6. *In vivo* imaging

Embryos were prepared for imaging as described previously (Engerer et al., 2016; Godinho, 2011): Between 10 and 18 hours post-fertilization (hpf), embryos were transferred to 0.3x Danieau's solution containing 0.003% 1-phenyl-2-thiourea (PTU, Sigma) to inhibit melanin formation (Karlsson et al., 2001). At 2 days post-fertilization (dpf), manually dechorionated embryos were anesthetized using 0.02% tricaine (PharmaQ) in medium containing PTU and, after screening on a dissecting fluorescence scope (Leica), embedded in low-melting agarose (0.7 – 0.8%, Sigma). Fish were imaged starting at 2 dpf on an Olympus FV1000 confocal/2-photon and an Olympus FVMPE-RS 2-photon microscope using water-immersion objectives (Olympus 20x/NA 0.95, Olympus 25x/NA 1.05, Zeiss 40x/NA 1.0, Nikon 25x/NA 1.1 and Nikon 40x/NA 0.8) or a silicon-immersion objective (Olympus 30x/ NA 1.05). Embryos were maintained at 28.5°C during all *in vivo* recordings. At each time-point z-stacks were acquired of the peripheral retina, encompassing its entire circumference.

## 2.7. Immunohistochemistry

Zebrafish embryos were anesthetized using tricaine and fixed in 4% (wt/vol) paraformaldehyde (PFA) in 1x PBS at 4°C overnight. For immunostaining on cryosections, an adaptation of a previously published protocol was used (Williams et al., 2010): Fixed embryos were washed several times in 1x PBS and incubated in 30% (wt/vol) sucrose in 1x PBS overnight. Samples were frozen in OCT (Tissue-Tek) and 30 µm coronal sections were cut in a Cryostat (Leica) and mounted on SuperFrost Plus slides (Thermo Scientific). Sections were washed several times with 1x PBS, incubated for 1 h in blocking serum (normal goat serum 10%, 0.2 to 0.5% Triton X-100), and subsequently overnight in one of the following primary antibodies: rabbit anti-pH3 (1:500, Upstate), mouse anti-pH3 (1:500, Abcam), rabbit anti-Crx (1:500, gift from Dr. P. Raymond, University of Michigan, Ann Arbor, USA), chicken anti-GFP (1:500, Abcam) and rabbit anti-PKC α/β (1:100, SCBT). After several washes with 1x PBS, sections were incubated in the appropriate Alexa dye-coupled secondary antibodies (1:1000, Invitrogen) for 1 h and finally mounted in Vectashield. For Crx immunostaining, an antigen retrieval step (two to ten minutes at 98°C in sodium citrate buffer; 10mM sodium citrate, 0.05% Tween 20, pH 6.0) was performed prior to primary antibody incubation.

For immunostaining on whole-mounts, an adaptation of a previously published protocol was used (Hunter et al., 2011): Following fixation and washes in 1x PBS, embryos were incubated in 0.25% Trypsin in 1x PBS on ice for 3 to 9 min. Embryos were then washed several times in 1x PBS, incubated for 1 h in 0.4% Blocking reagent (Roche) and subsequently in the primary antibody for two days at 4°C. Primary antibodies used were mouse or rabbit anti-pH3 (1:200), chicken anti-GFP (1:1000, Abcam) and mouse anti-myc (1:100, Sigma). Following several washes in 1x PBS, embryos were incubated in appropriate Alexa dye-coupled secondary

antibodies overnight (1:500, Invitrogen). DAPI (2 µg/ml, Roche) was added to the final washes in 1x PBS. Fish were mounted in low-melting agarose as for *in vivo* imaging.

## 2.8. *In situ* hybridization

*In situ* hybridizations were performed to detect the expression of *ribeye a* mRNA: Transgenic *ctbp2*:mGFP embryos were fixed in 4% PFA in 1x PBS overnight and subsequently dehydrated in a methanol series from 25% methanol in PBT (PBS with 0.1% Tween) to 100% methanol, and stored at -20°C. Following rehydration through a reverse methanol/PBT series, embryos were treated with proteinase K (10 µg/ml) at room temperature for 15 min and post-fixed in 4% PFA in 1x PBS for 20 min. They were pre-hybridized in $HYB^+$ (50% formamide; 5x SSC; 50 µg/ml heparin; 0.5 mg/ml yeast t-RNA; 0.1% Tween-20; 9.2 mM citric acid, pH 6.0) for 1 h at 68°C. Hybridization with the digoxygenin-labeled *ribeye a* riboprobe in $HYB^+$ was performed overnight at 68°C. Washes were performed at 68°C every 10 min with a mixture of $HYB^-$ (65% formamide; 5x SSC; 0.1% Tween-20) and 2x SSC in the following sequence: 75% $HYB^-$, 25% 2x SSC, followed by 50% $HYB^-$, 50% 2x SSC; and subsequently with 25% $HYB^-$ , 75% 2x SSC. Finally, embryos were washed in 2x SSC (twice for 30 min each at 68°C). Subsequent washes were performed at room temperature in 0.05x SSC, 50% 0.05x SSC; 50% PBT and finally PBT (each for 5 min), before incubating in block buffer (PBT; 2% normal goat serum; 2mg/ml bovine serum albumin) for 1 h. Fab fragments of anti-digoxygenin-alkaline phosphatase antibody (Roche) were preadsorbed in block buffer (1:100) for 24 h and diluted at a final concentration of 1:5000 in block buffer. Following 2 h incubation in the anti-digoxygenin antibody at room temperature, embryos were washed several times in PBT and subsequently left in PBT overnight. On the next day, embryos were rinsed in NTMT (100 mM Tris-HCl pH 9.5; 50 mM

$MgCl_2$, 100 mM NaCl; 0.1% Tween-20), and alkaline phosphatase activity was revealed using Fast Red TR/Napthol AS-MX (Sigma) to obtain a red fluorescent precipitate. Following extensive washes in PBT, embryos were immunostained for GFP and pH3, mounted in low-melting agarose as for *in vivo* imaging. (*In situ* hybridizations were performed in collaboration with Dr. Prisca Chapouton, Helmholtz Zentrum, München, Germany)

## 2.9. Hydroxyurea-aphidicolin treatment

Hydroxyurea (Sigma) and aphidicolin (BioViotica) were used at a final concentration of 20 mM and 150 µM respectively in 0.3x Danieau's containing 1.0 - 1.7% DMSO. Embryos were injected with a *p53* morpholino to ameliorate HUA induced apoptosis (Girdler et al., 2013). At 2 dpf embryos were mounted in agarose as described for *in vivo* imaging above, but leaving the tail fin un-embedded for better drug access. Retinas were imaged for one time-point prior to HUA administration. The 0.3x Danieau's medium was replaced with HUA-containing medium and time-lapse recording was immediately resumed. Recordings were generally limited to <16 h after HUA addition as high levels of cell death were observed thereafter.

## 2.10. DAPT treatment

DAPT {*N*-[*N*-(3,5-Difluorophenacetyl-L-alanyl)]-(*S*)-phenylglycine *t*-butyl ester (Enzo)} was used at a final concentration of 50 µM in 0.3x Danieau's containing 1 % DMSO. Embryos were injected with a *p53* morpholino (Gene Tools) at the one or two cell-stage to ameliorate DAPT induced toxicity (Girdler et al., 2013). At 2 dpf embryos were transferred into DAPT containing medium (or DMSO containing medium as a control) and incubated for approximately 20 h before analysis.

## 2.11. Statistics

Mean values and standard error of the mean (SEM) were calculated using Microsoft Excel. The Mann–Whitney U test was used to compare datasets with GraphPad Prism 5. Data are presented as mean ± SEM. p-values <0.05 are denoted with '*', <0.01 with '**' and <0.001 with '***'. For multiple comparisons, the significance of p-values were corrected according to the FDR principle (Benjamini and Hochberg, 1995).

## 2.12. Image processing

Images were viewed and processed using open-source ImageJ/Fiji software (http://fiji.sc). Image panels were assembled in Photoshop CS5 (Adobe) and combined into figures using Illustrator CS5 (Adobe). The "Gaussian blur" function was used to filter noise for clarity. Unless noted otherwise, the gamma-value was not adjusted.

## 2.13. Data analysis

**Estimation of post-mitotic cells in the laminated region of the retina**

I calculated the percentage of post-mitotic cells (y) in a given area by

$$y = \frac{2x}{(1 - x) + 2x}$$

where x is the percentage of *vsx1*$^{+}$ progenitors that have undergone mitoses. Given the ratio of cells dividing in the immature and mature part of the retina is approximately 60:40, I could calculate that the average mitotic *vsx1*$^{+}$ cell in the mature region will have 88.9% post-mitotic

*vsx1*$^+$ cells in the surround, with numbers ranging from 75% to 100% of post-mitotic *vsx1*$^+$ cells for individual *vsx1*$^+$ progenitors that divide in the mature region.

**Quantification of apically and non-apically dividing cells in *vsx1*:GFP sections**

To label cell membranes and clearly visualize the OPL and IPL in the retina, 2 dpf *vsx1*:GFP zebrafish embryos were incubated with the vital dye CellTrace BODIPY Texas Red methyl ester (Invitrogen) according to the manufacturer's instructions. Embryos were then fixed and processed for pH3 immunostaining (rabbit pH3 antibody) on cryosections as described above. Regions of the retina were assigned to be 'unlaminated' or 'laminated' based on the absence or presence respectively of a clearly discernable OPL and IPL. In each region we quantified the proportion of *vsx1*$^+$pH3$^+$ double-positive cells dividing apically and non-apically (at least one cell diameter away from the apical surface). The area between clearly 'unlaminated' and 'laminated' regions of the retina, which we refer to as 'intermediate', was excluded from analysis.

**Comparison of *vsx1*:GFP fluorescence intensity of dividing progenitors and cells in their vicinity**

Fluorescence intensities were measured on retinal sections from 2 dpf *vsx1*:GFP zebrafish that were immunostained with pH3 antibodies to label cells in $G_2$/M-phase. For each *vsx1*$^+$ dividing cell (*vsx1*:GFP$^+$ pH3$^+$ double-positive), GFP fluorescence in a region of interest (ROI) encompassing the soma in a single image plane of a confocal stack was measured and the background fluorescence averaged from three nearby *vsx1*$^-$ cells was subtracted to correct for auto-fluorescence and potential out-of-focus contributions. To calculate the fluorescence intensity of cells in the vicinity, 12 *vsx1*:GFP$^+$ pH3$^-$ cells were randomly chosen. Typically, surrounding cells were immediately adjacent to the mitotic cell (one to three somata away). However, the density of *vsx1*$^+$ cells was low in some instances in the unlaminated retina and therefore

surrounding cells needed to be selected farther afield. For comparison across different samples, fluorescence intensity values were normalized to the peak *vsx1*:GFP fluorescence intensity of BCs from the same section.

**Comparison of Crx fluorescence intensity of mitotic *vsx1*$^+$ cells and surrounding *vsx1*$^+$ cells**

*Vsx1*:GFP retinal sections were stained for Crx and pH3 as described above. Similar to the comparison of fluorescence intensities in mitotic *vsx1*$^+$ cells and the post-mitotic cells in their surround (described above), the average fluorescence intensity of the Crx stained cells was compared between a mitotic (pH3$^+$) *vsx1*$^+$ cell and 5 surrounding *vsx1*$^+$ cells. For comparison across different samples, fluorescence intensity values were normalized to the peak Crx fluorescence intensity of photoreceptors from the same section.

**Comparison of apical process retraction in mitotic *Q26* cells and surrounding, post-mitotic *Q26* cells**

The retinas of *Q26*; *UAS*:memYFP transgenic zebrafish were imaged *in vivo* starting at 2 dpf. In some experiments, we counterstained embryos with the vital dye CellTrace BODIPY Texas Red methyl ester (Invitrogen) or performed the experiments in the background of *Q01* transgenic fish, both of which permit visualizing the overall retinal architecture. We determined the time interval between when *vsx1*$^+$ progenitors retracted their cytoplasmic process from the apical surface and when they underwent mitotic division. At both time-points (*i.e.* retraction of the apical process and mitotic division) the presence or absence of an apical process was scored for at least five surrounding, post-mitotic Q26 cells (see also **Figure 2D**). During the course of a time-lapse recording, increasingly more BCs became visible due to the initiation of *Q26* transgene expression in these cells. Given their proximity to the progenitor, the emerging *Q26* BCs were additionally used for quantification at the mitosis time-point.

**Quantification of interkinetic nuclear migration**

The somal movements of *vsx1*$^{+}$ progenitors and post-mitotic cells were tracked by time-lapse imaging in the *vsx1*:GFP or *Q26*; *UAS*:memYFP lines. The position of *vsx1*$^{+}$ progenitors in the unlaminated regions of the retina was determined by the ratio of the distance between the most apical part of the soma and the (emerging) IPL, and the distance between the apical surface and IPL.

$$x = \frac{distance_{soma-IPL}}{distance_{apical-IPL}}$$

The position of *vsx1*$^{+}$ progenitors in the laminated regions and their neighboring post-mitotic BCs was determined by calculating the ratio of the distance between the most apical part of the soma and the IPL, and the distance between the OPL and IPL.

$$x = \frac{distance_{soma-IPL}}{distance_{OPL-IPL}}$$

To determine an average trajectory and correct for differing imaging intervals between recordings, higher resolution recordings were down-sampled to 15 min intervals by linear interpolation.

**Cell-cycle staging based on PCNA nuclear expression pattern**

We used the nuclear expression pattern of mOrange2-labeled PCNA (mRNA-based expression construct) to determine the phase of the cell-cycle *vsx1*$^{+}$ progenitors were in (Leonhardt et al., 2000; Leung et al., 2011). We classified cells as being in the beginning of late S phase when we could unambiguously identify fluorescent granules in the nucleus. As cells progressed through late S phase, individual granules became larger but their overall number decreased. The beginning of $G_2$ phase was marked by the sudden disappearance of granules. Entry into M phase

was marked by a noticeable loss of fluorescence in the nucleus and its diffusion into the entire cell due to nuclear membrane breakdown.

**Quantification of cell-cycle delay following HUA treatment**

*Vsx1*:GFP embryos were injected at the one or two cell stage with mOrange2-PCNA mRNA and p53 morpholino. For control (non-HUA treated) fish, the interval between the beginning of late S phase and the beginning of M phase was measured ($t_{control} = t_{M\ phase} - t_{S\ phase} = 142.4 \pm 3.8$ min). This interval was also measured for HUA treated fish ($t_{HUA} = t_{M\ phase} - t_{S\ phase}$). The HUA induced delay was calculated by subtracting the average interval between late S and M phases of control fish from the observed interval for each HUA treated progenitor ($t_{delay} = t_{HUA} - t_{control}$). Since all the HUA treated progenitors we used for quantification were in late S phase, but not necessarily at the beginning of late S phase as was the case in the control group, the HUA induced delay in cell-cycle progression could be underestimated.

**Prediction of mitosis location in HUA-treated retinas**

Dr. Leanne Godinho or myself were first given time-lapse datasets of control *vsx1*:GFP progenitors (no HUA treatment) to ascertain if the location of mitosis (apical or non-apical) could be predicted well before the mitotic division actually took place. The scorers were shown images from time-points in which the progenitor cell somata were elongated and located in the INL and when the mitotic division was known to occur within the next hour. Based on the general retinal cytoarchitecture of the region in which the progenitor was located, the morphology of the progenitor and the relative levels of *vsx1*:GFP fluorescence, scorers predicted the location of division with a high degree of accuracy (19 out of 22 instances). Progenitors that were located within an unlaminated region of the retina, had a cytoplasmic attachment to the apical surface and had relatively low levels of GFP were predicted to divide at the apical surface.

Conversely, progenitors within a laminated region and relatively high levels of GFP were predicted to divide in the INL. Scorers were then given time-lapse datasets of HUA-treated *vsx1*:GFP progenitors and asked to predict whether cells would undergo mitotic division at apical or non-apical locations, using the same criteria as for the control datasets.

**Cell type classification of *Q26*$^{+}$ cells**

*Q26*$^{+}$ cells were classified as BC or AC based on neurite morphology (presence or absence respectively of an apical process) and position of the soma (lower or upper part of the INL). To obtain the AC-BC ratio of different *Q26* genotypes, a maximum intensity projection (MIP) of a few imaging planes (typically 5) was obtained, and all *Q26*$^{+}$ cells (at least 70 per retina) in the MIP were classified. *Q26*$^{+}$ divisions were classified as BC-BC, AC-BC or AC-AC based on the criteria described above. *Q26*$^{+}$ progenitors which divided close to the end of a time-lapse recording (typically less than 6 hours prior to the end of the experiment) were excluded from analysis, if their daughter cells failed to establish an unambiguous cellular morphology.

**Quantification of Kaede recovery in photo-converted *Q26*$^{+}$ cells**

A tornado scan with 405 nm laser light was used to photo-convert Kaede in a local patch of *Q26*$^{+}$ cells (the diameter of the photo-converted area was approximately equal to the apico-basal extent of the INL). After photo-conversion, fish were unmounted and kept in the dark at 28.5°C until successive imaging time-points (after 24 h and 48h). Recovery of green fluorescent Kaede protein in *Q26*$^{+}$ ACs was assessed qualitatively as present (i.e. obvious gain in the green fluorescence channel similar to the surrounding *Q26*$^{+}$ BCs) or absent (i.e. no obvious gain in the green fluorescence channel similar to the surrounding *Q26*$^{+}$ BCs).

**Quantification of Notch:reporter levels in *Q26*$^+$ cells**

Notch:reporter (Tg(T2KTp1bglob:hmgb1-mCherry)jh11) fish express nuclear-targeted mCherry fluorescent protein in response to Notch activity (Parsons et al., 2009) Notch:reporter fluorescence intensity levels were determined in *Q26*$^+$ ACs and their potential sibling BCs. If at least one of the *Q26*$^+$ cells had a fluorescence intensity level twice above the background, the cell group was used for analysis (34/77 cell groups could be used). To classify a cell group as 'AC high', 'BC high' or 'equal', the Notch:reporter levels in the *Q26*$^+$ AC were compared to the surrounding *Q26*$^+$ BC with the highest Notch:reporter levels. If the *Q26*$^+$ AC had twice the brightness of the *Q26*$^+$ BC, the group was classified as 'AC high' (AC > BC). Similarly, in cases in which the *Q26*$^+$ BC had twice the brightness of the *Q26*$^+$ AC, the group was classified as 'BC high' (AC < BC). Otherwise (i.e. no cell had at least twice the fluorescence intensity of the other) the group was classified as 'equal' (AC = BC).

**Quantification of marker expression in *Q26*$^+$ ACs**

The expression of *crx*:mCFP, *ctbp*2:GFP, *gfap*:GFP, *ptf1a*:GFP and *vsx1*:GFP in all *Q26*$^+$ ACs was determined qualitatively as expressed (i.e. the presence of a *marker*$^+$ AC could be detected independently in the image channel of the marker, or in case of *vsx1*:GFP was similar to surrounding BCs) or not expressed (i.e. the AC could not be detected in the image channel of the marker, or in case of *vsx1*:GFP was not similar to surrounding BCs).

**Quantification of DAPT treatment**

The effect of DAPT treatment was quantified in two independent quadrants of the peripheral retina of *vsx1*:GFP fish. In a given quadrant, the total number of *vsx1*:GFP$^+$ ACs (i.e. with a brightness similar to surrounding BCs; see above) were counted in 10 z-planes (i.e. 17 µm).

## 2.14. Solutions and buffers

*Danieau's solution*

| Reagent | Quantity for 1 l of 30x concentrated solution |
|---|---|
| NaCl (Sigma, S7653) | 101.7 g |
| KCl (Sigma, P9541) | 1.56 g |
| $MgSO^4*7H_2O$ (Sigma, 230391) | 2.96 g |
| $Ca(NO_3)_2$ (Sigma, 202967) | 4.25 g |
| HEPES (Sigma, H3375) | 35.75 g |
| Distilled water | Up to 1 l |
| Adjust pH to 7.6 | |

Stock stored at 4°C. Used as a 0.3x working solution.

*Tricaine (3-Aminobenzoic Acid Ethyl Ester Methanesulfonate)*

| Reagent | Quantity for 100 ml 20x concentrated stock |
|---|---|
| Tricaine (PharmaQ) | 400 mg |
| 1M Tris pH 9 | 2.1 ml |
| Distilled water | Up to 100 ml |
| Adjust pH to 7 | |

Aliquots stored at -20°C. Used at 1x working solution in 0.3x Danieau's solution.

*PTU (1-phenyl-2-thiourea)*

| Reagent | Quantity for 100 ml 50x concentrated stock |
|---|---|
| PTU (Sigma, P7629) | 152 mg |
| Distilled water | Up to 100 ml |

Aliquots stored at -20°C. Used at 1x working solution in 0.3x Danieau's solution.

*PBS*

| Reagent | Quantity for 1 l 10x concentrated solution |
|---|---|
| $KH_2PO_4$ (Sigma, P9791) | 2.4 g |
| $Na_2HPO_4*2H_2O$ (Roth, 4984.1) | 17.8 g |
| KCl (Sigma, P9541) | 2 g |
| NaCl (Sigma, S7653) | 80 g |
| Distilled water | Up to 1 l |
| Adjust pH to 7.4 | |

Stock stored at room temperature. Used as 1x working solution.

*30% Sucrose*

| Reagent | Quantity for 100 ml 1x solution |
|---|---|
| Sucrose (Roth, 4661.1) | 30 g |
| 1x PBS | Up to 100 ml |

*4% Paraformaldehyde (PFA)*

| Reagent | Quantity for 1 l 10x concentrated solution |
|---|---|
| PFA (Sigma, P6148) | 40 g |
| NaOH (Roth, KK71.1) | 125 µl |
| 10x PBS | 100 ml |
| Distilled water | Up to 1 l |

PFA, NaOH and H2O were mixed on a heating plate at 50-60°C until the solution turned clear. PBS was added and the pH adjusted to 7.2 - 7.5. After the solution was filtered, aliquots of 4% PFA were stored at -20°C.

*Sodium Citrate buffer*

| Reagent | Quantity for 1 l 1x solution |
|---|---|
| $Na_3C_6H_5O_7$ (Roth, 4088.3) | 2.94 g |
| Tween 20 (Roth 9127.1) | 500 µl |
| Distilled water | Up to 1 l |

# 3. RESULTS

## 3.1. Uncoupling of neurogenesis and differentiation during CNS development

### 3.1.1. *Vsx1*$^{+}$ progenitors undergo mitosis in different proliferative zones and match the expression of molecular markers of surrounding post-mitotic BCs

To investigate the stereotypy of the developmental program in progenitors, I aimed to study the molecularly-defined *vsx1* progenitor population and compare individual progenitors thereof at the stage of mitosis. To this end, I used a transgenic line in which *vsx1* regulatory elements, derived from a bacterial artificial chromosome (BAC), drive the expression of cytosolic GFP (*vsx1*:GFP) (Kimura et al., 2008). In the zebrafish retina, *vsx1* is reported to be expressed at low levels in the vast majority of committed BC progenitors, up-regulated during BC differentiation and maintained at high levels in the vast majority of mature BCs (Vitorino et al., 2009). To corroborate the expression dynamics of *vsx1* in progenitor cells and post-mitotic BCs, I examined *vsx1*:GFP expression along the developmental gradient of the retina in a single field of view[4]. At 2 dpf I found low levels of GFP expression in the immature, unlaminated part of the retina in which *vsx1*:GFP$^{+}$ (henceforth referred to as *vsx1*$^{+}$) cells span the entire thickness of the retinal neuroepithelium, indicative of both progenitors and post-mitotic, undifferentiated BCs (Morgan et al., 2006; Randlett et al., 2013) (**Figure 3.1 A**, 'unlaminated'). In contrast, *vsx1*$^{+}$ cells in the more mature, laminated region of the retina showed high levels of GFP expression and confined their processes to the IPL and OPL, indicative of post-mitotic, differentiated BCs (**Fig. 3.1 A**, 'laminated'). Taken together, these differences in *vsx1* expression levels and morphologies along the developmental gradient suggest that progenitors divide in the immature, unlaminated region of the retina and that subsequently neuronal differentiation takes place to form the mature, laminated retina.

[4] See also **Figure 1.2** for the developmental gradient of the retina

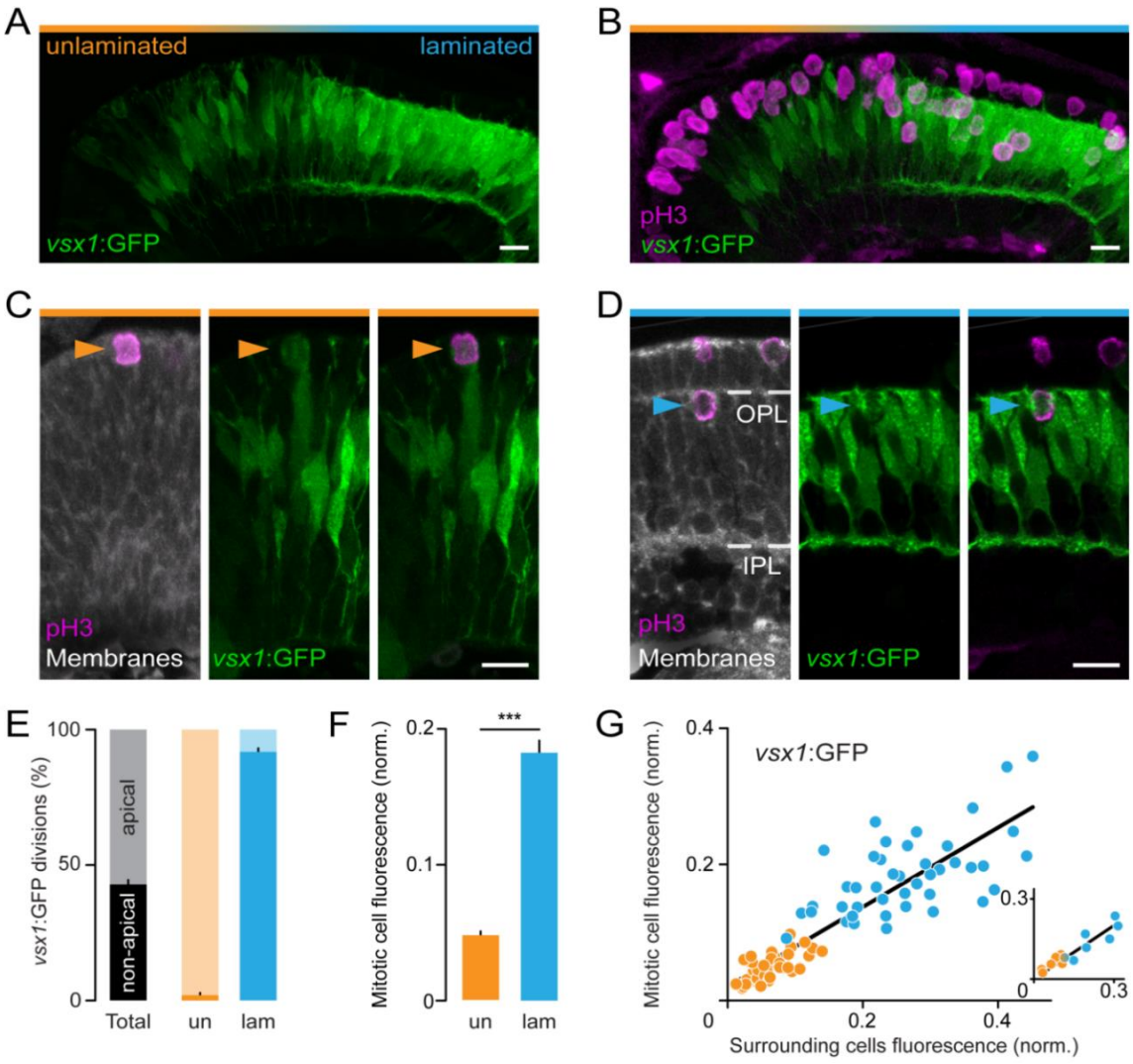


**Figure 3.1 - *Vsx1*$^+$ progenitors undergo mitosis in different proliferative zones and match *vsx1*:GFP expression of the post-mitotic BCs in their vicinity.**

**(A, B)** Confocal images of a coronal cryostat section from a 2 dpf *vsx1*:GFP retina with immature, unlaminated ('unlaminated', orange) and mature, laminated regions ('laminated', cyan). **(A)** *vsx1*:GFP; **(B)** *vsx1*:GFP shown in conjunction with pH3 antibody staining to label cells undergoing mitosis. **(C, D)** High magnification images of **(C)** an apically dividing *vsx1*$^+$ progenitor (orange arrowhead) in an unlaminated region where cells span the entire thickness of the retina and express GFP weakly and **(D)** a non-apically dividing *vsx1*$^+$ progenitor (blue arrowhead) in a laminated region where cells confine their processes to the OPL and IPL (dashed lines) and express high levels of GFP. Cellular membranes are labeled with BODIPY methyl ester in **C** and **D**. **(E)** Quantification of *vsx1*$^+$ progenitor mitoses at apical (lightly-shaded) and non-apical (darkly-shaded) locations in the unlaminated ('un', orange) and laminated ('lam', cyan) retina. 1391 mitotic divisions, 80 sections from at least 14 fish. **(F)** Quantification of *vsx1*:GFP fluorescence intensity of progenitors in the unlaminated and laminated retina. 86 progenitors, 43 sections from at least 13 eyes, $p \leq 0.0001$. **(G)** Correlation of *vsx1*:GFP fluorescence intensity in progenitors and their surrounding cells in the unlaminated (orange circles) and laminated (cyan circles) regions of the retina. 86 progenitors from 43 sections from at least 13 eyes, $r^2 = 0.78$. **Inset:** Analysis for all pH3$^+$cells (n=13) from a single section. Scale bar **A-D** 10 µm.

To my surprise, however, immunostaining of *vsx1*:GFP retinae for the mitosis marker phosphorylated histone H3 (pH3) revealed that *vsx1*$^+$ pH3$^+$ cells are not limited to the unlaminated part of the retina (**Figure 3.1 B**). In addition to the apically located *vsx1*$^+$ pH3$^+$ cells of the unlaminated retina (**Figure 3.1 C**), I also found substantial numbers of *vsx1*$^+$ pH3$^+$ cells which were located in the INL of the laminated retina (**Figure 3.1 D, E**). Thus not only post-mitotic BCs reside in the laminated regions of the retina but also BC progenitors which undergo mitoses at non-apical sites. As previous reports suggested that non-apically dividing progenitor cells can show signs of precocious neuronal differentiation (Attardo et al., 2008; Godinho et al., 2007), I next asked whether *vsx1*$^+$ progenitors in the laminated retina undergo neuronal differentiation similar to surrounding, post-mitotic BCs[5]. To this end, I first quantified GFP levels during mitotic division in *vsx1*$^+$ pH3$^+$ progenitors in the unlaminated and laminated regions of the developing retina and found a striking (3.8-fold) increase in GFP levels for progenitors dividing in the laminated part of the retina (**Figure 3.1 F**). Remarkably, when I compared individual *vsx1*$^+$ pH3$^+$ progenitors to surrounding *vsx1*$^+$ pH3$^-$ cells, I revealed a tight correlation of GFP levels in pH3$^+$ progenitors and pH3$^-$ surrounding cells across the entire developmental gradient ($r^2$= 0.78, **Fig. 3.1 G**). To corroborate this finding, I performed *in vivo* time-lapse recordings of *vsx1*:GFP retinae, in which a parallel increase of GFP levels in dividing *vsx1*$^+$ progenitors and surrounding *vsx1*$^+$ cells was observed (**Fig. 3.2**). Taken together, I found that BC progenitors do not have a single, constant level of *vsx1* promoter activity but rather that they form a large continuum in lock-step with surrounding *vsx1*$^+$ cells. Accordingly, at least with regard to *vsx1* expression, *vsx1*$^+$ progenitors of the mature retina are more similar to their post-mitotic BC neighbors than to *vsx1*$^+$ progenitors of the immature retina

[5] On average, approximately 90% of the *vsx1*$^+$ cells in the laminated retina are estimated to be post-mitotic; for calculation see **Materials and Methods.**

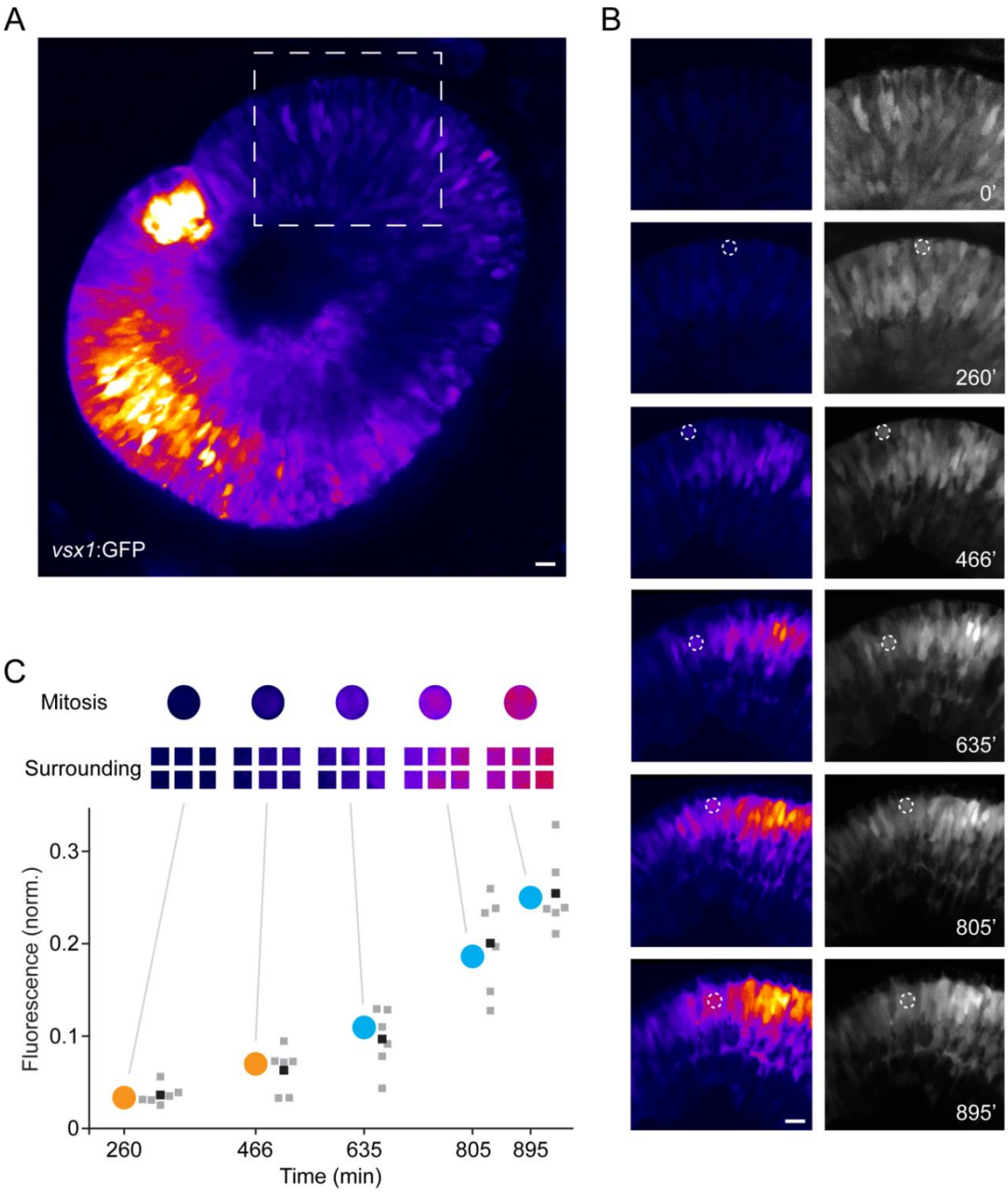


**Figure 3.2 - *In vivo* time-lapse recording of dividing BC progenitors in a *vsx1*:GFP retina.**

**(A)** Confocal *in vivo* image of a 2 dpf *vsx1*:GFP retina. Expression of GFP follows the retinal differentiation gradient, appearing first in the ventro-nasal patch and subsequently in the nasal, dorsal and temporal parts of the retina. **(B)** Time-lapse images of the boxed region in **A**. Left panels represent the raw levels of GFP fluorescence ('Fire' look-up table). Right panels depict GFP fluorescence adjusted for better visualization (grey). Dashed circles mark mitotic events. **(C)** Individual mitotic events marked in **B** at progressively later times during development. GFP fluorescence levels of the mitotic progenitors and that of 6 surrounding cells. Orange circles represent apical mitotic divisions; cyan circles represent non-apical mitotic divisions; grey squares represent individual surrounding cells; black squares represent average fluorescence of surrounding cells. Scale bar **A**, **B** 10 µm.

To further establish that the molecular differentiation of *vsx1*$^{+}$ progenitors differs profoundly between unlaminated and laminated parts of the retina but matches the differentiation state of surrounding *vsx1*$^{+}$ cells, I focused on two additional markers of BC differentiation: (1) Cone-rod homeobox (Crx) and (2) Ribeye a.

The transcription factor Crx is expressed in mature photoreceptors and BCs (Liu et al., 2001b; Shen and Raymond, 2004). In the unlaminated retina, antibody staining for Crx revealed little or no expression in *vsx1*$^{+}$ progenitors (pH3$^{+}$) and surrounding *vsx1*$^{+}$ cells (pH3$^{-}$). In the laminated retina, however, antibody staining for Crx revealed high levels of expression in *vsx1*$^{+}$ progenitors and surrounding post-mitotic *vsx1*$^{+}$ BCs (**Figure 3.3 A**). Similar to the correlation of GFP levels in *vsx1*:GFP (**Figure 3.1 F**), the intensity of Crx antibody staining in *vsx1*$^{+}$ progenitors along the differentiation gradient strongly correlated with that of the *vsx1*$^{+}$ cells in their immediate surround ($r^2$= 0.87, **Fig. 3.3 B**). Additionally, I performed time-lapse imaging recordings of a *crx*:mCFP transgenic fish line, in which I could regularly observe non-apically dividing *crx*:mCFP$^{+}$ progenitors in the laminated part of the retina (n = 97 divisions in 4 fish), **Figure 3.3 C, D**).

Finally, I analyzed the expression of Ribeye a, a structural protein of ribbon synapses in PRs and BCs (Wan et al., 2005). As expected, *ribeye a* mRNA was not present in the unlaminated retina, suggesting that both *vsx1*$^{+}$ progenitors and post-mitotic, undifferentiated BCs in the immature retina do not express *ribeye a*. In contrast, *ribeye a* mRNA was found in pH3$^{+}$ and pH3$^{-}$ cells located in the INL of the laminated retina, suggesting that both *vsx1*$^{+}$ progenitors and post-mitotic, differentiating BCs in the mature retina express *ribeye a* (**Figure 3.4 A, B**). Using *ctbp2*:mGFP (Odermatt et al., 2012), a stable transgenic line designed to report *ribeye a* expression in BCs, I observed little or no fluorescence in the unlaminated retina, but prominent expression in BCs in the laminated retina (**Figure 3.4 A**). In time-lapse recordings, I could

regularly observe *ctbp2*:mGFP$^{+}$ cells dividing at non-apical locations, giving rise to BCs (n = 87 divisions in 2 fish, **Figure 3.4 C**). Hence, even with regard to a marker linked to synaptic structures, I revealed that BC progenitors co-differentiate with post-mitotic BCs in the surround.

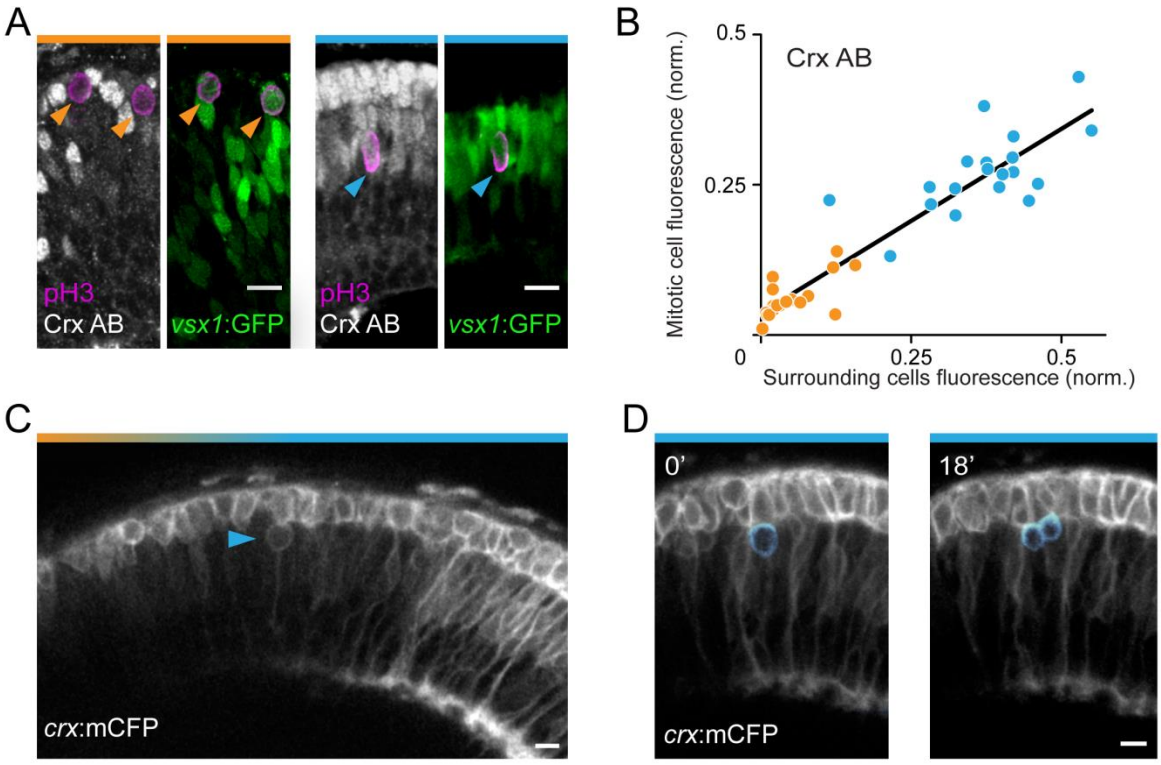


**Figure 3.3 - BC progenitors dividing in the laminated retina express Crx.**

(**A**) Confocal images of a coronal cryostat section from a 2 dpf *vsx1*:GFP retina immunostained with antibodies against pH3 and Crx. *Vsx1*$^{+}$ progenitors (GFP$^{+}$ pH3$^{+}$) are Crx negative (orange arrowheads) in the unlaminated retina (left panels), and are Crx positive (cyan arrowhead) in the laminated retina (right panels). (**B**) Correlation of Crx antibody staining intensity between mitotic *vsx1*$^{+}$ progenitors and surrounding *vsx1*$^{+}$ cells. 38 progenitors, 10 sections from at least 5 eyes, $r^2$= 0.87; orange circles represent apical mitoses, cyan circles represent non-apical mitoses. (C) *In vivo* image of a 2 dpf *crx*:mCFP retina. Expression of mCFP in the INL is largely limited to the 'laminated' region (blue bar above the figure panel) of the retina while only photoreceptors are labeled in the unlaminated parts of the retina (orange bar above panel). One mitotic *crx*:mCFP$^{+}$ progenitor (arrowhead) can be seen in the laminated region, which expresses *crx* stronger than surrounding BCs. (**D**) *In vivo* time-lapse of a *crx*:mCFP$^{+}$ progenitor undergoing mitotic division (pseudo-colored cyan) in the INL of a 2 dpf embryo. 97 such divisions were observed in 4 time-lapse recordings of a total of 32.1 h. Scale bar **A, C, D**, 10 µm.

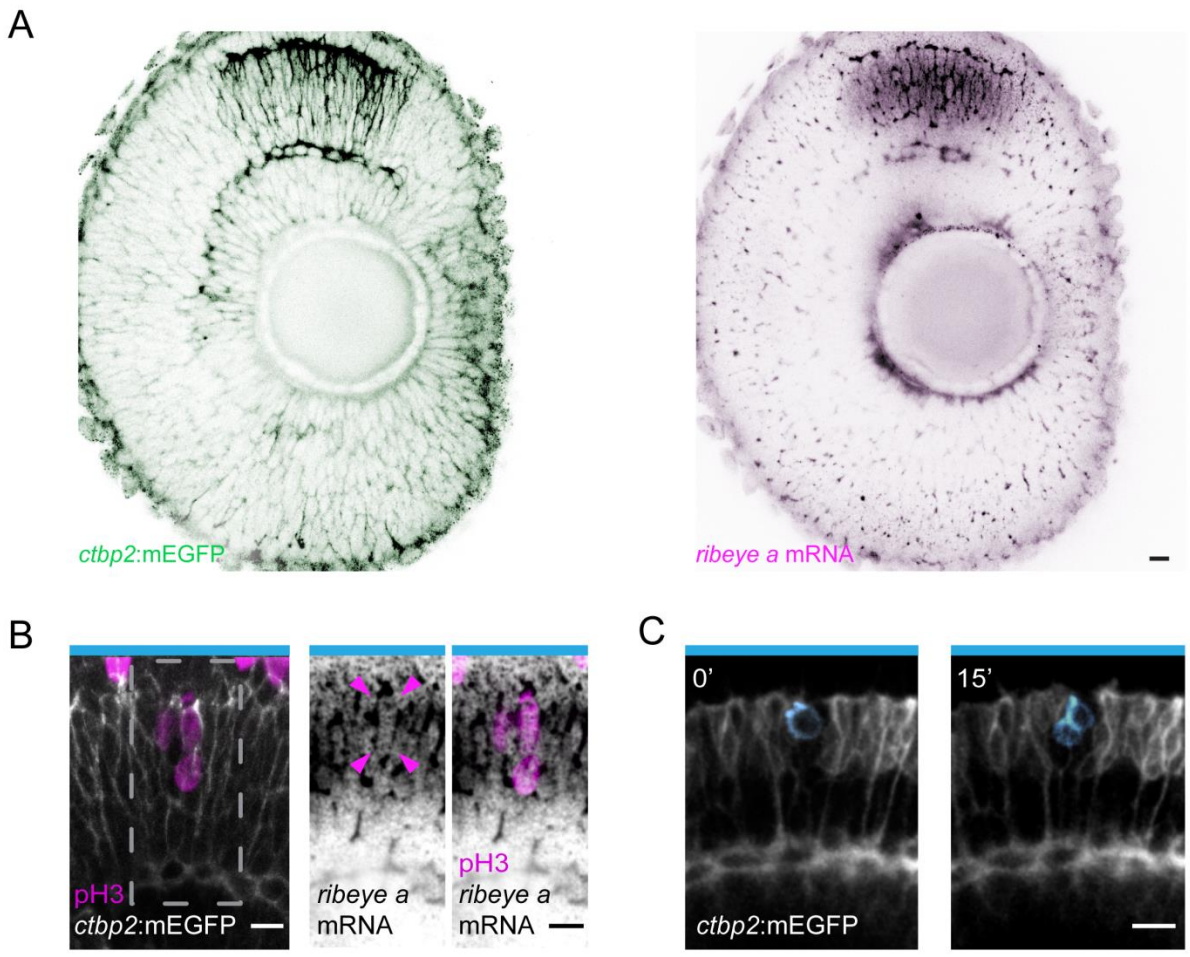


**Figure 3.4 - BC progenitors dividing in the laminated retina express *ribeye a.***

(**A)** Contrast inverted confocal images of an eye from a 2 dpf *ctbp2*:mGFP transgenic fish immunostained to visualize GFP (**left panel**) and processed for fluorescence *in situ* hybridization to detect expression of a *ribeye a* specific exon (**right panel**). (**B**) Confocal images of a 2 dpf *ctbp2*:mGFP retina labeled to detect GFP, pH3 and *ribeye a* mRNA. A *ribeye a*$^{+}$ pH3$^{+}$ non-apically dividing progenitor (magenta arrowheads, **middle panel**) can be seen in a laminated region of the retina (blue bars above panels). (**C**) *ctbp2*:mGFP$^{+}$ progenitor cell undergoing mitotic division (pseudo-colored cyan) in the INL during an *in vivo* time-lapse recording of a 2 dpf retina. 87 such divisions were observed in 2 time-lapse recordings totaling 32.8 h. Scale bar **A-C**, 10 µm.

### 3.1.2. Progenitor morphology and cell biology correspond to the surrounding post-mitotic bipolar cells

I next asked whether the similarity of *vsx1*$^{+}$ progenitors and surrounding (post-mitotic) cells extended beyond molecular markers to cellular morphology and kinetics. To be able to unambiguously study the developmental trajectory of individual *vsx1*$^{+}$ progenitors *in vivo* by time-lapse imaging, I used a transgenic *Gal4*-driver line (referred to as *Q26*) which uses a 3.2 kb fragment upstream of the *vsx1* gene as a promoter element (unpublished line, provided by Drs. S. Suzuki and T. Yoshimatsu, University of Washington, USA). *Q26* drives *Gal4* expression in a subset of *vsx1*$^{+}$ cells and thus allows for labeling of individual *vsx1*$^{+}$ progenitors and post-mitotic BCs if crossed to a *UAS*:XFP reporter fish. Since expression in *Q26* is virtually only present in the mature part of the retina, the vast majority of progenitor cell divisions occurred in the laminated retina at non-apical locations (**Figure 3.5**).

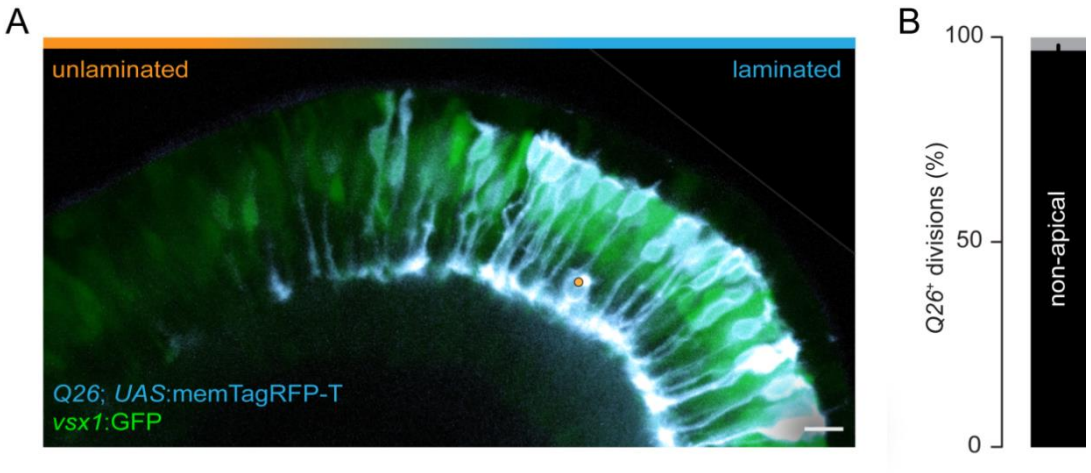


**Figure 3.5 - Characterization of BC subset transgenic line *Q26*.**

(**A**) Confocal *in vivo* image of a 2 dpf retina from a *vsx1*:GFP; *Q26*; *UAS*:memTagRFP-T compound transgenic fish. *Q26* drives transgene expression in BCs later than *vsx1*:GFP. Expression of *Q26* is initiated in the intermediate region between unlaminated (orange bar over panel) and laminated (cyan bar) parts of the retina and becomes robust in the laminated region. In addition to BCs, a single AC is labeled in the field of view (orange dot). The *Q26*$^{+}$ AC is *vsx1*:GFP negative. Scale bar 10 µm. (**B**) Quantification of the percentage of *Q26*$^{+}$ progenitor divisions occurring during *in vivo* time lapse recordings at apical (grey) and non-apical (black) locations. 158 progenitors, 20 fish.

The vast majority of non-apically dividing *Q26*$^{+}$ progenitor cells had confined their cytoplasmic processes to the OPL and IPL during mitosis (97.1 ± 1.5%; **Figure 3.6 A**, **B**), as is characteristic for post-mitotic, differentiated BCs of the mouse and zebrafish retina (Morgan et al., 2006; Randlett et al., 2013). None of the non-apically dividing *Q26*$^{+}$ progenitor cells spanned the entire thickness of the retina during mitosis, as is the case for progenitors undergoing mitosis at the apical surface (Das et al., 2003; Miyata et al., 2004; Noctor et al., 2004). Prior to mitotic division, however, the cytoplasmic processes of non-apically dividing progenitors are not limited to the OPL and IPL (**Figure 3.6 A** at -89'). Therefore, I asked whether the remodeling of the cytoplasmic processes to the synaptic layers occurs in a fixed time-window in relation to mitotic division. When I focused my analysis, for technical reasons[6], on the retraction of the apical process, I found that its remodeling to the OPL occurred over an extended period of time prior to mitotic division (18 min to > 9 h, **Figure 3.6 C**). In contrast, for apically dividing BC progenitors of the unlaminated retina, the remodeling of the apical process to the OPL was a post-mitotic event which similarly occurred over an extended period of time following mitotic division (a few min to > 8 h). Thus, a single differentiation step, the remodeling of the apical process to the OPL, can occur either pre- or post-mitotically, with a time span of more than 17 hours relative to mitosis. Notably however, time-lapse recordings suggested that apical process remodeling is locally coordinated. When I identified *Q26*$^{+}$ progenitors that had just confined their apical process to the OPL and asked whether post-mitotic BCs in the immediate vicinity had also done the same (**Figure 3.6 D**), I found that on the population level apical process remodeling occurred concurrently (**Figure 3.6 E**)[7]. Moreover, once confined to the OPL and IPL, the apical and basal

[6] I did not quantify the retraction of the basal process, as this event was only observable for 3/122 *Q26*$^{+}$ progenitors.

[7] Since whether an individual BC has an apical process or not is a binary event, the statistics of process retraction can be described by a Bernoulli distribution. Accordingly, in case of concurrent remodeling, ~50% of the BCs surrounding a progenitor cell should have an apical process.

processes of *Q26*$^{+}$ progenitors could form prominent arborizations. These arbors were transient (*i.e.* they were lost prior to mitosis), but were indistinguishable from the dendritic and axonal arborizations formed by the surrounding post-mitotic nascent BCs (**Figure 3.7 B** and **3.9 C**).

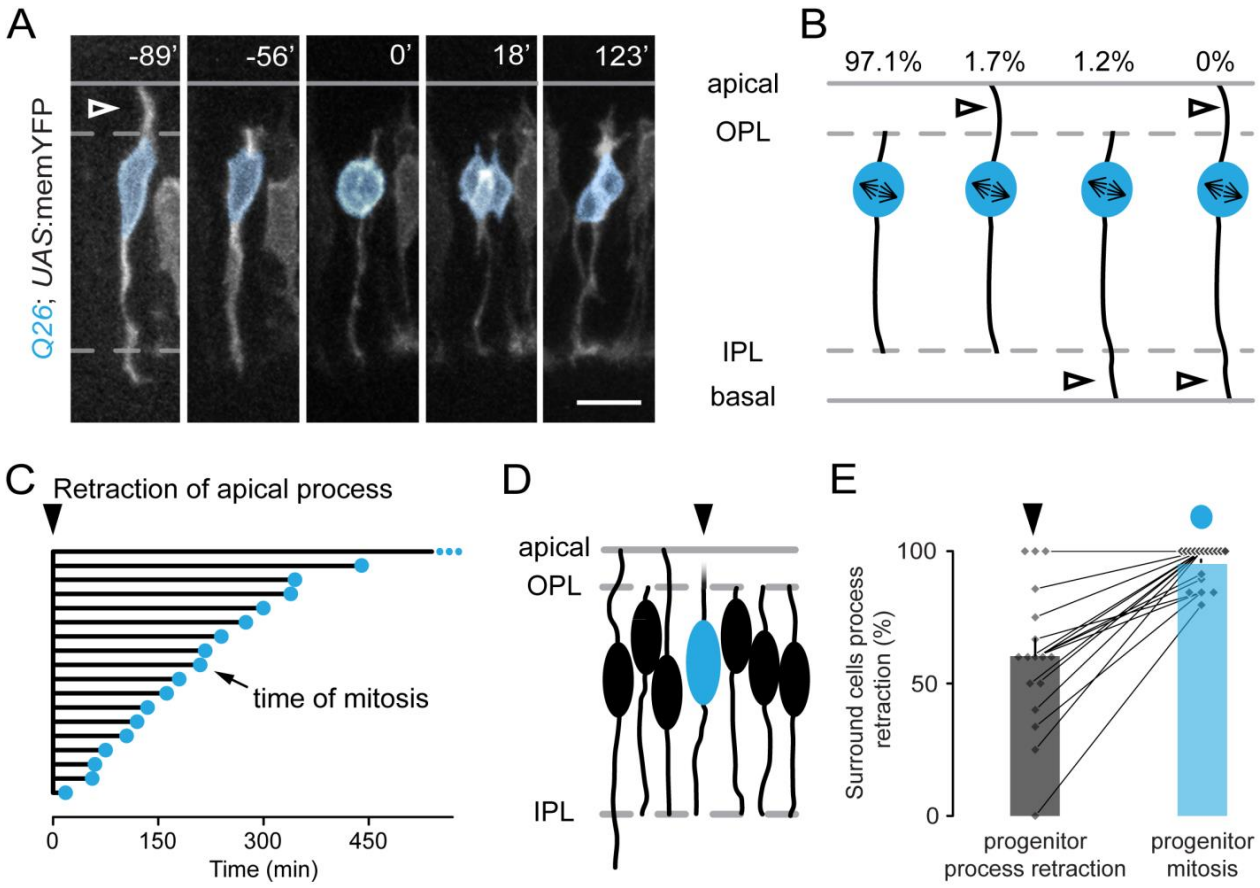


**Figure 3.6 - Morphological rearrangement of *vsx1*$^{+}$ progenitors matches surrounding BCs.**

(**A**) Confocal *in vivo* time-lapse recording of a retina (*Q26*; *UAS*:memYFP) showing a non-apically dividing *vsx1*$^{+}$ progenitor (pseudo-colored cyan) with processes restricted to the OPL and IPL (dashed lines) during mitosis (0'). The last time-point at which an apical process (open arrowhead) is detected is 89 min prior to mitosis. (**B**) Quantification of the distinct morphologies adopted by non-apically dividing *vsx1*$^{+}$ progenitors at mitosis entry (122 progenitors, 17 fish). Open arrowheads indicate cytoplasmic processes extending beyond the synaptic layers (OPL and IPL, dashed lines). (**C**) Quantification of the time interval between retraction of the apical process (triangle) and mitosis (cyan circle) of non-apically dividing *vsx1*$^{+}$ progenitors shows a range from 18 min to more than 540 min. As only mitosis, but not process retraction was observed for the progenitor depicted with small cyan dots, 540 min is the lowest estimate. 18 progenitors from 11 fish. (**D**) Schematic of apical process retraction (triangle) in a non-apical *vsx1*$^{+}$ progenitor (cyan soma) and the presence or absence of apical processes in the surrounding BCs. (**E**) Quantification of the percentage of surrounding BCs without an apical process at the time when pre-mitotic *vsx1*$^{+}$ progenitors undergo apical process retraction (triangle, 60.3 ± 6.6%) and at the time when these progenitors undergo mitosis (cyan circle, 95.1 ± 1.7%). 17 progenitors, 10 fish. Scale bar in A 10 µm.

Next, I examined whether *vsx1*$^{+}$ progenitors undergo interkinetic nuclear migration (IKNM), an oscillatory movement linked to specific cell-cycle phases (Baye and Link, 2007; Sauer, 1935) (see also **Figure 1.7**). To concurrently monitor the nuclear movements and cell-cycle phase of *vsx1*$^{+}$ progenitors, I generated an mRNA construct based on mOrange2-tagged proliferating nuclear antigen (PCNA). Cells expressing fluorescently-tagged PCNA display distinct nuclear localization patterns during the cell-cycle, thus making it possible to unequivocally follow the cell-cycle status of progenitors by time-lapse imaging (Leonhardt et al., 2000; Leung et al., 2011). *Vsx1*$^{+}$ progenitors dividing in the unlaminated region of the retina showed rapid apically-directed nuclear movement during the $G_2$-phase before undergoing mitosis at the apical surface (**Figure 3.7 A** and **3.8 A**), as is characteristic for classical (apical) progenitors (see also **Figure 1.7**). In contrast, this rapid apically-directed movement during $G_2$-phase was absent in *vsx1*$^{+}$ progenitors in the laminated region of the retina. Here, the nuclei of *vsx1*$^{+}$ progenitors were located in the outer part of the INL and showed little movement through S- and $G_2$-phase of the cell-cycle (**Figure 3.7 B** and **3.8 B**), as is also characteristic for post-mitotic BCs.

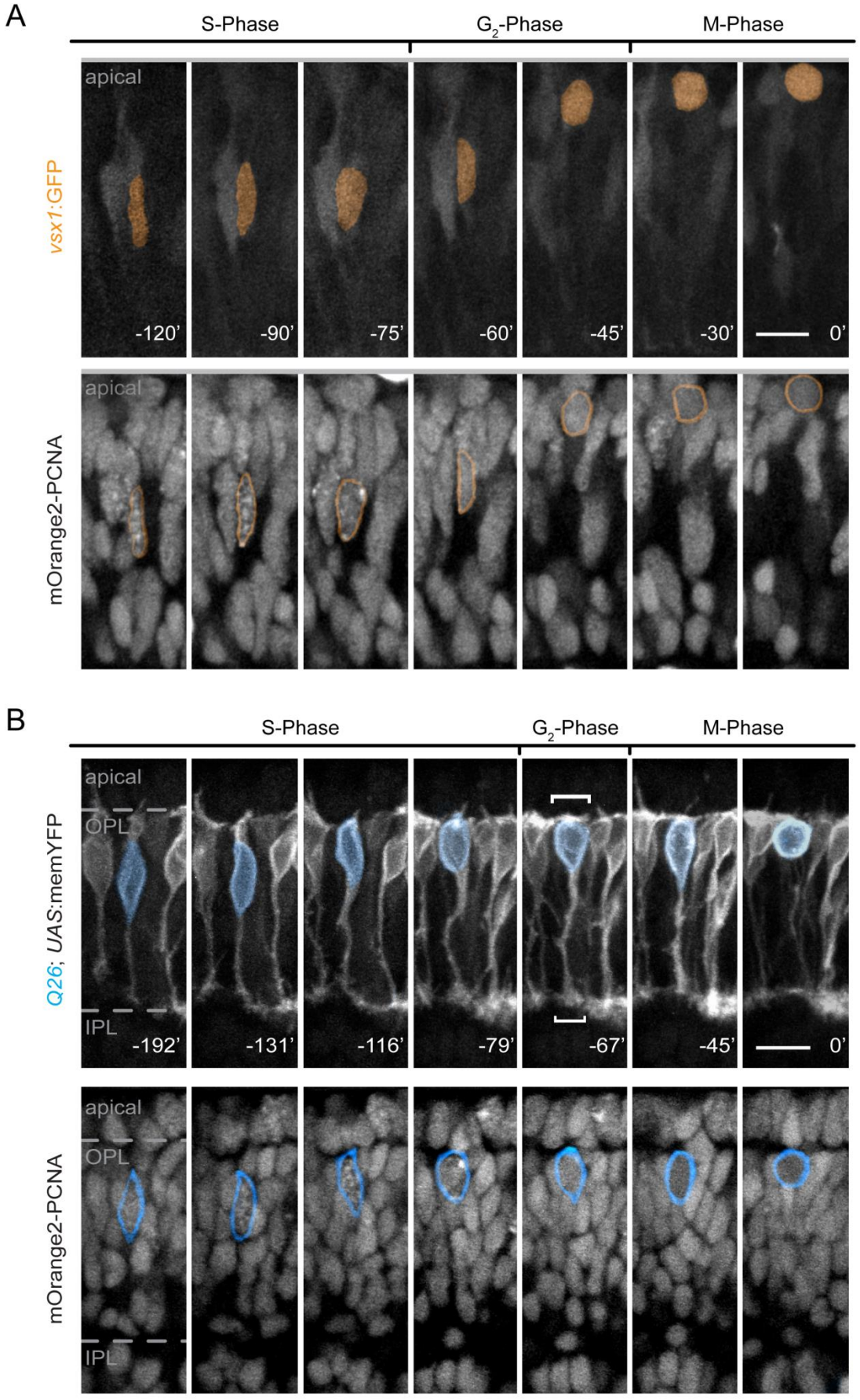
A
S-Phase
G2-Phase
M-Phase
vsx1:GFP
mOrange2-PCNA
apical
-120'
-90'
-75'
-60'
-45'
-30'
0'
B
S-Phase
G2-Phase
M-Phase
Q26; UAS:memYFP
mOrange2-PCNA
apical
OPL
IPL
-192'
-131'
-116'
-79'
-67'
-45'
0'

**Figure 3.7 – Distinct nucleokinesis of BC progenitors in the unlaminated and laminated retina.**

**(A)** *In vivo* confocal time-lapse recording of a 2 dpf *vsx1*:GFP retina (**upper panels**) expressing *mOrange2-PCNA* mRNA (**lower panels**). A *vsx1*$^+$ progenitor cell (pseudo-colored orange) is located in the middle of the retinal neuroepithelium and displays little movement during S-phase (granular nuclear pattern of PCNA**, bottom panels**). As it enters $G_2$-phase (disappearance of granular nuclear pattern, **bottom panels**), the *vsx1*$^+$ soma moves rapidly toward the apical surface to undergo mitosis at this location (0'). **(B)** *In vivo* confocal time-lapse recording of a 2 dpf *Q26*; *UAS*:memYFP retina (**upper panels**) expressing *mOrange2-PCNA* mRNA (**lower panels**). A *Q26*$^+$ progenitor cell (outlined in cyan) located in the INL displays little movement during S-phase (granular nuclear pattern of PCNA**, bottom panels**) and $G_2$-phase (disappearance of granular nuclear pattern, **bottom panels**). Prior to undergoing mitosis at the OPL, the *Q26*$^+$ progenitor cell shows transient lateral arborizations in the synaptic layers as wide as its soma (see brackets at -67'). Scale bar 10 µm.

Accordingly, analysis of nuclear movements in the laminated retina revealed largely indistinguishable migratory tracks for *vsx1*$^+$ progenitors and their surrounding post-mitotic BCs (**Figure 3.8 B**). However, close inspection of individual migratory tracks revealed one key difference: In contrast to the post-mitotic BCs, the non-apically dividing *vsx1*$^+$ progenitors always translocated their nuclei to the OPL prior to mitosis.

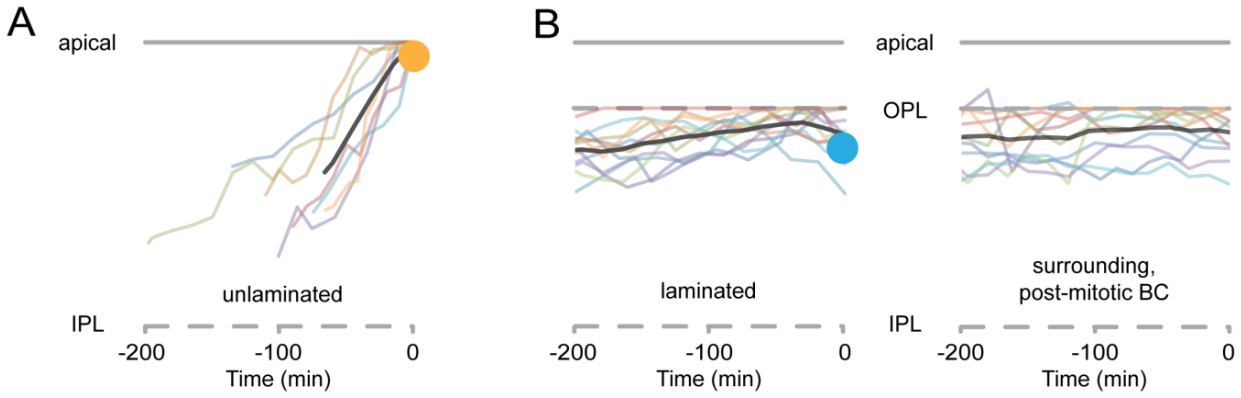


**Figure 3.8 – Nucleokinesis of *vsx1*$^+$ progenitors and nascent BCs.**

(**A**) Nuclear movement of *vsx1*$^+$ progenitors in the unlaminated region (*vsx1*:GFP) of the retina prior to mitosis at the apical surface (orange circle). 7 cells, 5 fish. (**B**) Nuclear trajectories of *vsx1*$^+$ progenitors in the laminated region that undergo mitosis next to the OPL (cyan circle, left panel) and post-mitotic BCs in their vicinity (right panel). 13 progenitors and 13 post-mitotic BCs, 5 fish. Black lines represent the average position of all *vsx1*$^+$ progenitors prior to mitosis in unlaminated (**A**) and laminated regions (**B**, **left panel**) and of the post-mitotic BCs (**B**, **right panel**).

As progenitors are known to translocate towards the centrosome during mitosis, I next aimed to concurrently monitor centrosome localization and nuclear movements of non-apically dividing progenitors. By expressing fluorescently-tagged centrin4, I found that centrosomes of post-mitotic BCs actively relocated from the apical surface to the OPL, resulting in a dendritic, rather than a somatic location at maturity (**Figure 3.9 A**, **B**). Similar to apical process retraction, centrosome relocation occurred at the same time for progenitors and surrounding, post-mitotic BCs (**Figure 3.9 C**). Thus, nucleokinesis and centrosome relocation represent further differentiation steps for which *vsx1*$^{+}$ progenitors are time-locked to their post-mitotic neighbors.

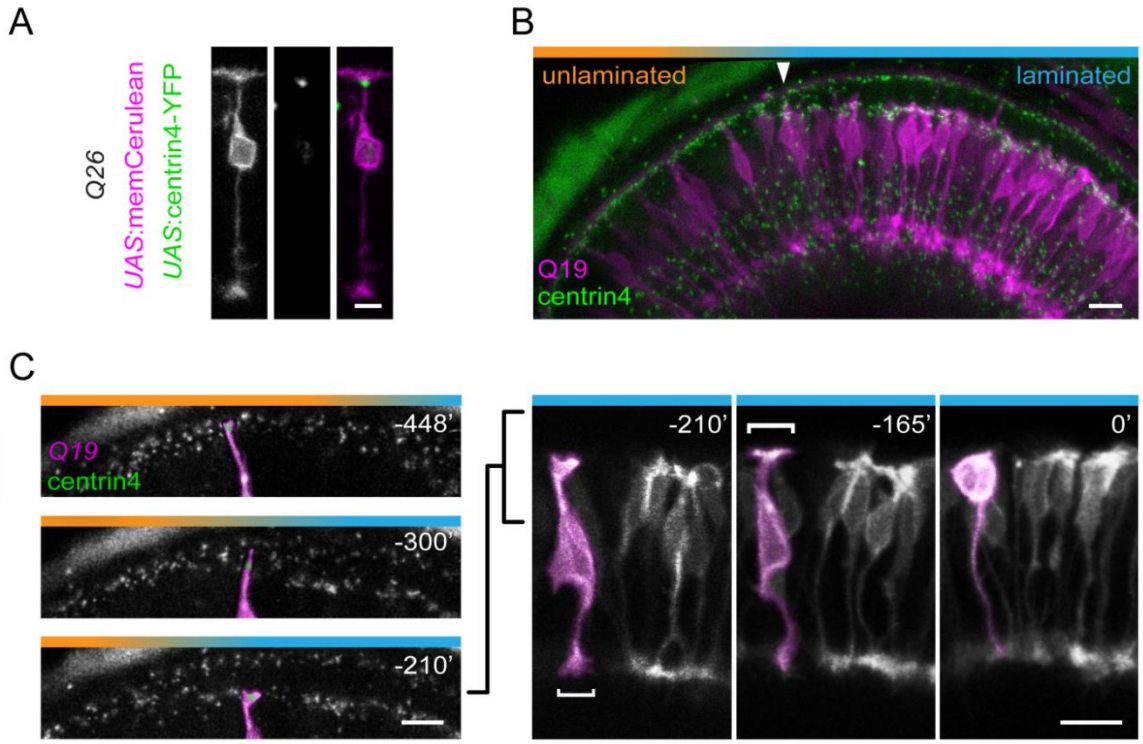


**Figure 3.9 – Centrosome dynamics in non-apically dividing *vsx1*$^{+}$ progenitors and post-mitotic BCs.**

(**A**) Confocal *in vivo* images of a 3 dpf retina (*Q26* injected with *UAS*:centrin4-YFP/*UAS*:memCerulean plasmid), in which the cellular membranes and centrosome of a single BC are labeled. The centrosome localizes to the dendritic tuft of the BC. (**B**) Confocal *in vivo* images of a 2 dpf retina, in which centrosomes (*centrin4-YFP* mRNA, green) and a subset of BCs (*Q19*, magenta) are labeled. The relocation of BC centrosomes from the apical surface to the OPL coincides with the retraction of the apical process (arrowhead). (**C**) Centrosomes (*centrin4-YFP* mRNA, grayscale) of a *vsx1*$^{+}$ progenitor (magenta mask, Q19) and post-mitotic BCs in the laminated region concurrently translocate to the OPL. The centrosome of the highlighted *vsx1*$^{+}$ progenitor is pseudo-colored green. The *vsx1*$^{+}$ progenitor shows transient lateral arborizations (see brackets at -210', -165'). Scale bar **A** 5 µm; **B, C** 10 µm.

### 3.1.3. The neurogenesis and differentiation programs of *vsx1*$^{+}$ progenitors are independent of each other

Taken together, my experiments established that along the developmental gradient of the retina, *vsx1*$^{+}$ progenitors blend into the differentiation landscape of surrounding BCs with regard to their morphological, cell biological and molecular characteristics. Two potential scenarios could account for this finding: (1) Multiple, 'fixed' *vsx1*$^{+}$ progenitors could exist, each of which undergoes mitosis at a stereotypic time-point in the cell's differentiation trajectory. (2) Alternatively, neurogenesis and differentiation could be uncoupled of each other, so that mitotic divisions could occur at various points in a cell's developmental trajectory. To distinguish between these two possibilities, I delayed *vsx1*$^{+}$ progenitor divisions by inhibiting DNA synthesis during S-phase with hydroxyurea and aphidicolin (HUA) (Harris and Hartenstein, 1991).

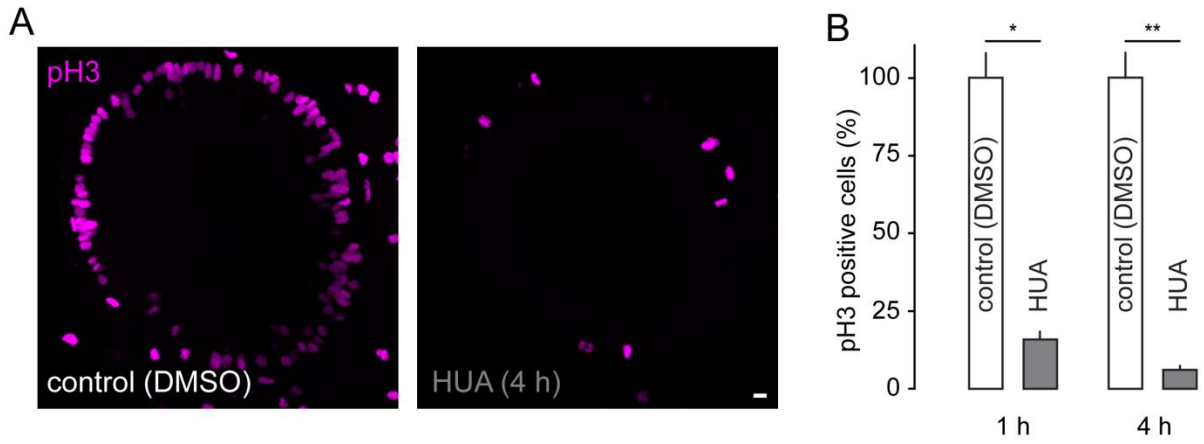


**Figure 3.10 – HUA rapidly inhibits progenitor cell mitosis.**

**(A)** Confocal images of the retina of pH3 immunostained whole-mount embryos in control conditions (DMSO, **left panel**) and following the administration of HUA for 4 h (**right panel**). Scale bar 10 µm. **(B)** Quantification of pH3$^{+}$ cells in control retinas (DMSO), and retinas treated for 1 or 4 h with HUA prior to fixation. A significant reduction in the number of cells undergoing mitosis was observed following HUA treatment (reduction to 15.9 ± 2.5% after 1 h HUA, p = 0.0121, 5 fish; 6.1 ± 1.3% after 4 h HUA, p = 0.0027, 10 fish). Abbreviation: hydroxyurea and aphidicolin (HUA).

HUA treatment rapidly reduced the number of cells entering mitosis (**Figure 3.10)**, but a small number of progenitor cells continued to divide albeit with a prominent delay[8]. I could now ask whether during delayed progenitor cell mitosis, differentiation stalled (as predicted by the 'fixed' progenitor scenario) or whether it continued and remained in synchrony with surrounding post-mitotic BC differentiation (as predicted by the 'uncoupling' scenario; **Figure 3.11**).

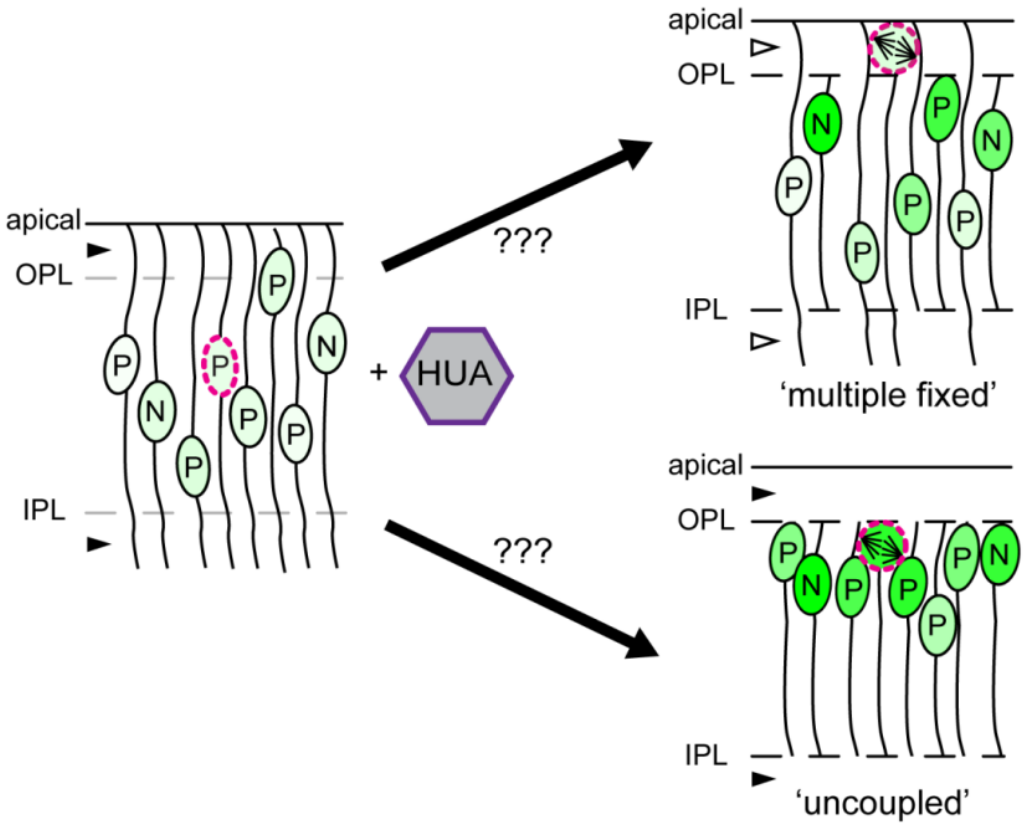


**Figure 3.11 – Potential phenotypes of *vsx1*$^{+}$ cells after HUA treatment.**

(A) Schematic representation of expected outcomes if the immature retina is treated with HUA to delay the cell-cycle. Upper panel: If there are multiple 'fixed' progenitors, a block of cell division should stall progenitors at the differentiation state in which they normally would have undergone mitosis. The result would be a 'salt-and-pepper' pattern of undifferentiated (light green) and differentiating progenitors (dark green). Lower panel: If cell-cycle and differentiation are independent, all progenitors should homogenously differentiate. Open arrowheads indicate cytoplasmic processes not confined to the OPL and IPL, filled arrowheads indicate cytoplasmic processes confined to the synaptic layers. Abbreviations: progenitor cell (P), neuron (N), hydroxyurea and aphidicolin (HUA).

[8] A detailed explanation of how I calculated the delay for individual *vsx1*$^{+}$ progenitor cell division follows in **Figure 3.12**

I tracked 10 *vsx1*$^{+}$ progenitors in HUA-treated embryos from late S-phase until mitosis. Knowing that progenitors in control experiments divided with an average of 142 ± 3.9 min after the onset of late S-phase, I could determine when a HUA-treated cell should have divided ('expected' mitosis) and measured the delay with which the division actually occurred ('observed' mitosis, delay range approximately 3.5 to 9 h; **Figure 3.12** and **3.13 A**).

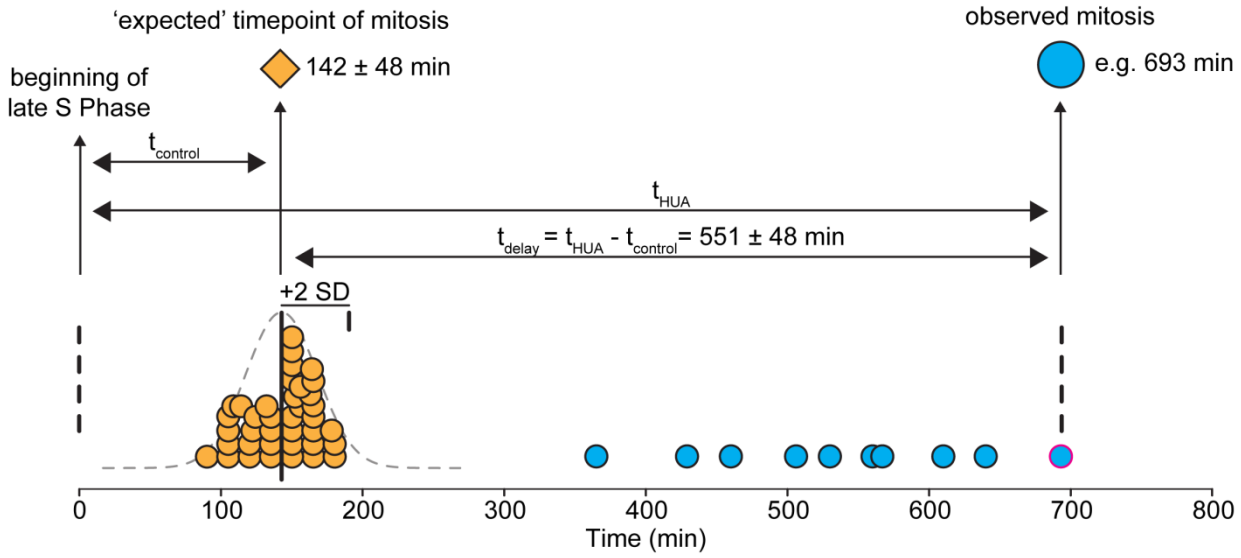


**Figure 3.12 – Calculation of HUA-induced mitosis delay in individual *vsx1*$^{+}$ progenitors.**

Time-lapse imaging of *vsx1*:GFP retinae expressing mOrange2-PCNA was used to determine the time interval between the beginning of late S-phase and the beginning of M-phase for progenitors. In control fish the average time for this interval was 142 ± 48 min (mean ± 2 standard deviations, SD, 38 cells from 6 fish, orange circles represent single cells). HUA treated progenitors were significantly delayed compared to controls, with an average time interval of 534 ± 32 min (10 cells from 4 fish, $p < 0.0001$, blue circles). The delay with which each of the 10 HUA-treated progenitors entered mitosis was calculated by subtracting the average 'expected' time interval between S- and M-phase (obtained from control cells, orange diamond) from the observed time interval between S- and M-phase for each HUA-treated progenitor (blue circles). An example for this calculation is shown for a progenitor which divides with a calculated delay of 551 ± 48 min.

Because we[9] could predict with a high degree of accuracy (86.4%), whether progenitor cells, in control conditions, would undergo mitosis at the apical surface or in the INL (i.e. at non-apical location) well before the divisions occurred (see **Materials and Methods**), we could ask whether the HUA-induced delay of mitosis would shift divisions from apical to non-apical locations. Nine of the 10 HUA treated *vsx1*$^{+}$ progenitors fulfilled criteria that identified them to be destined to divide apically. However, all 10 *vsx1*$^{+}$ progenitors instead underwent mitosis in the INL after process remodeling, suggesting that they had been shifted from an apical to a non-apical phenotype simply by delaying mitosis (**Figure 3.13 B**). Furthermore, *vsx1*:GFP expression levels in the 10 delayed *vsx1*$^{+}$ progenitors increased from the point of expected mitosis to observed mitosis (**Figure 3.13 A, C**). Importantly, even after hours of delayed mitosis, progenitors still matched the fluorescence levels of BCs in their immediate surround (**Figure 3.13 D**). Accordingly, these findings support the 'uncoupling' scenario laid out above and thus argue for the independence of neurogenesis and differentiation programs during BC development.

[9] My supervisor Dr. Leanne Godinho and myself

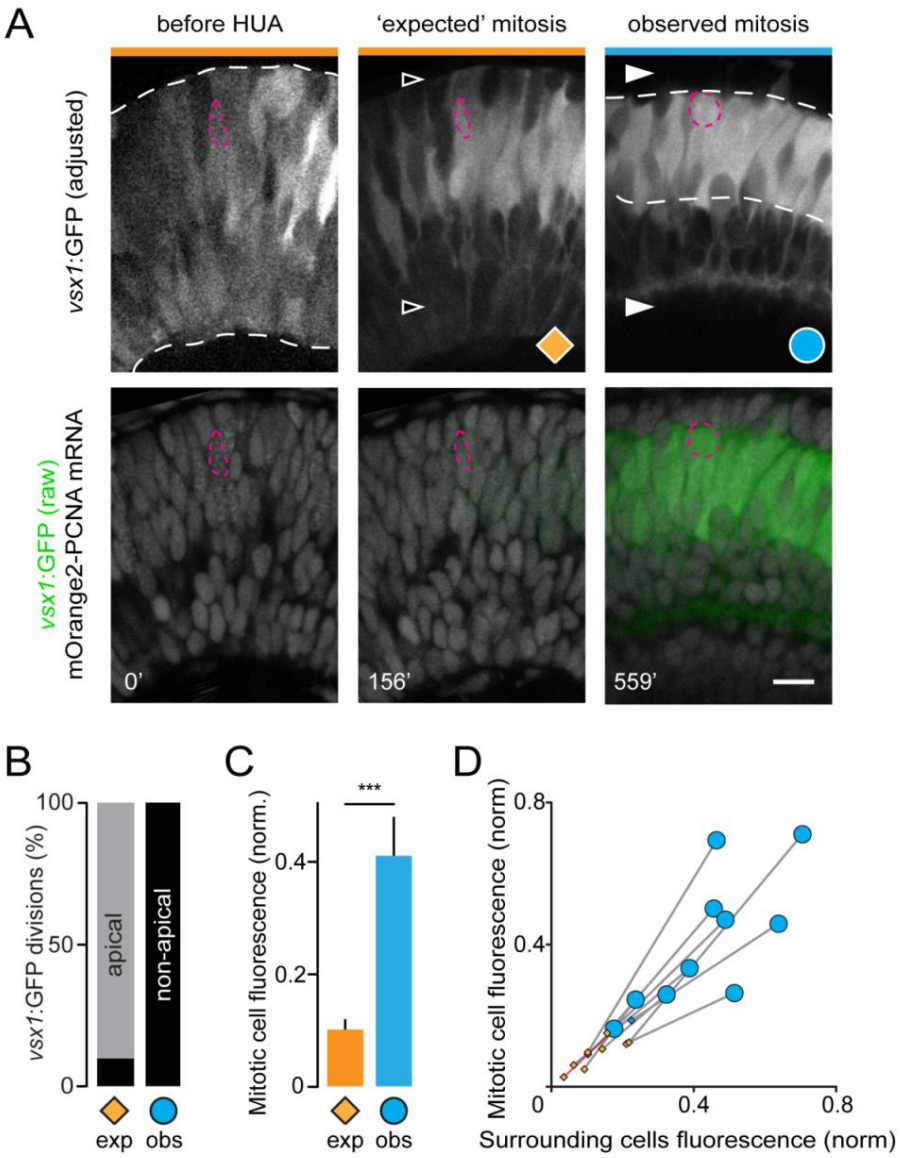


**Figure 3.13 – Neurogenesis and differentiation of *vsx1*$^+$ progenitors are independent of each other**.

(**A**) Confocal images of a 2 dpf retina from a *vsx1*:GFP and mOrange2-PCNA mRNA retina. A *vsx1*$^+$ progenitor (dashed magenta outline) is shown before HUA treatment (left panel), at the time when it would have been 'expected' to undergo mitosis (middle panel, orange diamond) and when it actually underwent mitosis (right panel, cyan circle). The retina and the vsx1+ progenitor continue to mature after the 'expected' mitosis (retraction of cytoplasmic processes, mitosis at non-apical location and up-regulation of GFP). Open arrowheads indicate cytoplasmic processes not confined to the synaptic layers, filled arrowheads indicate cytoplasmic processes confined to the synaptic layers. Dashed lines indicate extent of *vsx1*$^+$ cell somata across retinal thickness. Scale bar 10 µm. (**B**) Progenitors that were expected to divide at the apical surface (exp), divided non-apically (obs). 10 progenitors, 4 fish. (**C**) Quantification of *vsx1*:GFP fluorescence intensity of progenitors at the time when they were expected to undergo mitosis (exp) and when they underwent mitotic division (obs). 10 progenitors, 4 fish, p = 0.0002. (**D**) The fluorescence intensity of HUA-treated *vsx1*:GFP progenitors at the time when they were expected to undergo mitosis (diamonds), and when they were underwent mitosis (circles), plotted against the intensity of the surrounding cells (10 progenitors, 4 fish).

## 3.2. Re-specification of neuronal identity during CNS development

### 3.2.1. *Vsx1*$^{+}$ progenitor cells can undergo terminal, asymmetric division to generate an AC-BC pair

So far, my experiments were limited to the (non-)stereotypy of *vsx1*$^{+}$ progenitors during retinal development. To ask whether some sort of plasticity could also be found in post-mitotic *vsx1*$^{+}$ cells, I followed the daughter cells of *vsx1*$^{+}$ progenitor divisions by time lapse recordings of *Q26*; *UAS*:memYFP retinae [henceforth referred to as *Q26* wt (wildtype)]. As expected from previous publications (He et al., 2012; Vitorino et al., 2009), I found that *Q26*$^{+}$ progenitors can undergo terminal, symmetric divisions to generate two BCs (54.2 ± 5.7% of all mitotic divisions in *Q26* wt, 141 mitotic divisions, 17 fish; see also **Figure 3.6 A**). To my surprise, however, I found that *Q26*$^{+}$ progenitors can also undergo terminal, asymmetric divisions to generate an AC-BC pair (44.4 ±5.6% of all mitotic divisions in *Q26* wt*;* **Figure 3.14**).

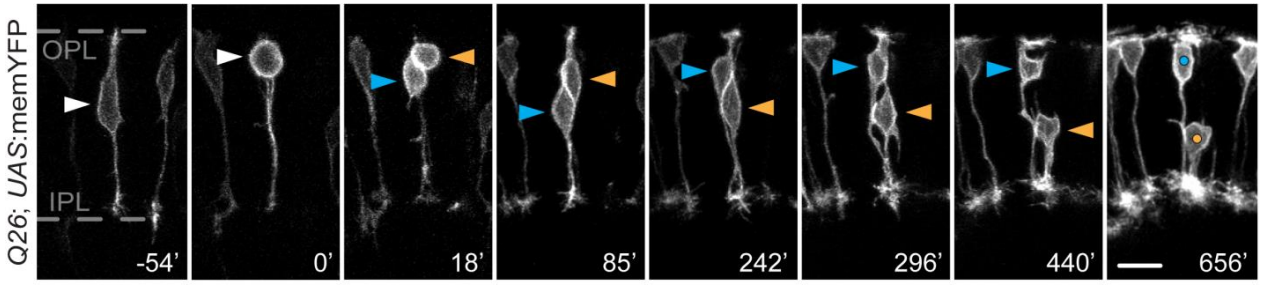


**Figure 3.14 – *In vivo* time-lapse imaging of an AC-BC division of a non-apically dividing *Q26*$^{+}$ progenitor**.

Confocal *in vivo* time-lapse recording of a 2 dpf retina (*Q26; UAS*:memYFP) showing a non-apically dividing *Q26*$^{+}$ progenitor (white arrowhead) which generates an AC (orange arrowhead) and a BC (cyan arrowhead). The two daughter cell somata remain in contact for more than 242 minutes post-mitosis. Subsequently, the nascent AC undergoes radial migration to the inner INL without any lateral displacement. Scale bar 10 µm.

As I based the cell-type classification of *Q26*$^{+}$ daughter cells on morphology (see also **Figure 1.1 B**), I next aimed to corroborate the AC phenotype of *Q26*$^{+}$ cells molecularly. To this end, I

crossed *Q26* wt to the *ptf1a*:GFP reporter fish, in which all inhibitory neurons of the retina, including ACs, are labeled by cytosolic GFP (Godinho et al., 2005). Using *Q26* wt; *ptf1a*:GFP compound embryos, I could confirm that $Q26^+$ progenitors indeed generate $ptf1a^+$ ACs (99.2 ± 0.8% $Q26^+$ ACs were positive for *ptf1*a:GFP, 60 cells, 12 fish; **Figure 3.15**).

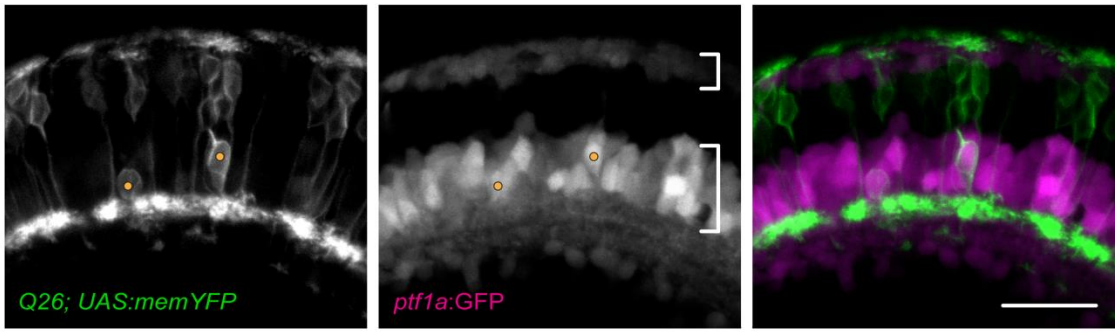


**Figure 3.15 – *Q26*$^+$ ACs are *ptf1a*$^+$.**

Confocal *in vivo* images of a 3 dpf retina (*Q26*; *UAS*:memYFP; *ptf1a*:GFP). $Ptf1a^+$ cells next to the OPL are HCs [mono-layer of *ptf1a*:$GFP^+$ cells at the top of the image (upper bracket)]; p$tf1a^+$ cells in the lower part of the INL are ACs [thick layer of *ptf1a*:$GFP^+$ cells in the middle of the image (lower bracket)]. Two $Q26^+$ cells in the lower part of the INL (orange circles) express GFP under control of the *ptf1a* promoter and thus also molecularly qualify as ACs. On the contrary, $Q26^+$ BCs are negative for *ptf1a*. Scale bar 20 µm.

If indeed ~40% of all $vsx1^+$ progenitors divided asymmetrically to produce an AC- BC pair, it would be expected that ~20% of all post-mitotic $vsx1^+$ cells in the retina are ACs[10]. However, analysis in *vsx1*:GFP retinae revealed that there are only a few, irregularly-spaced $vsx1^+$ ACs and that the proportion of $vsx1^+$ cells with an ACs phenotype is much lower than expected (0.8 ± 0.2% of all $vsx1^+$ cells are ACs; **Figure 3.16**). These low numbers of $vsx1^+$ ACs could be due to at least two distinct factors.

[10] Assuming there are 100 $vsx1^+$ progenitors, of which 60 divide in a BC-BC mode and 40 divide in an AC-BC mode. Accordingly, we would get 60 x (BC + BC) + 40 x (AC + BC) = 160 BCs + 40 ACs. This in turn means that out of 200 post-mitotic $vsx1^+$ cells 40 would be ACs, i.e. 20%.

(1) The estimate that ~40% of *vsx1*$^{+}$ progenitors undergo terminal asymmetric divisions is based on observations in the *Q26* line. As *Q26* labels only a subset of *vsx1*$^{+}$ cells, the proportion of asymmetrically dividing progenitors could be heavily overestimated due to biased labeling in this transgenic line. However, using an unbiased labelling approach based on heat-shock induction, a recent study indicated that ~25% of BC-generating progenitor divisions are terminal and asymmetric (He et al., 2012). Furthermore, using transient injections of an *ath5*:Gal4 construct into *UAS*:memYFP fish, I found that a substantial fraction of BC-generating progenitors indeed divide in an AC-BC mode (8/21 progenitor divisions which generated at least one BC, 5 fish). Therefore, three independent approaches suggest that a substantial proportion (~25 to ~40%) of BC-generating progenitors divide asymmetrically to produce an AC-BC pair. As the vast majority of BC progenitors are *vsx1*$^{+}$ (Vitorino et al., 2009), it would be expected that more than ~1% of the *vsx1*$^{+}$ cells are ACs (**Figure 3.16**).

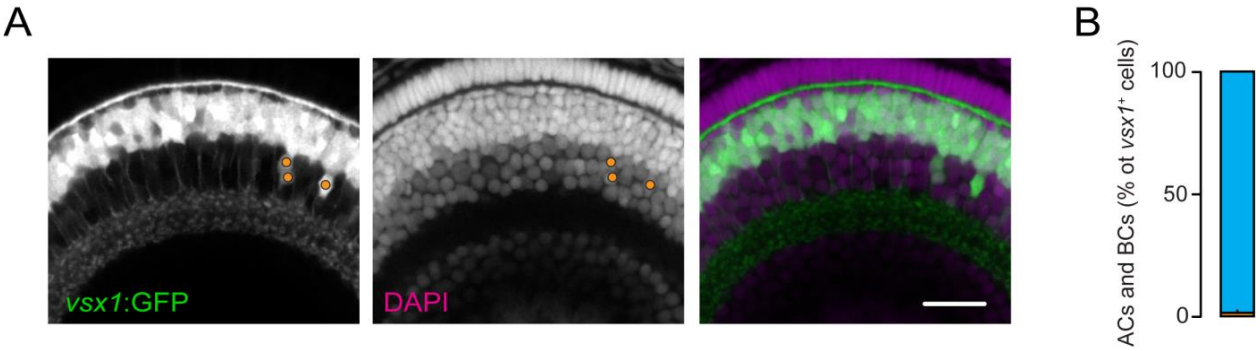


**Figure 3.16 – Only a small minority of *vsx1*$^{+}$ cells are ACs**.

(**A**) Confocal images of a 3 dpf *vsx1*:GFP retina counterstained with DAPI. Only few, irregularly spaced *vsx1*$^{+}$ ACs are visible (orange circles). Scale bar 20 µm. (**B**) Proportion of ACs (orange; 0.8 ± 0.2%) and BCs (cyan; 99.2 ± 0.2%) on total *vsx1*$^{+}$ cells in 3 dpf *vsx1*:GFP retinae (2276 *vsx1*$^{+}$ cells from 8 fish).

(2) *Vsx1* expression could be transient in ACs from the *vsx1*$^{+}$ lineage, i.e. it is expressed at the progenitor stage but not in post-mitotic ACs. Indeed, when I analyzed ACs in *Q26, UAS*:memTagRFP-T, *vsx1*:GFP compound embryos, I found that virtually all *Q26*$^{+}$ ACs are

*vsx1*:GFP$^-$ (22/23 cells showed no or very little GFP fluorescence, 5 fish; see also **Figure 3.5**). This discrepancy in AC labeling could likely be explained by the fact that fluorescence protein expression in *Q26* is mediated by the *Gal4*/*UAS* system and as such, is amplified and prolonged (Brand and Perrimon, 1993; Koster and Fraser, 2001; Scheer et al., 2002). Support for this hypothesis comes from three independent lines of experiments: First, *Q19* is a transgenic line (see also **Figure 3.9**), in which the same 3.2 kb fragment of the *vsx1* promoter element as in *Q26* directly drives expression of membrane-targeted Cerulean, (i.e. no involvement of the *Gal4*/*UAS* system). Despite a broad overlap of labeled BCs in *Q19* and *Q26*, virtually no ACs could be observed in *Q19* (*Q19*: 0.3 ± 0.2 vs. *Q26* wt: 8.4 ± 0.8 ACs per retina, p = 0.0002). Second, as labeling in *Q26* is only prominent in the laminated part of the retina (see also **Figure 3.5**), the vast majority of BCs appearing newly during time-lapse imaging are already post-mitotic (> 95%) and, accordingly, only for a small minority of BCs the progenitor cell mitosis which gave birth to them could be observed (< 5%). In stark contrast, for the vast majority of newly-appearing *Q26*$^+$ ACs, the mitotic event could be observed (for 16/17 *Q26*$^+$ ACs the mitosis could be observed, 3 fish). These observations suggest that in most *Q26*$^+$ ACs, *vsx1* is only expressed prior to mitosis and thus the post-mitotic AC labeling is due to a 'spill-over' of Gal4 and fluorescent protein from the progenitor. Third, when I photo-converted the fluorescence protein Kaede to its red fluorescent state in *Q26; UAS*:Kaede embryos, I did not observe a sizeable recovery of the unconverted green fluorescent protein in *Q26*$^+$ ACs (0/13 *Q26*$^+$ ACs showed a recovery of green fluorescence comparable to surrounding *Q26*$^+$ BCs, 5 fish). Therefore, the lack of newly-synthetized green Kaede protein can serve as direct evidence for the loss of *vsx1* promoter activity in most *Q26*$^+$ ACs.

Taken together, these observations strongly suggest that a least a quarter of all *vsx1*$^+$ progenitors divides asymmetrically to produce an AC-BC pair of daughter cells. Furthermore, the vast

majority of these ACs (estimated to be ~95%[11]) loses signs of the BC lineage, including expression of the BC markers *vsx1*, *crx* and *ribeye a*, which were all expressed at the progenitor stage (see also **chapter 3.1.1**). Accordingly, only a small fraction of ACs from the *vsx1*$^+$ lineage (the remaining ~5% of *vsx1*$^+$ ACs) continues to express BC markers (**Figure 3.17**). Therefore, I next aimed to investigate what enables the vast majority of *vsx1*$^+$ AC daughter cells to switch their fate from a nascent BC to a proper AC.

[11] As about 25-40% of *vsx1*$^+$ progenitors divide asymmetrically to produce an AC-BC pair, about 12-20% of cells derived from the *vsx1*$^+$ lineage are ACs. As only about 1% of mature *vsx1*$^+$ cells are ACs, the vast majority of ACs (11/12 to 19/20, i.e. about 95%) loses *vsx1* expression.

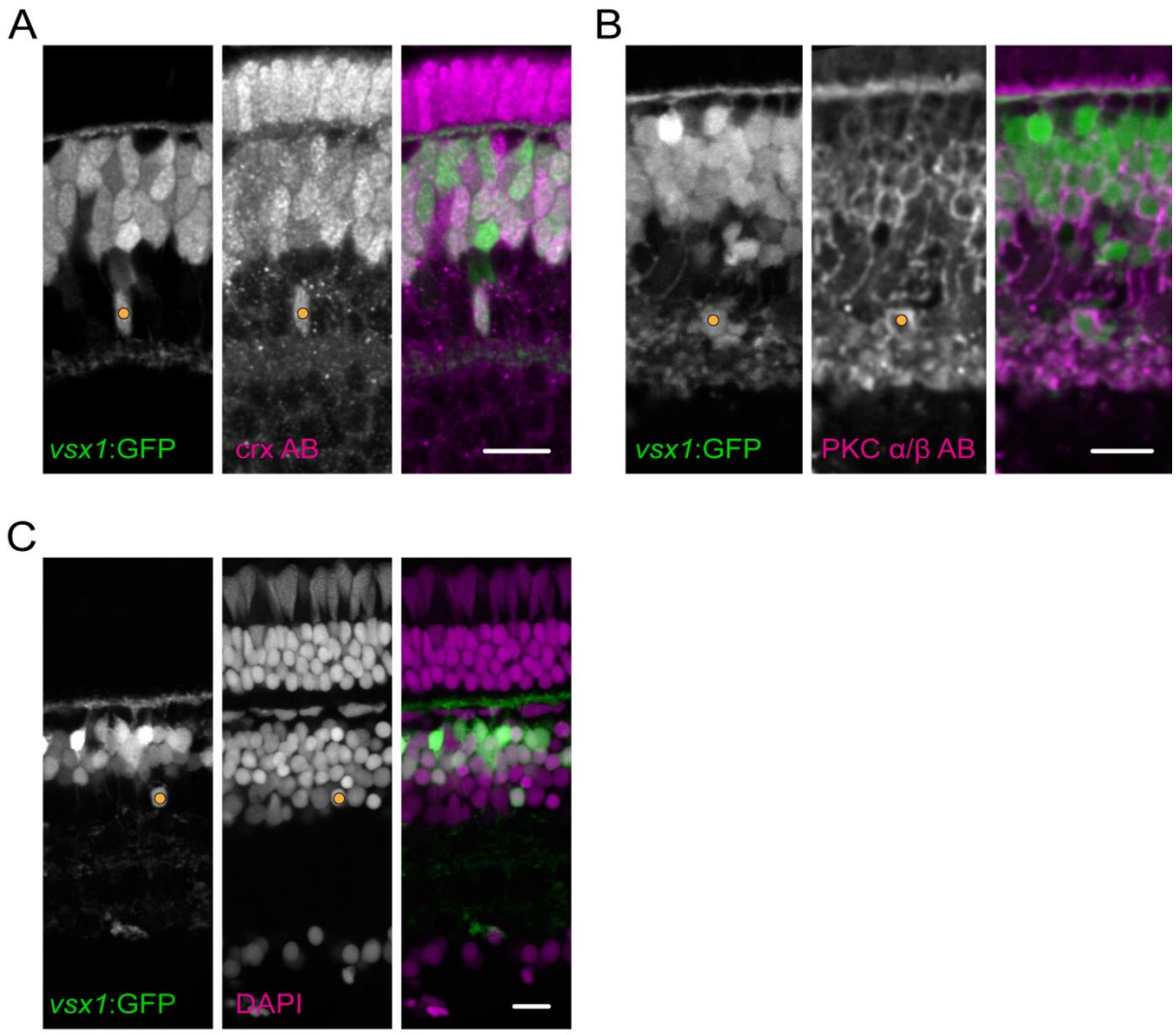


**Figure 3.17 – Upregulation and maintenance of BC markers in a subset of ACs from the *vsx1*$^{+}$ lineage.**

(**A**) Confocal images of a retinal section from a 2.5 dpf *vsx1*:GFP retina stained for Crx. Crx expression in a *vsx1*$^{+}$ AC (orange circle) is similar to surrounding BCs, suggesting that Crx is expressed in some post-mitotic *vsx1* ACs. (**B**) Confocal images of a retinal section from a 5.5 dpf *vsx1*:GFP retina stained for PKC α/β. PKC α/β expression cannot be found in *vsx1*$^{+}$ progenitors but only in post-mitotic *vsx1*$^{+}$ cells, including ACs from the *vsx1* lineage (orange circle). (**C**) Confocal images from a retinal section of an adult *vsx1*:GFP retina counterstained with DAPI. The expression of *vsx1* in some ACs (orange circle) is maintained into adulthood. Scale bar 10 µm.

### 3.2.2. The role of Notch in AC specification of cells from the *vsx1*$^{+}$ lineage

To understand how *vsx1*$^{+}$ progenitor divisions can generate distinct cellular fates, I first analyzed the spindle orientation during mitosis and the position of the daughter cells along the apico-basal axis after mitosis (Siller and Doe, 2009), but I did not detect any striking pattern or predictive trait (**data not shown**). However, these analyses revealed that the somata of *Q26*$^{+}$ daughter cells always remained in contact for several hours after mitosis (3.9 ± 0.5 h, 20 cell pairs, 6 fish; see also **Figure 3.14**), potentially allowing for cell signaling between daughter cells.

A signaling pathway which has been implicated in binary fate decisions throughout the nervous system of vertebrates is the Notch pathway (Jadhav et al., 2006b; Kimura et al., 2008; Mizuguchi et al., 2006; Peng et al., 2007; Shin et al., 2007). Notch is expressed during retinal development and gain- and loss-of-function experiments have yielded prominent phenotypes (Bao and Cepko, 1997; Bernardos et al., 2005; Del Bene et al., 2008; Jadhav et al., 2006a; Jadhav et al., 2006b; Kechad et al., 2012; Mizeracka et al., 2013; Scheer et al., 2001)[12]. To ask whether the Notch pathway is differentially activated in *Q26*$^{+}$ daughter cells and thus could instruct distinct cellular fates, I took advantage of a transgenic line in which activation of the Notch pathway is reported by expression of nuclear-targeted mCherry fluorescent protein [(T2KTp1bglob:hmgb1-mCherry)$^{jh11}$ henceforth referred to as Notch:reporter] (Parsons et al., 2009). When I crossed *Q26* wt to the Notch:reporter fish, I observed a strong bias for high Notch:reporter signals in AC daughter cells (in 29/34 ACs I found a higher Notch:repoter fluorescence intensity than in the surrounding BCs, at least 10 fish; **Figure 3.18**). Therefore, I hypothesized that high Notch levels instruct AC fate, while low levels lead to a BC phenotype. To test this hypothesis, I next aimed to manipulate Notch signaling in the *vsx1*$^{+}$ lineage.

[12] Since Notch signaling controls numerous processes (e.g. the maintenance of 'steminess' in progenitor cells or the promotion of gliogenesis), these phenotypes are not necessarily related to binary fate decisions.

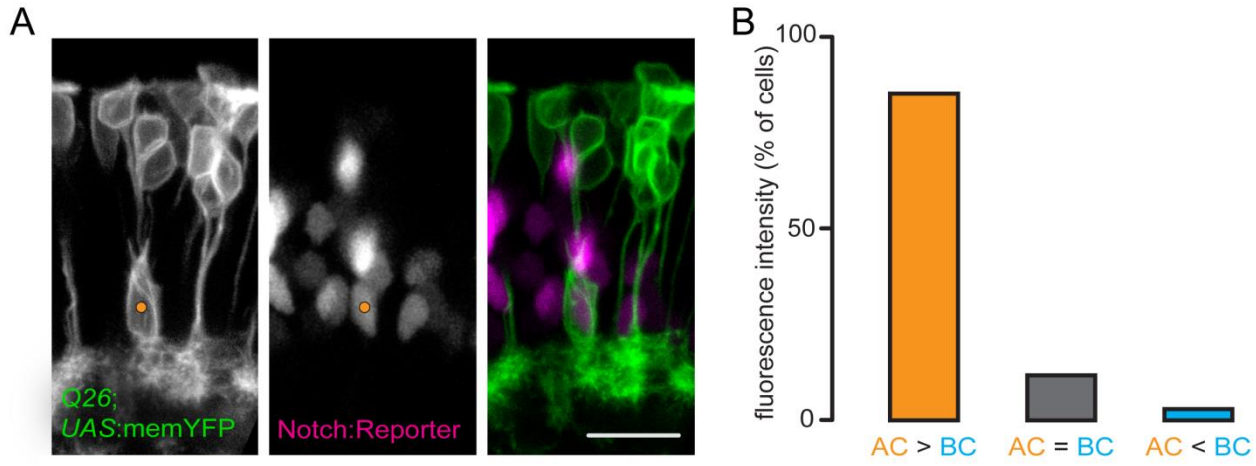


**Figure 3.18 – High levels of Notch pathway activity in *Q26*$^+$ ACs.**

(**A**) Confocal *in vivo* images of a 3 dpf retina (*Q26*, *UAS*:memYFP, Notch:reporter) indicate distinct levels of Notch pathway activity in *Q26*$^+$ cells. High levels of Notch:reporter fluorescence (i.e. Notch activity) could be found in the *Q26*$^+$ AC daughter cell (orange circle), while no detectable levels of Notch activity could be found in its surrounding *Q26*$^+$ BCs. Scale bar 10 µm. (**B**) Quantification of fluorescence intensity of the Notch:reporter signal in *Q26*$^+$ ACs and BCs. The vast majority of ACs (29/34) had higher fluorescence intensity than their surrounding (sibling) BCs.

As predicted, the pharmacological inhibition of γ-secretase, an enzyme which cleaves the Notch receptor and thus enables the Notch intracellular domain (NICD) to act as a transcription factor, lowered the number of *vsx1*$^+$ ACs in *vsx1*:GFP retinae (the numbers of *vsx1*$^+$ ACs were lowered to 60.0 ± 7.2% of DMSO-treated controls (4.1 ± 0.5 ACs per region) in DAPT-treated fish (2.4 ± 0.3 ACs per region), 12 fish, $p = 0.005$). However, I was not able to block Notch signaling specifically in *Q26*$^+$ cells with a dominant-negative *Su(H)* construct (Chapouton et al., 2010; Wettstein et al., 1997). Even though I screened several newly-generated *UAS*:dnSu(H) and *UAS*:mem:YFP-P2A- dnSu(H) founder fish by crosses to the pan-neuronal *Gal4* line *s1101t* (Mason et al., 2009), the offspring did not develop a phenotype similar to what has been described for small molecule inhibitors and classical mutants of the Notch pathway (Geling et al., 2002; Itoh et al., 2003). As the pan-neuronal expression of *dnSu(h)* did not reveal any obvious defects, I concluded that the *dnSu(H)* construct is an inefficient tool for blocking the Notch

signaling pathway during nervous system development and thus not suitable for manipulating Notch activity in nascent *Q26*$^{+}$ cells.

On the contrary, as the pan-neuronal activation of Notch signaling by over-expression of *UAS*:NICD in *s1101t* severely impaired retinal development (**data not shown**), I concluded that *UAS*:NICD fish (Scheer et al., 2001) could be a suitable tool for studying the effect of Notch activation in a cell-specific manner (i.e. in *Q26*$^{+}$ cells). Indeed, when I assayed the effect of Notch activation in *Q26*; *UAS*:memYFP; *UAS*:NICD embryos (henceforth referred to as *Q26* NICD fish), I found a dramatic increase of ACs (8.6-fold more *Q26*$^{+}$ ACs per retina, $p = 0.003$; see also **Figure 3.23**). Moreover, time-lapse imaging of *Q26* NICD retinae revealed the emergence of AC-AC divisions (0.0 ± 0.0% of all mitotic divisions in *Q26* wt vs. 38.6 ± 8.0% of all mitotic in *Q26* NICD, 44 mitotic divisions, 8 fish, $p < 0.001$; **Figure 3.19 A**). Since the proportion of BC-BC divisions was unaffected in *Q26* NICD retinae (54.2 ± 5.7% in *Q26* wt vs. 51.9 ± 10.1% in *Q26* NICD, $p = 0.762$; see also **Figure 3.24 A**), AC-AC divisions emerged at the expense of AC-BC divisions (reduction from 44.4 ± 5.6% to 9.4 ± 3.8%, $p < 0.001$; see also **Figure 3.24 A**).

A shift of AC-BC divisions to AC-AC divisions would roughly predict a doubling of ACs per retina in *Q26* NICD. However, I consistently observed larger numbers of ACs per retina (8.6-fold more ACs), suggesting that an additional source for ACs exists in *Q26* NICD. During my time-lapse experiments, I could reveal that the additional ACs are derived from events which I refer to as 'AC transformations' (**Figure 3.19 B**). In these transformations, *Q26*$^{+}$ cells exhibit a bipolar morphology well after mitosis - in some cases even including the elaboration of prominent axonal and dendritic arbors (**Figure 3.19 B** at 264') - and only subsequently transform into cells with the morphology and somal localization of ACs (**Figure 3.19 B** from 432' to 672').

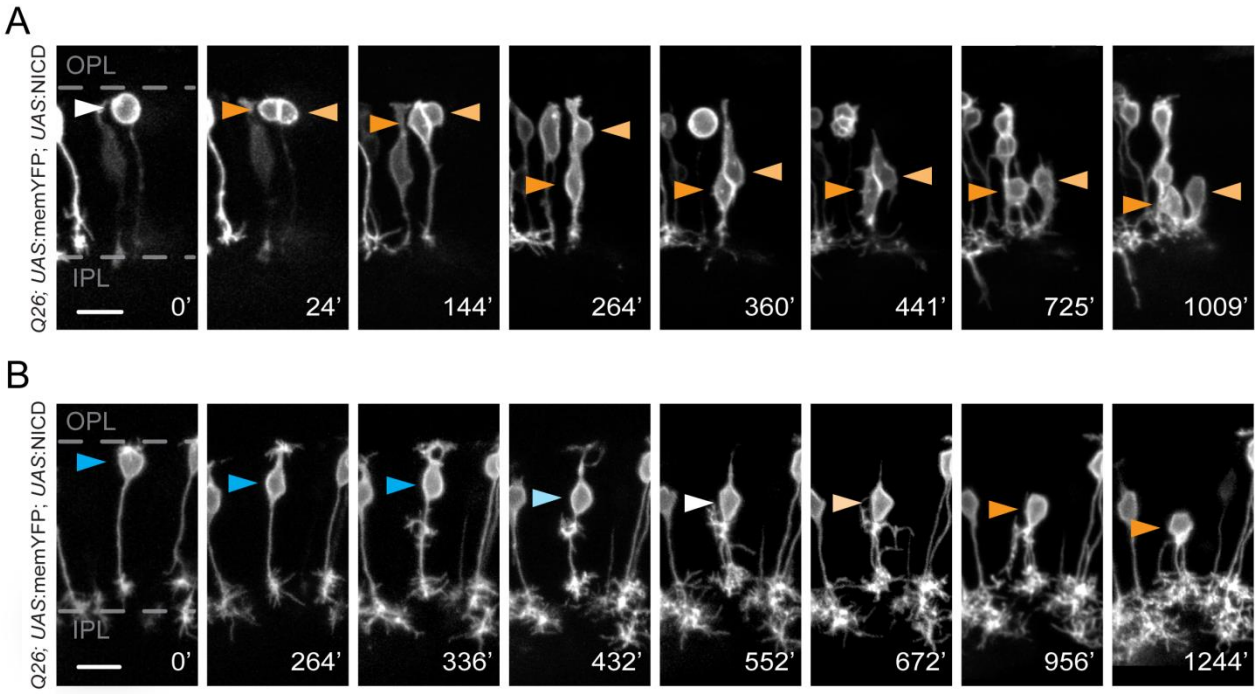


**Figure 3.19 – Over-expression of NICD in *Q26*$^{+}$ cells promotes AC fate.**

Confocal *in vivo* images of a 2.5 dpf retina (*Q26*; *UAS*:memYFP; *UAS*:NICD) in which the Notch pathway is specifically activated in *Q26*$^{+}$ cells via the *Gal4*/*UAS* system. (**A**) A *Q26*$^{+}$ progenitor (white arrowhead) divides to generate two ACs (orange arrowheads). In wild-type retinae, an AC-AC division mode of *Q26*$^{+}$ progenitor cells was not observed. (**B**) A cell with BC morphology (cyan arrowhead) transforms well after mitosis to an AC (orange arrowhead). While undergoing transformation, the cell grows additional processes (336') sheds the apical process (552') and migrates slowly towards the IPL (entire recording). Scale bar 10 µm.

To confirm the AC phenotype of transformed cells molecularly, I crossed *Q26* NICD to *ptf1a*:GFP fish. Surprisingly, I found that not only the transformed ACs were *ptf1a*$^{+}$ (97.2 ± 1.2% of ACs in *Q26* NICD are *ptf1a*$^{+}$, 111 ACs, 2 fish: **Figure 3.20** and **3.22**), but also a substantial portion of cells with BC morphology were *ptf1a*$^{+}$ (0.2 ± 0.2% in *Q26* wt vs. 26.0 ± 6.5% in *Q26* NICD, 365 BCs, 3 fish, p = 0.04; **Figure 3.20**). This observation suggests that some *Q26*$^{+}$ cells likely initiated the transformation to ACs molecularly but failed to adopt a morphological transformation. One explanation for this observation could be the existence of a limited time window for AC transformations. Indeed, during time-lapse imaging of *Q26* NICD; *ptf1a*:GFP

retinae, I could virtually not observe AC transformations after the formation of the HC layer[13] (99.3 ± 0.1% of the BCs mainted their morphology after the formation of the HC layer, 399 cells, 2 fish; **Figure 3.20**). Nevertheless, the acquisition of an AC phenotype via the transformation of nascent BCs into ACs in *Q26* NICD took a longer time than the generation of ACs after mitotic divisions in *Q26* wt (3.9 ± 0.5 h in *Q26* wt vs. 10.6 ± 1.3 h in *Q26* NICD, 13 AC transformations in 3 fish, $p < 0.001$; see also **Figures 3.14** and **3.19 B**). Therefore, I next asked whether the transformed *Q26*$^+$ ACs displayed a high(er) degree of BC differentiation.

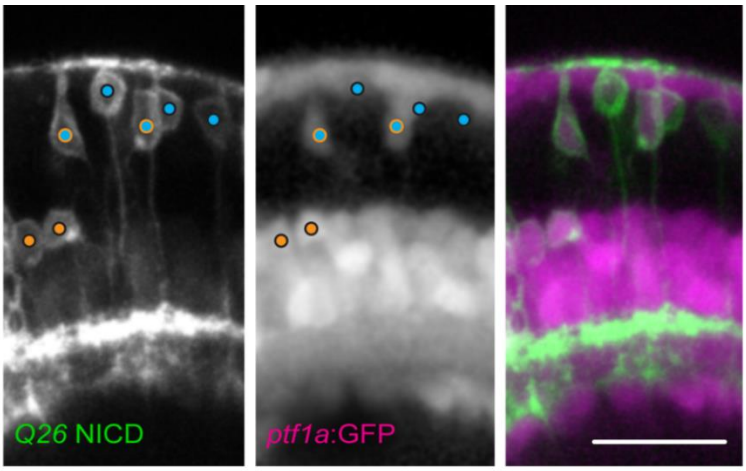


**Figure 3.20 – *Q26*$^+$ ACs and BCs are *ptf1a*$^+$.**

Confocal *in vivo* images of a 3.5 dpf retina (*Q26*; *UAS*:memYFP; *UAS*:NICD; *ptf1a*:GFP) in which the Notch pathway is specifically activated in *Q26*$^+$ cells via the *Gal4*/*UAS* system, and bona-fide inhibitory cells are labeled by *ptf1a*:GFP. *Q26*$^+$ cells with the morphology and somal location of ACs are *ptf1a*$^+$ (orange circles with black outline). In contrast to *Q26* wt, BCs in *Q26* NICD are frequently *ptf1a*$^+$ (*ptf1*$^+$ BCs are labeled by cyan circles with orange outline; *ptf1a*$^-$ BCs are labeled by cyan circles with black outline). The gamma-value of the *ptf1a*:GFP image was adjusted for better visualization. Scale bar 20 µm.

To this end, I crossed *Q26* NICD either to *vsx1*:GFP (i.e. *vsx1* expression, see also **Figure 3.1**), to *crx*:mCFP (i.e. *crx* expression, see also **Figure 3.3**) or to *ctbp2*:mEGFP fish (i.e. *ribeye a* expression, see also **Figure 3.4**), and asked whether I could find large numbers of *Q26*$^+$ ACs positive for these BC markers. However, I virtually did not detect any BC marker expression in

[13] The formation of the HC layer was used as an independent timestamp of retinal development

ACs of *Q26* NICD (*vsx1*:GFP: 4.7 ± 1.1%, 85 ACs, 3 fish; *crx*:mCFP: 0.0 ± 0.0%, 65 ACs, 3 fish; *ctbp2*:mEGFP: 1.9 ± 1.1%, 95 ACs, 4 fish; **Figure 3.22**), suggesting that even though some transformed cells undergo an extended morphological BC differentiation before transformation, a molecular imprint of this cannot be detected.

On the other hand, since AC transformations presumably require some sort of 'progenitor-like potency' in order to allow for changes in cellular fate, I next asked whether transformed ACs show signs of immaturity markers, such as expression of GFAP. In *gfap*:GFP embryos, neural progenitors which express **g**lial **f**ibrillary **a**cidic **p**rotein (GFAP) are labeled (Bernardos and Raymond, 2006). Accordingly, while *gfap*:GFP is widely expressed in the retina during early retinal development (at the stage of a neuroepithelium, see also **Figure 1.2**), it is virtually only expressed in Müller glia, the 'stem-cells' of the retina, when retinal neurogenesis is complete at 3 dpf (Bernardos and Raymond, 2006). Strikingly, however, I found that in *Q26* NICD, *gfap*:GFP fish *Q26*$^{+}$ ACs are largely *gfap*$^{+}$ [11.1 ± 5.1% of ACs in *Q26* wt (7 fish) vs. 60.9 ± 3.9% of ACs in *Q26* NICD (6 fish), p = 0.001; **Figure 3.21** and **3.22**). The expression of this immaturity marker in *Q26*$^{+}$ ACs suggests that cells have been or are in some sort of 'rejuvenated' state, which allows for changes in cellular fate.

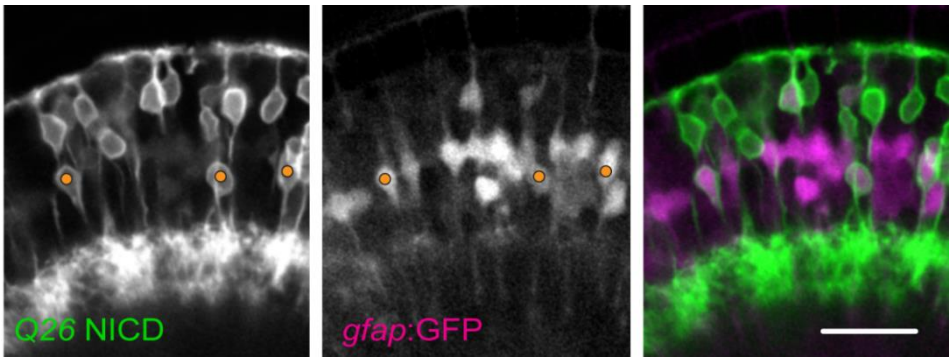


**Figure 3.21 – The majority of *Q26*$^{+}$ ACs in *Q26* NICD is positive for the immaturity marker GFAP.**

Confocal *in vivo* images of a 4 dpf retina (*Q26*; *UAS*:memYFP; *UAS*:NICD; *gfap*:GFP) showing that *Q26*$^{+}$ ACs are largely *gfap*$^{+}$ (orange circles). Scale bar 20 µm.

Taken together, experiments in *Q26* NICD show that Notch can instruct AC fate in *Q26*$^{+}$ cells, and that Notch is able to push nascent BCs to a 'rejuvenated' state, which, in turn, allows for their transformation into ACs. However, Notch seems to only induce AC fate in a subset of *Q26*$^{+}$ cells, as I did not detect any changes in the proportion of BC-BC divisions in *Q26* NICD, suggesting that BCs originating from BC-BC divisions are inert to Notch manipulation (see also **Figure 3.24 B**). To further address the molecular mechanism driving the generation of ACs in the *vsx1*$^{+}$ lineage, I next aimed to investigate the role of the inhibitory transcription factor *ptf1a*, which controls the specification of all retinal ACs (Dullin et al., 2007; Fujitani et al., 2006; Jusuf and Harris, 2009; Nakhai et al., 2007) .

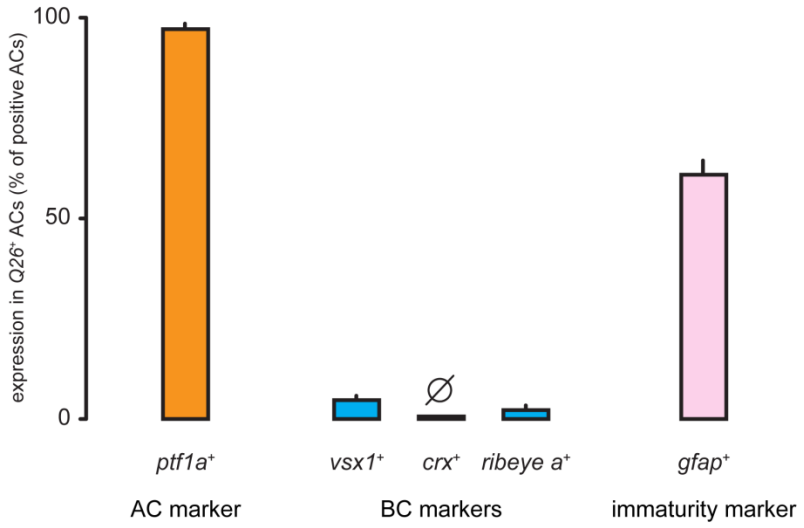


**Figure 3.22 – Effects of Notch activation on marker expression in *Q26*$^{+}$ ACs.**

Quantification of marker expression in *Q26* NICD retinae (3 or 4 dpf). *Q26*$^{+}$ ACs are virtually all positive for the AC marker *ptf1a*, and virtually all negative for BC markers *vsx1*, *crx* and *ribeye a*. Additionally, a large portion of *Q26*$^{+}$ ACs is *gfap*$^{+}$.

### 3.2.3. Ptf1a can induce AC fate in all *Q26*$^{+}$ cells but its action has a limited time window

When I crossed *Q26*; *UAS*mem:YFP to newly-generated *UAS*:Ptf1a fish (henceforth referred to as *Q26* Ptf1a), I found a prominent AC phenotye. Similarly to *Q26* NICD, I detected more *Q26*$^{+}$ ACs per retina (3.4-fold increase in comparison to *Q26* wt; $p < 0.001$; see also **Figure 3.23**). Moreover, I also observed the emergence of *Q26*$^{+}$ AC-AC divisions (23.1 ± 9.6% of all mitotic divisions in *Q26* Ptf1a, 33 mitotic divisions, 5 fish; **Figure 3.24 A**). However, the proportions of the three division modes (i.e. BC-BC, AC-BC and AC-AC divisions) were very distinct when compared to *Q26* wt or *Q26* NICD (**Figure 3.24 A**). While Q26 NICD only shifted AC-BC to AC-AC divisions, *Q26* Ptf1a affected both BC-BC and AC-BC divisions. Therefore, the number of divisions involving at least one AC was significantly higher than in *Q26* wt (increase from 44.4 ± 5.6% to 93.1 ± 2.8%, $p < 0.001$) and *Q26* NICD (increase from 48.0 ± 10.0% to 93.1 ± 2.8%, $p = 0.02$; see also **Figure 3.24 B**). Accordingly, in contrast to NICD, the over-expression of Ptf1a was able to induce AC fate in *Q26*$^{+}$ cells which originated from BC-BC divisions (**Figure 3.24 B**), suggesting that *ptf1a* can impact all newly-born BCs.

Given these shifts in division mode of *Q26*$^{+}$ progenitors, it would be expected that more *Q26*$^{+}$ ACs can be found in *Q26* Ptf1a than in *Q26* NICD. However, quantification of *Q26*$^{+}$ ACs showed significantly more ACs in *Q26* NICD (2.5-fold more ACs than in *Q26* Ptf1a, $p = 0.006$; **Figure 3.23**). This conundrum could be explained by the lack of AC transformations in *Q26* Ptf1a. Therefore, the potency of Ptf1a is apparently restricted to cells at mitosis or briefly thereafter. This hypothesis may also explain why Ptf1a over-expression is rather inefficient in inducing AC-AC divisions, since the time for Ptf1a to exert its effect might be too short in some *Q26*$^{+}$ daughter cells. To test this hypothesis, I next obtained *Q26*; *UAS*:memYFP; *UAS*:NICD; *UAS*:Ptf1a embryos (henceforth referred to as *Q26* NICD Ptf1a), and asked whether I could

observe a synergistic effect of NICD and Ptf1a over-expression. To my surprise[14], I found that the vast majority of *Q26*$^{+}$ cells are ACs in *Q26* NICD Ptf1a (36.6-fold increase compared to *Q26* wt, p = 0.003; see also **Figure 3.23**). Moreover, time-lapse recordings revealed that the bulk of *Q26*$^{+}$ progenitors divided in an AC-AC mode (82.3 ± 11.2%, 30 mitotic divisions, 5 fish, see also **Figure 3.24 A**). Therefore, in *Q26* NICD Ptf1a, the distinct effects of NICD and Ptf1a act synergistically: On the one hand, NICD confers plasticity, i.e. it makes nascent post-mitotic *Q26*$^{+}$ cells responsive for fate determinants. On the other hand, Ptf1a on its own is able to induce AC fate in all newly-born *Q26*$^{+}$ cells. Since in the presence of NICD the effect of Ptf1a is no longer restricted to cells at mitosis or briefly thereafter, the vast majority of *Q26*$^{+}$ cells could be shifted to ACs in *Q26* NICD Ptf1a.

[14] I first thought I may have mixed-up fish lines

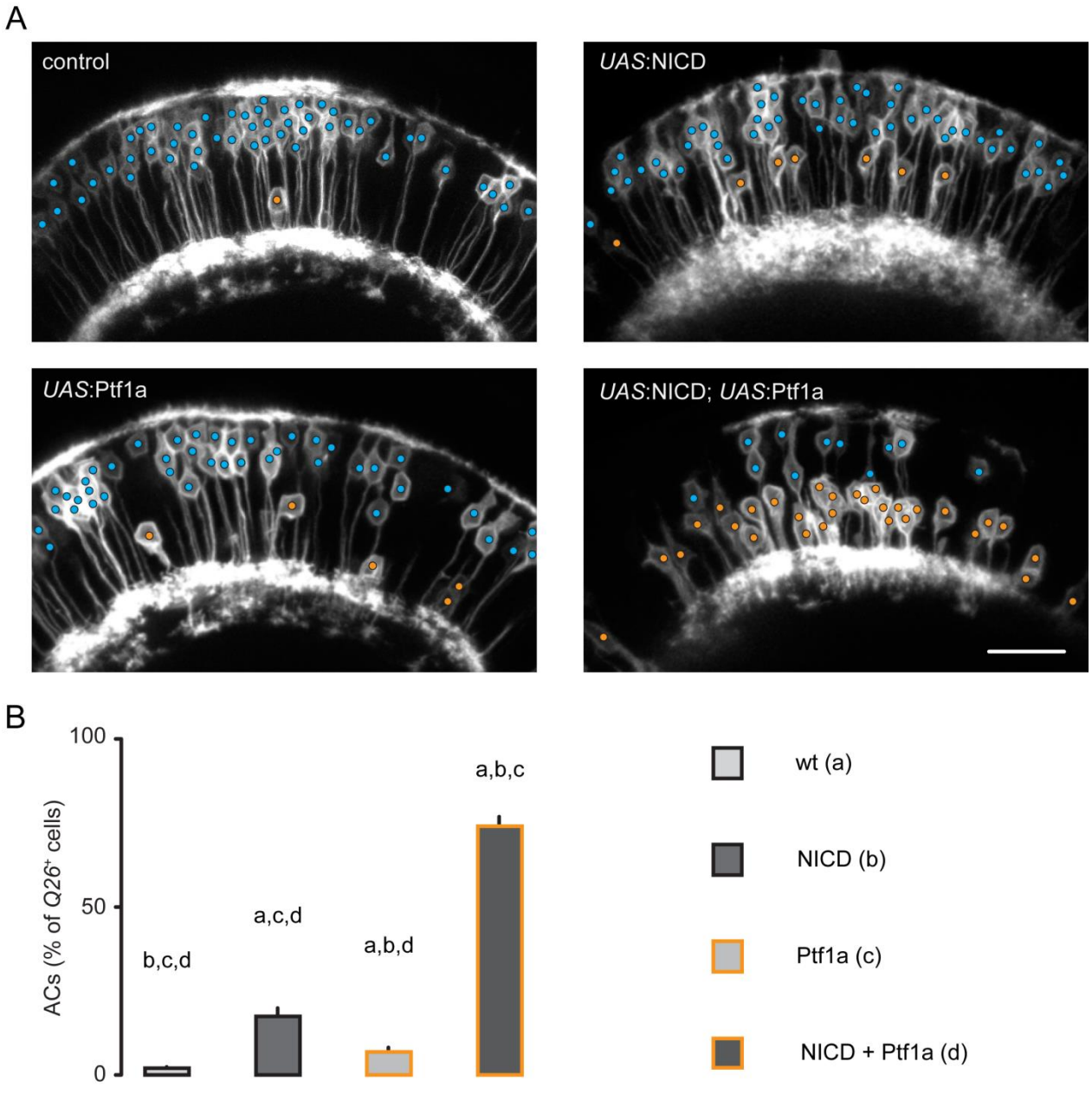


**Figure 3.23 – Quantification of ACs numbers in *Q26* wt, *Q26* NICD, *Q26* Ptf1a and *Q26* NICD Ptf1a.**

(A) Representative confocal *in vivo* images of 3 dpf *Q26* wt, *Q26* NICD, *Q26* Ptf1a and *Q26* NICD Ptf1a retinae. ACs are marked by orange circles, BCs are marked by cyan circles. Scale bar 20 µm. (B) Proportion of ACs in *Q26* wt, *Q26* NICD, *Q26* Ptf1a and *Q26* NICD Ptf1a retinae. P-values ≤ 0.05 (after FDR correction) are denoted by letters a (significantly different to *Q26* wt), b (significantly different to *Q26* NICD), c (significantly different to *Q26* Ptf1a) and d (significantly different to *Q26* NICD Ptf1a).

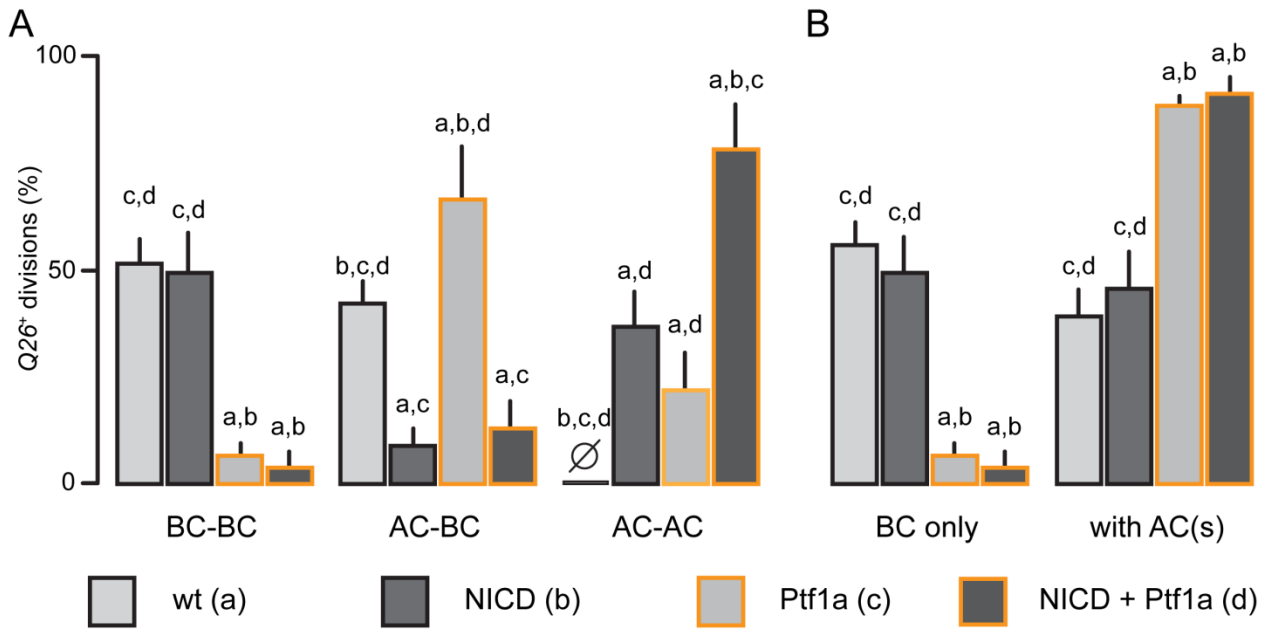


**Figure 3.24 – Quantification of division modes in *Q26* wt, *Q26* NICD, *Q26* Ptf1a and *Q26* NICD Ptf1a.**

(A) Quantification of BC-BC, AC-BC and AC-AC divisions in *Q26* wt (light grey bar with black outline), *Q26* NICD (dark grey bar with black outline), *Q26* Ptf1a (light grey bar with orange outline) and *Q26* NICD Ptf1a (dark grey bar with orange outline) retinae. (B) Quantification of divisions generating only BCs (i.e. BC-BC divisions) and divisions generating at least one AC (i.e. AC-BC and AC-AC divisions) in *Q26* wt (light grey bar with black outline), *Q26* NICD (dark grey bar with black outline), *Q26* Ptf1a (light grey bar with orange outline) and *Q26* NICD Ptf1a (dark grey bar with orange outline) retinae. P-values $\leq 0.05$ (after FDR correction) are denoted by letters a (significantly different to *Q26* wt), b (significantly different to *Q26* NICD), c (significantly different to *Q26* Ptf1a) and d (significantly different to *Q26* NICD Ptf1a).

Taken together, experiments in which I over-expressed NICD, Ptf1a or both in $Q26^+$ cells suggest a dual role for Notch in terminal, asymmetric $vsx1^+$ divisions (**Figure 3.25**): First, Notch confers some degree of immaturity/plasticity (see also **Figure 3.21** and **3.22**), allowing nascent post-mitotic BCs to dedifferentiate and change cellular fate. Second, Notch itself is sufficient to induce *ptf1a* expression (see also **Figure 3.20** and **3.22**), which, in turn, induces AC fate.

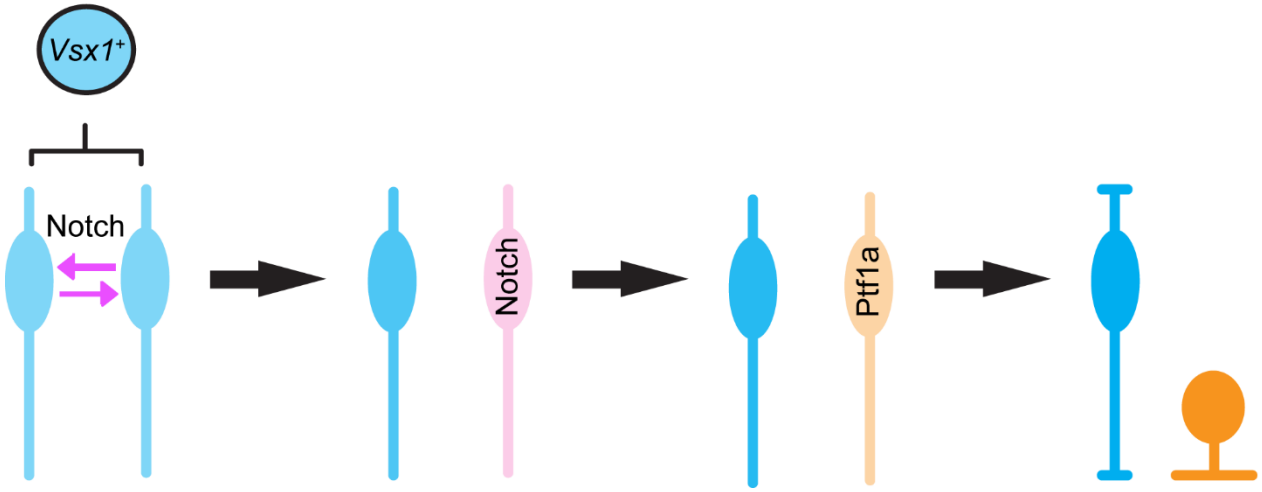


**Figure 3.25 – Model for AC specification in the *vsx1*$^{+}$ lineage.**

Model for AC specification in terminal, asymmetric *vsx1*$^{+}$ divisions. After mitotic division of the *vsx1*$^{+}$ progenitor, the daughter cells stay in contact to establish Notch signaling (**first panel**). While one daughter cell does not up-regulate Notch activity and continues to mature as a BC (cyan cell), the other daughter cell up-regulates Notch activity, which, in turn, pushes the cell to a plastic state (**second panel**, light pink cell). Additionally, Notch signaling induces *ptf1a* expression (**third panel**, light orange cell), which, in turn, promotes AC fate (**fourth panel**, orange cell).

### 3.2.4. Induction of RGC-like cells in the *vsx1*$^+$ lineage

A role for Notch in conferring immaturity/plasticity to post-mitotic *vsx1*$^+$ cells is surprising, as this function of Notch is supposedly restricted to progenitor cells (Bao and Cepko, 1997; de la Pompa et al., 1997; Dorsky et al., 1995; Ishibashi et al., 1994; Lardelli et al., 1996; Nye et al., 1994). Therefore, to directly test the extent to which Notch confers plasticity in post-mitotic *vsx1*$^+$ cells, I next aimed to challenge the temporal competence model (see also **Figure 1.6**).

To this end, I over-expressed NICD along with Atoh7 in the *vsx1*$^+$ lineage. *Atoh7* is a transcription factor which is critical for the induction of RGC fate (Brown et al., 2001; Kanekar et al., 1997; Kay et al., 2001; Liu et al., 2001a; Masai et al., 2005). According to birth-dating studies and the temporal competence model (see also **Figure 1.5** and **1.6**), once a progenitor cell lineage expresses *vsx1*$^+$, it should have long passed its competence to produce RGCs. Surprisingly, however, I could find cells with an RGC morphology, albeit a low numbers, in *Q26*; *UAS*:memYFP; *UAS*:NICD; *UAS*:Atoh7 embryos (henceforth referred to as *Q26* NICD Atoh7 fish) which were injected with *ptf1a* morpholino (2.5 ± 0.7 RGC-like cells per retina, 11 fish; **Figure 3.26**). Moreover, RGC-like cells could not be observed in *Q26* Atoh7 (i.e. without NICD) embryos, suggesting that the presence of NICD is necessary for RGC induction in the *vsx1*$^+$ lineage.

To corroborate the transformation of *Q26*$^+$ cells to RGC-like cells, I performed *in vivo* time-lapse recordings and could indeed monitor RGC-like transformations (14 RGC-like transformations in 3 fish; **Figure 3.27**). Taken together, the induction of RGC-like cells in the *vsx1*$^+$ lineage is unexpected and argues for extensive Notch-mediated plasticity in newly-born post-mitotic neurons.

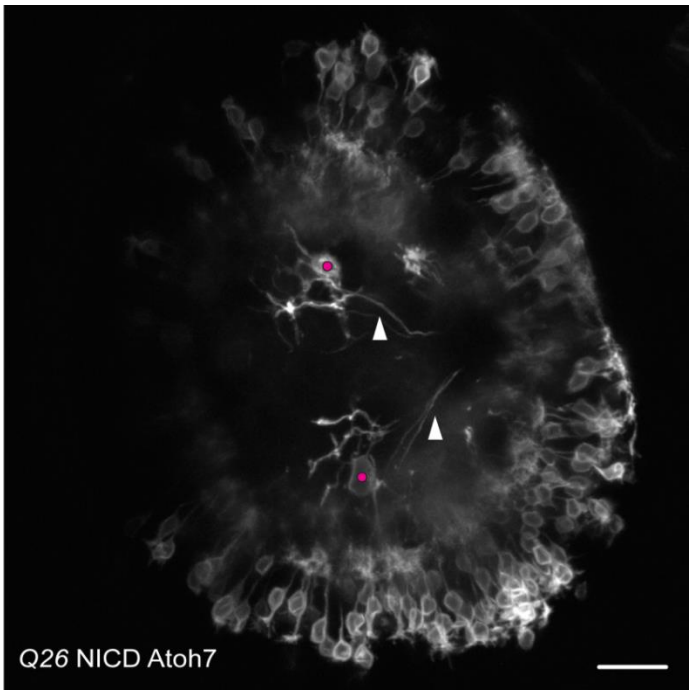


**Figure 3.26 – Induction of RGC-like cells in *Q26* NICD Atoh7.**

Confocal *in vivo* image of a 3 dpf *Q26* NICD Atoh7 retina (*Q26*; *UAS*:memYFP; *UAS*:NICD; *UAS*:Atoh7) injected with *ptf1a* morpholino. Two $Q26^{+}$ cells (magenta circles) are located in the GCL (towards the center of the eye) and have the morphology of RGCs (arrowheads point at presumptive axons).

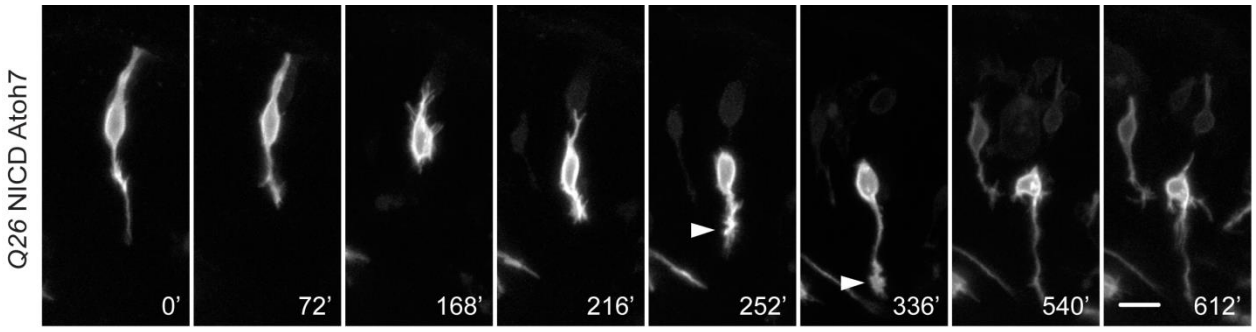


**Figure 3.27 – *In vivo* time-lapse imaging of an RGC-transformation.**

Confocal *in vivo* time-lapse recording of a 2 dpf *Q26* NICD Atoh7 retina (*Q26*; *UAS*:memYFP; *UAS*:NICD; *UAS*:Atoh7) injected with *ptf1a* morpholino. A retina-spanning $Q26^{+}$ cell loses its bipolar morphology (0' to 72'), migrates basally (72' to 252'), and grows out an axon (252' to 540'; arrowhead) and small apically-directed processes (540' to 612'). Scale bar 10 µm.

# 4. DISCUSSION

As *in vivo* studies of the development of the CNS are challenging in most vertebrate models, our knowledge about vertebrate CNS development largely builds on experiments in fixed-tisssue and/or *in vitro*. However, such preparations seem to be especially unfavourable for studying dynamic processes of neural development, as single time-points (fixed-tissue) and/or the lack of tissue context (cell culture) could only serve as a decalcomania of the complex situation *in vivo*. Consequently, little is known about the plasticity of CNS progenitor cells and newly-born post-mitotic neurons *in vivo*. Taking advantage of the zebrafish retina as a model system which is conducive for *in vivo* imaging and genetic interference, I aimed to directly observe and manipulate the development of prognitor cells and interneurons of the *vsx1*$^{+}$ lineage *in vivo*. In contrast to the widely-accepted view and my expectations, I did not encounter a linear and stereotypical progression of developmental events but rather a high degree of plasticity in progenitor cells (see **chapter 3.1**) and newly-born neurons (see **chapter 3.2**) of the *vsx1*$^{+}$ lineage.

## 4.1. Uncoupling of neurogenesis and neuronal differentiation during CNS development

In my first project, I aimed to address the stereotypy of the developmental program in CNS progenitor cells *in vivo*. To this end, I determined the relative timing of neurogenesis, neuronal migration and neuronal differentiation in a moleculary-defined CNS progenitor population. Unexpectedly, I found that developing *vsx1*$^{+}$ neurons do not adopt a stereotypical and fixed sequence of neurogenesis, neuronal migration and neuronal differentiation (see also **Figure 1.3**). Rather, to my surprise, the differentiation status of *vsx1*$^{+}$ progenitor cells at mitosis was quite

variable with regard to molecular, morphological and cell biological characteristics. However, the occurrence of a specific differentiation status in *vsx1*$^{+}$ progenitor cells was not random: *Vsx1*$^{+}$ progenitor cells dividing in the unlaminated part of the retina showed only a few signs of BC differentiation (e.g. low expression of BC markers; retina-spanning processes; somata not restricted to the outer part of the INL). On the contrary, *vsx1*$^{+}$ progenitor cells dividing in the laminated part of the retina showed prominent signs of BC differentiation (e.g. robust expression of the BC markers *vsx1*, *crx* and *ribeye a*; processes confined to synaptic layers; somata in the outer part of the INL). Importantly, progenitors dividing in the unlaminated and laminated part of the retina do not represent distinct *vsx1*$^{+}$ progenitor cell populations but lie along the continuum of the developmental gradient of the retina in 'lock-step' with the differentiation of surrounding post-mitotic BCs. Accordingly, *vsx1*$^{+}$ progenitor cells dividing in the laminated part of the retina are more similar to their surrounding post-mitotic BCs than to *vsx1*$^{+}$ progenitor cells dividing in the unlaminated part of the retina. Indeed, without the help of *in vivo* imaging or cell cycle phase markers, it would have been virtually impossible for me to distinguish, on a single cell level, between pre-mitotic *vsx1*$^{+}$ progenitors and post-mitotic nascent BCs. Strikingly, I found that *vsx1*$^{+}$ progenitor cells can even be the most differentiated cell along the differentiation gradient of the retina (see also **Figure 3.3 C**). Taken together, my results lead to the conclusion that a stereotypical and fixed sequence of ontogenetic events is not necessary during neuronal development. Therefore, at least for terminally-dividing progenitors, which generate a large part of CNS neurons (He et al., 2012; Nakashima et al., 2015), mitosis does not have to occur before neuronal differentiation commences (or at any specific point thereafter), but rather can be flexibly intercalated between other developmental steps.

### 4.1.1. Uncoupling of neurogenesis and neuronal differentiation could be a general principle of neuronal development

The uncoupling of neurogenesis and neuronal differentiation may explain three previously intriguing observations: First, that some neuronal progenitors in various parts of the nervous system display signs of neuronal differentiation prior to cell-cycle exit (Attardo et al., 2008; DiCicco-Bloom et al., 1990; Godinho et al., 2007; Miyata et al., 2004; Prasov and Glaser, 2012; Rohrer and Thoenen, 1987; Rothman et al., 1980). Second, that blocking neurogenesis does not prevent neuronal differentiation throughout the *Xenopus* CNS including the retina, spinal cord and brain stem (Harris and Hartenstein, 1991). Third, that during neuronal development in *Xenopus* (Bestman et al., 2012) and in the adult zebrafish telencephalon (Barbosa et al., 2015) neuronal stem cells can directly convert into neurons without the need of (self-sustaining) mitotic divisions. My findings in the *vsx1*$^{+}$ lineage now offer a unifying explanation for these observations, suggesting that they might simply result from a fundamental uncoupling of cell-cycle and neuronal differentiation during neuronal development. Indeed, the increasingly recognized prevalence of precociously-differentiating progenitors in a range of species and neuronal structures [e.g. basal progenitors in the neocortex of mice and primates (Betizeau et al., 2013; Haubensak et al., 2004; Miyata et al., 2004; Noctor et al., 2004; Wang et al., 2016); neural crest-derived PNS progenitors of mice (DiCicco-Bloom et al., 1990; Rohrer and Thoenen, 1987; Rothman et al., 1980) and retinal progenitors of zebrafish and mice (Godinho et al., 2007; Prasov and Glaser, 2012)], implies that such uncoupling may be a general principle of neural development. However, it will require technically challenging experiments (i.e. being able to concurrently monitor the cell-cycle and differentiation status of individual cells across developmental time) to elucidate whether uncoupling mechanisms are at play during mammalian CNS development. Nevertheless, a recently published study on the development of the neocortex

in mice suggests that early-dividing progenitors, late-dividing progenitors and post-mitotic neurons may form a differentiation continuum (Telley et al., 2016).

### 4.1.2. Uncoupling of neurogenesis and neuronal differentiation could allow for fast and synchronous CNS development *in vivo*

What could be the advantage(s) of uncoupling neurogenesis and neuronal differentiation? In comparison to the classical model and its orderly sequence of developmental events, the uncoupled model provides two advantages, namely speed and synchrony (**Figure 4.1**).

**1. Speed**

In the 'classical model', differentiation can only be initiated following mitosis. Therefore, the time required to reach maturity is delayed for the majority of cells by their (late) birth dates (note the mitotic division on the furthest right (white circle) in the **'classical model**' of **Figure 4.1**, in which neuronal differentiation only commences when some of the earlier-born BCs have almost reached maturity). By contrast, in the 'uncoupled model', differentiation steps can already occur at the progenitor stage, permitting the acquisition of full maturity across the population faster (note the mitotic division on the furthest right (dark green circle) in the **'uncoupled model'** of **Figure 4.1**, which has undergone substantial neuronal differentiation prior to mitosis).

**2. Synchrony**

In the 'classical model', every developmental trajectory is the same and thus the time from mitosis to completed differentiation is constant for every daughter cell. This, in turn, also means

that the first and last developmental trajectory (resulting from the first and the last mitotic division) are separated exactly by the time period between the first and last mitotic division, i.e. asynchronous (see the large shift of individual differentiation trajectories in the **'classical model'** of **Figure 4.1**). Furthermore, as the developmental trajectories are constant in the 'classical model', also the time period between the first- and last-born daughter cell to reach full maturity equals the time period between the first and last mitotic division (see the large spread of elliptical cells (representing full maturity of daughter cells) in the **'classical model'** of **Figure 4.1**). On the contrary, developmental trajectories in the 'uncoupled model' are variable and thus the time from mitosis to completed differentiation is different for every daughter cell. As developmental trajectories in the 'uncoupled model' are arranged according to their differentiation (but not cell cycle status), progenitors and daughter cells of a given population differentiate in relative synchrony despite the extended time span over which mitotic divisions occur (see the concentration of developmental trajectories and elliptical cells (representing full maturity of daughter cells) in the **'uncoupled model'** of **Figure 4.1**).

Furthermore, it should be noted that 'uncoupling' is the only mechanism to gain developmental synchrony without changing the rates of neuronal differentiation (a changing rate of differentiation could be conceived as variable slopes of the developmental trajectories in **Figure 4.1**) as in every 'coupled' model the time period of mitoses equals the time period of completed neuronal differentiation across the entire population of newly-born daughter cells. Consequently, even if progenitors underwent a stereotypic neuronal differentiation prior to mitoses, the time period of mitoses and completed neuronal differentiation would be equal and thus neuronal differentiation asynchronous.

Taken together, the uncoupling of neurogenesis and neuronal differentiation allows for fast and synchronous development of the CNS. Therefore, this mechanism might be particularly

important for the assembly of rapidly developing circuits, e.g. for escape and prey capture (Nikolaou and Meyer, 2015), or circuits which form over an extended period of neuronal development, such as the neocortex (Wilsch-Bräuninger et al., 2016).

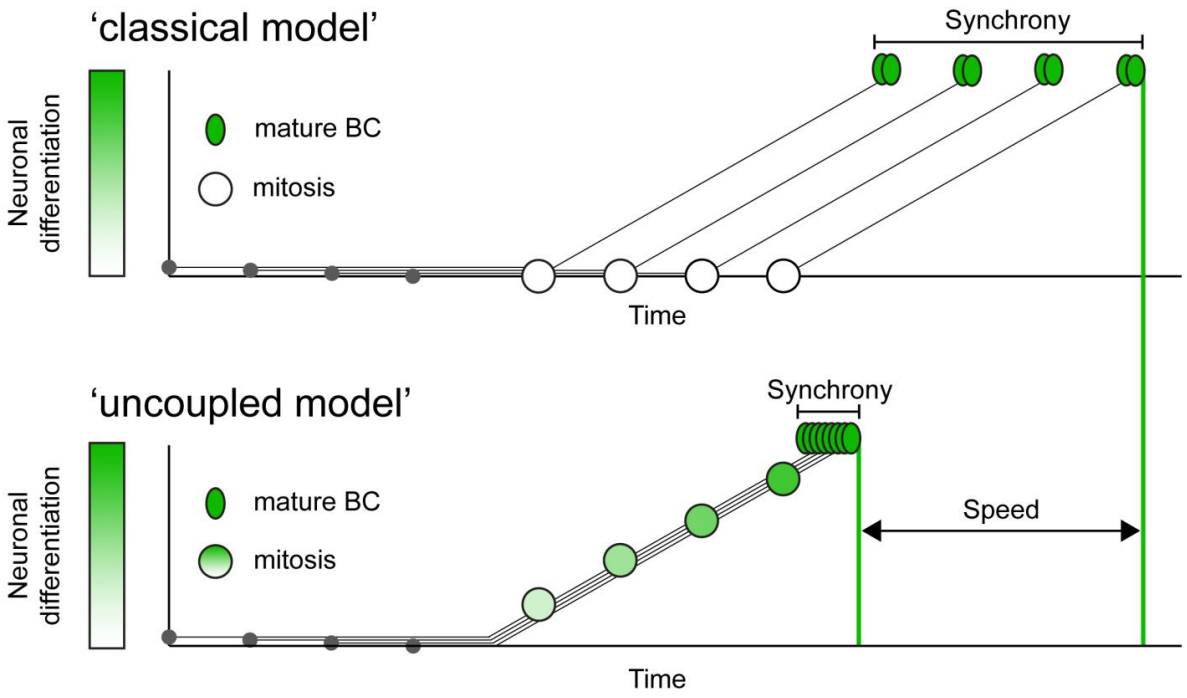


**Figure 4.1 – Comparison of the 'classical model' and 'uncoupled model' of neuronal development.**

The developmental trajectories of four progenitors (circles) are schematically tracked over time until they differentiate and reach maturity (ellipses). The time period of neurogenesis is the same for cells in the 'classical' and the 'uncoupled' model. As compared to the 'classical' model in which differentiation commences only after cell-cycle exit, 'uncoupling' neurogenesis and differentiation permits a cell population to differentiate faster and in relative synchrony.

## 4.2. Re-specification of neuronal identity

In a second project, while exploring mechanisms of fate specification in retinal interneurons, I uncovered a high degree of plasticity in nascent *vsx1*$^{+}$ cells. Using *in vivo* time-lapse microscopy, I found that a substantial proportion of *vsx1*$^{+}$ progenitors undergoes asymmetric division to give birth to an AC-BC pair of daughter cells. The generation of ACs by *vsx1*$^{+}$ progenitors is surprising *per se*, as the retinal *vsx1*$^{+}$ lineage is widely-accepted to be committed to the generation of BCs (Vitorino et al., 2009). Indeed, the generation of ACs by *vsx1*$^{+}$ progenitors is particularly surprising in zebrafish, as my own work demonstrated that *vsx1*$^{+}$ progenitors undergo precocious neuronal differentiation and display the phenotype of nascent BCs prior to mitotic division (see **chapter 3.1**). Consequently, one daughter cell of the asymmetric *vsx1*$^{+}$ division has to lose signs of BC differentiation and is re-specified as an AC. The re-specification process seems to be rather efficient, as the vast majority (~95%) of ACs from the *vsx1*$^{+}$ lineage does not maintain or up-regulate expression of BC markers. Furthermore, it is unlikely that the ACs which maintain BC characteristics consitute one or more distinct AC subtype(s), as the distribution of *vsx1*:GFP ACs does not suffice to account for the regular retinal mosaics adopted by other AC subtypes (Kay et al., 2012).

To my knowledge, there has been no report on the re-specification of neuronal identity as a mechanism for generating cellular diversity during vertebrate CNS development. Nevertheless, there are a few examples for cellular plasticity of post-mitotic neurons in vertebrates, including the activity-dependent re-specification of neurotransmitters (Spitzer, 2012) and the unstable cellular fate of nascent DRG neurons (Wright et al., 2010). However, the most extensive (as well as impressive) insights regarding cellular plasticity of post-mitotic cells have been provided by re-progamming studies (Amamoto and Arlotta, 2014): Here, using powerful transcription factors

as instructive signals, differentiated cells (including astrocytes, fibroblasts, hepatocytes and pericytes) could be directly converted to neurons (Berninger et al., 2007; Caiazzo et al., 2011; Karow et al., 2012; Marro et al., 2011; Pang et al., 2011; Vierbuchen et al., 2010). While most re-programming studies were performed *in vitro* and showed the conversion of non-neuronal cells to neurons, the conversion of (immature) spiny neurons of layer 4 to corticospinal motor neurons (CSMNs) as well as the conversion of (immature) callosal projection neurons to CSMNs have recently been achieved *in vivo* by over-expression of the transcription factor *Fezf2* (De la Rossa et al., 2013; Rouaux and Arlotta, 2013). Therefore, there is evidence that post-mitotic neurons in the mammalian CNS, in principle, have the capacity to switch their fate after mitosis (at least in conjunction with the over-expression of instructive transcription factors). However, whether the re-specification of neuronal identity also operates during normal neural development in mammals (i.e. without over-expression of exogenous transcription factors) remains to be determined.

### 4.2.1. Implications of the re-specification of neuronal identity

While I have described in great detail the advantages of uncoupling neurogenesis and neuronal differentiation in *vsx1*$^{+}$ progenitors for BC differentation (see **chapter 4.1.2**), the uncoupling mechanism would seem detrimental to the large proportion of asymmetric *vsx1*$^{+}$ division that generate AC-BC pairs: At first glance, it does not seem advantageous for *vsx1*$^{+}$ cells to undergo BC differentiation until mitotic division and subsequently to be re-specified as an AC. Therefore, I next want to address the implications of the uncoupling of neurogenesis and neuronal differentiation for asymmetric *vsx1*$^{+}$ divisions.

First, it should be considered as an ameliorating factor that only a small proportion (less than 10%)[15] of all post-mitotitc *vsx1*$^+$ cells actually undergo extensive re-specification to become ACs. Therefore, the vast majority of cells originating from the *vsx1*$^+$ lineage either profits from (all BCs) or is only marginally affected by (ACs derived from undifferentiated *vsx1*$^+$ progenitors of the unlaminated retina) the uncoupling of neurogenesis and neuronal differentiation. Second, it is conceivable that the zebrafish retina initally (i.e. when it starts to function) rather works as a simple light sensor than as a sophisticated device that provides the animal with detailed information about the outside world. Strikingly, well before a functional retina forms, a simple photomotor response (PMR) mediated by the hindbrain has been described for 1 dpf zebrafish (Kokel et al., 2010; Kokel et al., 2013), highlighting the immediate importance of phototactic behaviours. Furthermore, it was reported for various species that the retinal synaptic circuitry undergoes refinement over an extendend time period after the establishment of first visual function (Tian, 2008). Therefore, I would like to speculate that for the acquisition of rudimentary visual function, differentiated BCs (which are essential for the channeling of information from PRs to RGCs) are more vital than differentiated ACs (which are important for lateral processing), and that the uncoupling mechanism could accordingly prioritize for these needs. Third, there could also be benefits in keeping *vsx1*$^+$ daughter cells in a plastic state for an elongated time period, e.g. to balance excitation (BCs) and inhibiton (ACs) in the retina. Indeed, in experiments in which I lowered the number of retinal ACs by *ptf1a* morpholino injection, I could observe that addtional *vsx1*$^+$ cells commenced the differentiation of inhibitory cellular fate as assayed by *ptf1a*:GFP expression (11.4 ± 1.8 *Q26*$^+$*ptf1a*$^+$ double-positive cells per retina in *Q26* controls vs.

[15] Only 20% of *vsx1*$^+$ daughter cells are ACs and thus potentially have to undergo AC re-specification. However, since the majority of *vsx1*$^+$ progenitors divides in the unlaminated part of the retina and does not undergo an extensive BC differentiation prior to mitosis (estimated to be 60% of all *vsx1*$^+$ mitotic divisions), the majority of ACs from the *vsx1*$^+$ lineage are not generated by progenitors that underwent extensive BC differentiation. Consequently, only a minority of *vsx1*$^+$ ACs (40%) is derived from 'differentiated' *vsx1*$^+$ progenitors and thus only about 8% (40% x 20%) of all post-mitotic *vsx1*$^+$ cells have to undergo extensive AC re-specification.

21.9 ± 2.5 *Q26*$^{+}$*ptf1a*$^{+}$ double-positive cells per retina in *Q26 ptf1a* morphants, p = 0.01). Therefore, the possibility of converting BCs to ACs during late(r) stages of neural development could be employed as a strategy to fine-tune excitation and inhibition in the retina. This possibility seems to be especially plausible in zebrafish, as here, in contrast to many other vertebrates (Yeo and Gautier, 2004), developmental cell death is not neccesarily a mechanism for the selection of the appropiate neuronal numbers (Biehlmaier et al., 2001). Fourth, it has been reported that in the neocortex the origin from a shared progenitor lineage helps to establish preferential synaptic connectivity between (excitatory) sister neurons (Li et al., 2012a; Yu et al., 2009; Yu et al., 2012). So far, I do not have compelling evidence that AC-BC daughter cells are synaptically connected, but light-microscopic images strongly suggest a close proximity of AC-BC neurites (**Figure 4.2**). Nevertheless, a formal proof of preferential synaptic connectivity is particularly challenging in the zebrafish retina, as it would depend on at least one of these three experimental strategies: (1) Paired electrophysiological recordings (the method of choice for the studies in the neocortex): The application of targeted-recordings (not to mention targeted paired-recordings) in the larval retina has not been achieved yet. (2) Optogenetic stimulation and readout: As the retina itself expresses opsins in photoreceptors and thus is sensitive to blue-light stimulation (Sethuramanujam et al., 2016), optogenetic experiments in the retina are not straightforward and thus far were largely restricted to time-points before the complete assembly of retinal circuitry (Yonehara et al., 2011) or to the restoration of PR function (Busskamp et al., 2010). (3) Volumetric EM techniques: Techniques to acquire large EM volumes in zebrafish are only beginning to be established and particularly the analysis (the tracing of neurites) involves exuberant hours of human labor (Helmstaedter et al., 2013; Kasthuri et al., 2015). Therefore, it will be difficult to directly address the concept of preferential synaptic connectivity among AC-BC daughter cells.

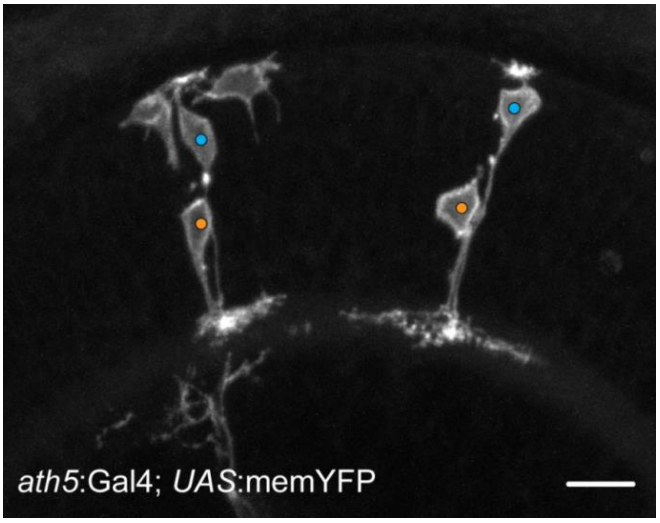


**Figure 4.2 – Neurites of AC and BC siblings overlap on the light microscopic level.**

Confocal image of a fixed 3 dpf retina (injection of *ath5*:Gal4 into *UAS*:memYFP fish) showing two isolated AC-BC pairs (orange and cyan circles). Since *ath5* is not expressed in post-mitotic ACs and BCs, the labeling of an isolated AC-BC cell pair suggests its origin from a common (*vsx1*$^{+}$) progenitor. In each of the two isolated AC-BC pairs, the axonal arbor of the BC stratifies in the dendritic field of the AC (the axonal arbor of the BC can be identified as the brightest spot in the AC-BC neuropil).

However, I propose that the expression patterns of family members of the synaptic adhesion molecules Dscam and Sidekick could alternatively be used as a proxy for synaptic connectivity. Various subtypes of Dscam and Sidekick proteins are expressed in non-overlapping populations of retinal interneurons and RGCs of the chicken retina, which, in turn, homophilically interact to form synapses in distinct sub-laminae of the IPL (Yamagata and Sanes, 2008; Yamagata et al., 2002). Therefore, it is conceivable that the expression of the same Dscam or Sidekick subtype in AC-BC daughter cells should facilitate a synaptic interaction amongst them. Intriguingly, it is even conceivable that Dscam or Sidekick molecules are already expressed in *vsx1*$^{+}$ progenitors, and thus a link between the targeting of neurites and the 'precocious' neuronal differentiation in *vsx1*$^{+}$ progenitors seems apparent. Indeed, in a pioneering experiment, I could observe non-apically dividing *Dscamb*$^{+}$ progenitors in a novel *Dscamb* transgenic fish line (collaboration with

Alvaro Sagasti, UCLA, Los Angeles). Nevertheless, as the cellular fate of the daugther cells generated by *Dscamb*$^{+}$ progenitors is unknown for now (it is possible that non-apically dividing *Dscamb*$^{+}$ progenitors do not give birth to AC-BC pairs) and as Dscam molecules could also mediate homophilic repulsion (Fuerst et al., 2009; Fuerst et al., 2008), further experiments will be neccesary to gauge the significance of *Dscamb*$^{+}$ progenitors.

### 4.2.2. The role of Notch during re-specification of post-mitotic *vsx1*$^{+}$ cells

The Notch pathway has been implicated in numerous processes during neural development in invertebrates and vertebrates, most notably (1) to keep progenitors as undifferentiated cells in the cell cycle (de la Pompa et al., 1997; Dorsky et al., 1995; Fortini et al., 1993; Imayoshi et al., 2010; Nye et al., 1994), (2) to control binary fate decisions (Cooper and Bray, 1999; Dong et al., 2012; Fanto and Mlodzik, 1999; Kechad et al., 2012; Kimura et al., 2008; Peng et al., 2007; Quillien et al., 2011; Shin et al., 2007), and (3) to promote gliogenesis (Bernardos et al., 2005; Morrison et al., 2000; Scheer and Campos-Ortega, 1999; Scheer et al., 2001; Taylor et al., 2007). Using cell-type specific activiation of the Notch pathway by NICD over-expression in *Q26*$^{+}$ cells, I could reveal a dual role for Notch in the re-specification of ACs (see also **Figure 3.25**): First, Notch confers a degree of plascticity which allows for changes in cellular fate. Accordingly, nascent *Q26*$^{+}$ cells committed to the BC fate become responsive to instructive transcripton factors. Second, Notch itself is sufficient to induce *ptf1a* expression (the master regulator for inhibitory cell specification in the nervous systems of vertebrates) and thus AC fate is instructed in the *Q26*$^{+}$ daughter cell with high Notch activity. Despite the pleiotropy of Notch, the Notch-mediated effects in *Q26*$^{+}$ cells were rather specific: First, Notch did not prevent the molecular

and morphologic differentiation of ACs in *Q26* NICD. Second, Notch did not exert a gliogenic effect in *Q26* NICD. Third, the competence of Notch to instruct AC fate in *Q26* NICD was restricted to a subset of BCs, presumably to BCs derived from asymmetric *vsx1*$^{+}$ divisions. However, virtually all *Q26*$^{+}$ post-mitotic cells adopted AC fate in *Q26* NICD Ptf1a, suggesting that, in principle, all BCs have the capabaility to acquire an AC fate but that in *Q26* NICD in a subset of BCs (presumably BCs derived from symmetric BC-BC divisions) the signaling cascade triggering AC specification cannot be activated by Notch alone. Fourth, however, I did observe exuberant neuritic growth as a potential side effect of NICD over-expression in *Q26*$^{+}$ cells (see the loss of the ON- and OFF-lamination in the IPL of *Q26* NICD retinae as consequence of excessive axonal arbors of *Q26*$^{+}$ cells in **Figure 3.23**). The observed over-growth of neurites in *Q26* NICD stands in contrast to the previously reported growth inhibiting effect of Notch on neurites during cortical development (Šestan et al., 1999).

In my experiments, the question of how distinct Notch activity levels are established in daughter cells remains unanswered. While a stereotypic cleavage plane orientation during mitotic divisions and the resulting asymmetric distibution of Notch pathway modulators (e.g. Numb and Par3) have been proposed as mechanism for binary fate decisions in invertebrates and vertebrates (Bultje et al., 2009; Cayouette et al., 2001; Frise et al., 1996; Rhyu et al., 1994; Shen et al., 2002), I found neither a stereotypic division plane orientation (**data not shown**) nor the asymmetric distribution of Numb and Par3 (**data not shown**) in retinal *vsx1*$^{+}$ progenitors. Nevertheless, for the generation of V2a and V2b interneurons by *vsx1*$^{+}$ progenitors of the zebrafish spinal cord, a model has been proposed in which initially stochastic differences in Notch signalling activity are amplified by a feedback mechanism and thus lead to daughter cells with distinct Notch activity (Kimura et al., 2008). Therefore, it is conceivable that a similar stochastic mechanism is at play in retinal *vsx1*$^{+}$ progenitors.

To my knowledge, I describe for the first time a role for Notch in conferring plasticity/immaturity during binary fate decisions in the developing nervous system. While this function of Notch is well described for neuronal progenitors (de la Pompa et al., 1997; Dorsky et al., 1995; Fortini et al., 1993; Imayoshi et al., 2010; Nye et al., 1994), I now propose that during binary fate decisions Notch-mediated cellular plasticity allows for tissue homeostasis by elongating the time window in which cellular fates can be switched. In this context, I uncovered that the extent of Notch-mediated plasticity can be remarkable: First, using the transcription factor *Atoh7* [which is naturally suppressed in cells with high Notch activity (Maurer et al., 2014)] in combination with NICD, I showed that post-mitotic *vsx1*$^{+}$ cells can be transformed to RGC-like cells in *Q26* NICD Atoh7. While the RGC phenotype of transformed cells has still to be confirmed molecularly, these experiments are the first to suggest that restrictions of the temporal competence model (Cepko, 2014; Kohwi and Doe, 2013) can, in principle, be overcome *in vivo* (see also **Figure 1.5** and **1.6**). Second, as re-programming of neurons is increasingly recognized as a potential therapeutic strategy for brain damage (Amamoto and Arlotta, 2014), it will be pivotal to find genes which confer plasticity to post-mitotic neurons. In this context, since NICD over-expression is able to elongate the time period for the re-specification of neuronal identity, it will be informative to express NICD along with instructive transcription factors to test if the time period for the neuronal re-specification can be prolonged in conjunction with NICD (as is the case for *ptf1a* in *Q26*$^{+}$ cells). For example, it was shown that callosal projection neurons and spiny neurons of layer 4 can only be converted to corticospinal motor neurons before the establishment of synaptic circuitry (De la Rossa et al., 2013; Rouaux and Arlotta, 2013). Indeed, it is well conceivable that in such a setting a pulse of Notch expression could prolong the time period in which the conversion of neuronal subtypes can be instructed, and thus contribute to a

modern re-interpretation of Virchow's famous third tenet of cell theroy: All cells come from cells.

# 5. PUBLICATIONS

Engerer P, Williams PR, Suzuki SC, Yoshimatsu T, Misgeld T, Godinho L. **Re-specification of neuronal identity during CNS development.** *In preparation*

Engerer P, Suzuki SC, Yoshimatsu T, Chapouton P, Obeng N, Odermatt B, Williams PR, Misgeld T, Godinho L. **Uncoupling of neurogenesis and differentiation during CNS development.** *In revision*

Engerer P, Fecher C, Misgeld T. **Super-resolution microscopy writ large.** *Nat Biotechnol* (2016)

Engerer P, Plucinska G, Thong, R, Trovo L, Paquet D, and Godinho L. **Imaging Subcellular Structures in the Living Zebrafish Embryo.** *J Vis Exp.* (2016).

Held K, Bhonsle-Deeng L, Siewer K, Sato W, Beltran E, Schmidt S, Ruhl G, Ng JK, Engerer P, Moser M, Klinkert WE, Babbe H, Misgeld T, Wekerle H, Laplaud DA, Hohlfeld R, Dornmair K. **αβ T-cell receptors from multiple sclerosis brain lesions show MAIT cell-related features.** *Neurol Neuroimmunol Neuroinflamm* (2015)

Engerer P, Yoshimatsu T, Suzuki SC, Godinho, L. **CentrinFish permit the visualization of centrosome dynamics in a cellular context in vivo.** *Zebrafish* (2014)

Kleele T, Marinkovic P, Williams PR, Stern S, Weigand EE, Engerer P, Naumann R, Hartmann J, Karl RM, Bradke F, Bishop D, Herms J, Konnerth A, Kerschensteiner M, Godinho L, Misgeld T. **An assay to image neuronal microtubule dynamics in mice.** *Nat Commun* (2014)

Wang K, Milkie DE, Saxena A, Engerer P, Misgeld T, Bronner ME, Mumm J, Betzig E. **Rapid adaptive optical recovery of optimal resolution over large volumes.** *Nat Methods* (2014)

# 6. REFERENCES


Amamoto, R., and Arlotta, P. (2014). Development-inspired reprogramming of the mammalian central nervous system. Science 343, 1239882.

Anderson, S.A., Eisenstat, D.D., Shi, L., and Rubenstein, J.L. (1997). Interneuron migration from basal forebrain to neocortex: dependence on Dlx genes. Science 278, 474-476.

Attardo, A., Calegari, F., Haubensak, W., Wilsch-Brauninger, M., and Huttner, W.B. (2008). Live imaging at the onset of cortical neurogenesis reveals differential appearance of the neuronal phenotype in apical versus basal progenitor progeny. PLoS One 3, e2388.

Bao, Z.Z., and Cepko, C.L. (1997). The expression and function of Notch pathway genes in the developing rat eye. J Neurosci 17, 1425-1434.

Barbosa, J.S., Sanchez-Gonzalez, R., Di Giaimo, R., Baumgart, E.V., Theis, F.J., Gotz, M., and Ninkovic, J. (2015). Neurodevelopment. Live imaging of adult neural stem cell behavior in the intact and injured zebrafish brain. Science 348, 789-793.

Barnes, A.P., Lilley, B.N., Pan, Y.A., Plummer, L.J., Powell, A.W., Raines, A.N., Sanes, J.R., and Polleux, F. (2007). LKB1 and SAD Kinases Define a Pathway Required for the Polarization of Cortical Neurons. Cell 129, 549-563.

Baye, L.M., and Link, B.A. (2007). Interkinetic nuclear migration and the selection of neurogenic cell divisions during vertebrate retinogenesis. J Neurosci 27, 10143-10152.

Beis, D., and Stainier, D.Y. (2006). In vivo cell biology: following the zebrafish trend. Trends Cell Biol 16, 105-112.

Belliveau, M.J., and Cepko, C.L. (1999). Extrinsic and intrinsic factors control the genesis of amacrine and cone cells in the rat retina. Development 126, 555-566.

Benjamini, Y., and Hochberg, Y. (1995). Controlling the False Discovery Rate: A Practical and Powerful Approach to Multiple Testing. Journal of the Royal Statistical Society Series B (Methodological) 57, 289-300.

Bernardos, R.L., Lentz, S.I., Wolfe, M.S., and Raymond, P.A. (2005). Notch-Delta signaling is required for spatial patterning and Muller glia differentiation in the zebrafish retina. Dev Biol 278, 381-395.

Bernardos, R.L., and Raymond, P.A. (2006). GFAP transgenic zebrafish. Gene Expression Patterns 6, 1007-1013.

Berninger, B., Costa, M.R., Koch, U., Schroeder, T., Sutor, B., Grothe, B., and Gotz, M. (2007). Functional properties of neurons derived from in vitro reprogrammed postnatal astroglia. J Neurosci 27, 8654-8664.

Berson, D.M., Dunn, F.A., and Takao, M. (2002). Phototransduction by retinal ganglion cells that set the circadian clock. Science 295, 1070-1073.

Bestman, J.E., Lee-Osbourne, J., and Cline, H.T. (2012). In vivo time-lapse imaging of cell proliferation and differentiation in the optic tectum of Xenopus laevis tadpoles. J Comp Neurol 520, 401-433.

Betizeau, M., Cortay, V., Patti, D., Pfister, S., Gautier, E., Bellemin-Ménard, A., Afanassieff, M., Huissoud, C., Douglas, Rodney J., Kennedy, H., and Dehay, C. (2013). Precursor Diversity and Complexity of Lineage Relationships in the Outer Subventricular Zone of the Primate. Neuron 80, 442-457.

Biehlmaier, O., Neuhauss, S.C., and Kohler, K. (2001). Onset and time course of apoptosis in the developing zebrafish retina. Cell Tissue Res 306, 199-207.

Blackshaw, S., Harpavat, S., Trimarchi, J., Cai, L., Huang, H., Kuo, W.P., Weber, G., Lee, K., Fraioli, R.E., Cho, S.H., *et al.* (2004). Genomic analysis of mouse retinal development. PLoS Biol 2, E247.

Boije, H., Rulands, S., Dudczig, S., Simons, B.D., and Harris, W.A. (2015). The Independent Probabilistic Firing of Transcription Factors: A Paradigm for Clonal Variability in the Zebrafish Retina. Dev Cell 34, 532-543.

Bradke, F., and Dotti, C.G. (2000). Establishment of neuronal polarity: lessons from cultured hippocampal neurons. Current Opinion in Neurobiology 10, 574-581.

Brand, A.H., and Perrimon, N. (1993). Targeted gene expression as a means of altering cell fates and generating dominant phenotypes. Development 118, 401-415.

Brown, N.L., Patel, S., Brzezinski, J., and Glaser, T. (2001). Math5 is required for retinal ganglion cell and optic nerve formation. Development 128, 2497-2508.

Brzezinski, J.A.t., Kim, E.J., Johnson, J.E., and Reh, T.A. (2011). Ascl1 expression defines a subpopulation of lineage-restricted progenitors in the mammalian retina. Development 138, 3519-3531.

Bultje, R.S., Castaneda-Castellanos, D.R., Jan, L.Y., Jan, Y.N., Kriegstein, A.R., and Shi, S.H. (2009). Mammalian Par3 regulates progenitor cell asymmetric division via notch signaling in the developing neocortex. Neuron 63, 189-202.

Busskamp, V., Duebel, J., Balya, D., Fradot, M., Viney, T.J., Siegert, S., Groner, A.C., Cabuy, E., Forster, V., Seeliger, M., *et al.* (2010). Genetic reactivation of cone photoreceptors restores visual responses in retinitis pigmentosa. Science 329, 413-417.

Cahoy, J.D., Emery, B., Kaushal, A., Foo, L.C., Zamanian, J.L., Christopherson, K.S., Xing, Y., Lubischer, J.L., Krieg, P.A., Krupenko, S.A., *et al.* (2008). A transcriptome database for astrocytes, neurons, and oligodendrocytes: a new resource for understanding brain development and function. J Neurosci 28, 264-278.

Caiazzo, M., Dell'Anno, M.T., Dvoretskova, E., Lazarevic, D., Taverna, S., Leo, D., Sotnikova, T.D., Menegon, A., Roncaglia, P., Colciago, G., *et al.* (2011). Direct generation of functional dopaminergic neurons from mouse and human fibroblasts. Nature 476, 224-227.

Cajal, S.R. (1899). Comparative study of the sensory areas of the human cortex.

Cayouette, M., Whitmore, A.V., Jeffery, G., and Raff, M. (2001). Asymmetric segregation of Numb in retinal development and the influence of the pigmented epithelium. J Neurosci 21, 5643-5651.

Cepko, C. (2014). Intrinsically different retinal progenitor cells produce specific types of progeny. Nat Rev Neurosci 15, 615-627.

Chapouton, P., Skupien, P., Hesl, B., Coolen, M., Moore, J.C., Madelaine, R., Kremmer, E., Faus-Kessler, T., Blader, P., Lawson, N.D., and Bally-Cuif, L. (2010). Notch activity levels control the balance between quiescence and recruitment of adult neural stem cells. J Neurosci 30, 7961-7974.

Chen, S.K., Badea, T.C., and Hattar, S. (2011). Photoentrainment and pupillary light reflex are mediated by distinct populations of ipRGCs. Nature 476, 92-95.

Chow, R.L., and Lang, R.A. (2001). Early eye development in vertebrates. Annu Rev Cell Dev Biol 17, 255-296.

Chow, R.L., Snow, B., Novak, J., Looser, J., Freund, C., Vidgen, D., Ploder, L., and McInnes, R.R. (2001). Vsx1, a rapidly evolving paired-like homeobox gene expressed in cone bipolar cells. Mech Dev 109, 315-322.

Chow, R.W., Almeida, A.D., Randlett, O., Norden, C., and Harris, W.A. (2015). Inhibitory neuron migration and IPL formation in the developing zebrafish retina. Development 142, 2665-2677.

Connaughton, V.P. (2011). Bipolar cells in the zebrafish retina. Vis Neurosci 28, 77-93.

Cooper, M.T., and Bray, S.J. (1999). Frizzled regulation of Notch signalling polarizes cell fate in the Drosophila eye. Nature 397, 526-530.

Das, T., Payer, B., Cayouette, M., and Harris, W.A. (2003). In vivo time-lapse imaging of cell divisions during neurogenesis in the developing zebrafish retina. Neuron 37, 597-609.

de la Pompa, J.L., Wakeham, A., Correia, K.M., Samper, E., Brown, S., Aguilera, R.J., Nakano, T., Honjo, T., Mak, T.W., Rossant, J., and Conlon, R.A. (1997). Conservation of the Notch signalling pathway in mammalian neurogenesis. Development 124, 1139-1148.

De la Rossa, A., Bellone, C., Golding, B., Vitali, I., Moss, J., Toni, N., Luscher, C., and Jabaudon, D. (2013). In vivo reprogramming of circuit connectivity in postmitotic neocortical neurons. Nat Neurosci 16, 193-200.

Deans, M.R., Krol, A., Abraira, V.E., Copley, C.O., Tucker, A.F., and Goodrich, L.V. (2011). Control of neuronal morphology by the atypical cadherin Fat3. Neuron 71, 820-832.

Del Bene, F., Wehman, A.M., Link, B.A., and Baier, H. (2008). Regulation of neurogenesis by interkinetic nuclear migration through an apical-basal notch gradient. Cell 134, 1055-1065.

Demb, J.B., and Singer, J.H. (2012). Intrinsic properties and functional circuitry of the AII amacrine cell. Vis Neurosci 29, 51-60.

DiCicco-Bloom, E., Townes-Anderson, E., and Black, I.B. (1990). Neuroblast mitosis in dissociated culture: regulation and relationship to differentiation. J Cell Biol 110, 2073-2086.

Distel, M., Hocking, J.C., Volkmann, K., and Koster, R.W. (2010). The centrosome neither persistently leads migration nor determines the site of axonogenesis in migrating neurons in vivo. J Cell Biol 191, 875-890.

Dong, Z., Yang, N., Yeo, S.Y., Chitnis, A., and Guo, S. (2012). Intralineage directional Notch signaling regulates self-renewal and differentiation of asymmetrically dividing radial glia. Neuron 74, 65-78.

Dorsky, R.I., Rapaport, D.H., and Harris, W.A. (1995). Xotch inhibits cell differentiation in the xenopus retina. Neuron 14, 487-496.

Dowling, J.E. (2012). The Retina - An Approachable Part of the Brain, Vol Revised Edition.

Dullin, J.P., Locker, M., Robach, M., Henningfeld, K.A., Parain, K., Afelik, S., Pieler, T., and Perron, M. (2007). Ptf1a triggers GABAergic neuronal cell fates in the retina. BMC Dev Biol 7, 110.

Emerson, M.M., Surzenko, N., Goetz, J.J., Trimarchi, J., and Cepko, C.L. (2013). Otx2 and Onecut1 promote the fates of cone photoreceptors and horizontal cells and repress rod photoreceptors. Dev Cell 26, 59-72.

Engerer, P., Plucinska, G., Thong, R., Trovo, L., Paquet, D., and Godinho, L. (2016). Imaging Subcellular Structures in the Living Zebrafish Embryo. J Vis Exp.

Engerer, P., Yoshimatsu, T., Suzuki, S.C., and Godinho, L. (2014). CentrinFish permit the visualization of centrosome dynamics in a cellular context in vivo. Zebrafish 11, 586-587.

Fanto, M., and Mlodzik, M. (1999). Asymmetric Notch activation specifies photoreceptors R3 and R4 and planar polarity in the Drosophila eye. Nature 397, 523-526.

Fortini, M.E., Rebay, I., Caron, L.A., and Artavanis-Tsakonas, S. (1993). An activated Notch receptor blocks cell-fate commitment in the developing Drosophila eye. Nature 365, 555-557.

Frise, E., Knoblich, J.A., Younger-Shepherd, S., Jan, L.Y., and Jan, Y.N. (1996). The Drosophila Numb protein inhibits signaling of the Notch receptor during cell-cell interaction in sensory organ lineage. Proc Natl Acad Sci U S A 93, 11925-11932.

Fuerst, P.G., Bruce, F., Tian, M., Wei, W., Elstrott, J., Feller, M.B., Erskine, L., Singer, J.H., and Burgess, R.W. (2009). DSCAM and DSCAML1 function in self-avoidance in multiple cell types in the developing mouse retina. Neuron 64, 484-497.

Fuerst, P.G., Koizumi, A., Masland, R.H., and Burgess, R.W. (2008). Neurite arborization and mosaic spacing in the mouse retina require DSCAM. Nature 451, 470-474.

Fujitani, Y., Fujitani, S., Luo, H., Qiu, F., Burlison, J., Long, Q., Kawaguchi, Y., Edlund, H., MacDonald, R.J., Furukawa, T., *et al.* (2006). Ptf1a determines horizontal and amacrine cell fates during mouse retinal development. Development 133, 4439-4450.

Gahwiler, B.H., Capogna, M., Debanne, D., McKinney, R.A., and Thompson, S.M. (1997). Organotypic slice cultures: a technique has come of age. Trends Neurosci 20, 471-477.

Gamlin, P.D., McDougal, D.H., Pokorny, J., Smith, V.C., Yau, K.W., and Dacey, D.M. (2007). Human and macaque pupil responses driven by melanopsin-containing retinal ganglion cells, Vol 47.

Gao, P., Postiglione, M.P., Krieger, T.G., Hernandez, L., Wang, C., Han, Z., Streicher, C., Papusheva, E., Insolera, R., Chugh, K., *et al.* (2014). Deterministic progenitor behavior and unitary production of neurons in the neocortex. Cell 159, 775-788.

Geling, A., Steiner, H., Willem, M., Bally-Cuif, L., and Haass, C. (2002). A gamma-secretase inhibitor blocks Notch signaling in vivo and causes a severe neurogenic phenotype in zebrafish. EMBO Rep 3, 688-694.

Girdler, G.C., Araya, C., Ren, X., and Clarke, J.D. (2013). Developmental time rather than local environment regulates the schedule of epithelial polarization in the zebrafish neural rod. Neural Dev 8, 5.

Godinho, L. (2011). Live imaging of zebrafish development. Cold Spring Harbor protocols 2011, 770-777.

Godinho, L., Mumm, J.S., Williams, P.R., Schroeter, E.H., Koerber, A., Park, S.W., Leach, S.D., and Wong, R.O. (2005). Targeting of amacrine cell neurites to appropriate synaptic laminae in the developing zebrafish retina. Development 132, 5069-5079.

Godinho, L., Williams, P.R., Claassen, Y., Provost, E., Leach, S.D., Kamermans, M., and Wong, R.O. (2007). Nonapical symmetric divisions underlie horizontal cell layer formation in the developing retina in vivo. Neuron 56, 597-603.

Goldman, D. (2014). Muller glial cell reprogramming and retina regeneration. Nat Rev Neurosci 15, 431-442.

Gomes, F.L., Zhang, G., Carbonell, F., Correa, J.A., Harris, W.A., Simons, B.D., and Cayouette, M. (2011). Reconstruction of rat retinal progenitor cell lineages in vitro reveals a surprising degree of stochasticity in cell fate decisions. Development 138, 227-235.

Gotz, M., and Huttner, W.B. (2005). The cell biology of neurogenesis. Nat Rev Mol Cell Biol 6, 777-788.

Harris, W.A., and Hartenstein, V. (1991). Neuronal determination without cell division in xenopus embryos. Neuron 6, 499-515.

Haubensak, W., Attardo, A., Denk, W., and Huttner, W.B. (2004). Neurons arise in the basal neuroepithelium of the early mammalian telencephalon: a major site of neurogenesis. Proc Natl Acad Sci U S A 101, 3196-3201.

He, J., Zhang, G., Almeida, A.D., Cayouette, M., Simons, B.D., and Harris, W.A. (2012). How variable clones build an invariant retina. Neuron 75, 786-798.

Helmstaedter, M., Briggman, K.L., Turaga, S.C., Jain, V., Seung, H.S., and Denk, W. (2013). Connectomic reconstruction of the inner plexiform layer in the mouse retina. Nature 500, 168-174.

Hinds, J.W., and Hinds, P.L. (1978). Early development of amacrine cells in the mouse retina: an electron microscopic, serial section analysis. J Comp Neurol 179, 277-300.

Hinds, J.W., and Hinds, P.L. (1983). Development of retinal amacrine cells in the mouse embryo: evidence for two modes of formation. J Comp Neurol 213, 1-23.

Holt, C.E., Bertsch, T.W., Ellis, H.M., and Harris, W.A. (1988). Cellular determination in the Xenopus retina is independent of lineage and birth date. Neuron 1, 15-26.

Hoon, M., Okawa, H., Della Santina, L., and Wong, R.O. (2014). Functional architecture of the retina: development and disease. Prog Retin Eye Res 42, 44-84.

Hu, M., and Easter, S.S. (1999). Retinal neurogenesis: the formation of the initial central patch of postmitotic cells. Dev Biol 207, 309-321.

Hunter, P.R., Nikolaou, N., Odermatt, B., Williams, P.R., Drescher, U., and Meyer, M.P. (2011). Localization of Cadm2a and Cadm3 proteins during development of the zebrafish nervous system. J Comp Neurol 519, 2252-2270.

Imayoshi, I., Sakamoto, M., Yamaguchi, M., Mori, K., and Kageyama, R. (2010). Essential roles of Notch signaling in maintenance of neural stem cells in developing and adult brains. J Neurosci 30, 3489-3498.

Ishibashi, M., Moriyoshi, K., Sasai, Y., Shiota, K., Nakanishi, S., and Kageyama, R. (1994). Persistent expression of helix-loop-helix factor HES-1 prevents mammalian neural differentiation in the central nervous system. EMBO J 13, 1799-1805.

Itoh, M., Kim, C.H., Palardy, G., Oda, T., Jiang, Y.J., Maust, D., Yeo, S.Y., Lorick, K., Wright, G.J., Ariza-McNaughton, L., *et al.* (2003). Mind bomb is a ubiquitin ligase that is essential for efficient activation of Notch signaling by Delta. Dev Cell 4, 67-82.

Jadhav, A.P., Cho, S.H., and Cepko, C.L. (2006a). Notch activity permits retinal cells to progress through multiple progenitor states and acquire a stem cell property. Proc Natl Acad Sci U S A 103, 18998-19003.

Jadhav, A.P., Mason, H.A., and Cepko, C.L. (2006b). Notch 1 inhibits photoreceptor production in the developing mammalian retina. Development 133, 913-923.

Jusuf, P.R., Almeida, A.D., Randlett, O., Joubin, K., Poggi, L., and Harris, W.A. (2011). Origin and determination of inhibitory cell lineages in the vertebrate retina. J Neurosci 31, 2549-2562.

Jusuf, P.R., and Harris, W.A. (2009). Ptf1a is expressed transiently in all types of amacrine cells in the embryonic zebrafish retina. Neural Dev 4, 34.

Kanekar, S., Perron, M., Dorsky, R., Harris, W.A., Jan, L.Y., Jan, Y.N., and Vetter, M.L. (1997). Xath5 Participates in a Network of bHLH Genes in the Developing Xenopus Retina. Neuron 19, 981-994.

Karlsson, J., von Hofsten, J., and Olsson, P.E. (2001). Generating transparent zebrafish: a refined method to improve detection of gene expression during embryonic development. Mar Biotechnol (NY) 3, 522-527.

Karow, M., Sanchez, R., Schichor, C., Masserdotti, G., Ortega, F., Heinrich, C., Gascon, S., Khan, M.A., Lie, D.C., Dellavalle, A., *et al.* (2012). Reprogramming of pericyte-derived cells of the adult human brain into induced neuronal cells. Cell Stem Cell 11, 471-476.

Kasthuri, N., Hayworth, K.J., Berger, D.R., Schalek, R.L., Conchello, J.A., Knowles-Barley, S., Lee, D., Vazquez-Reina, A., Kaynig, V., Jones, T.R., *et al.* (2015). Saturated Reconstruction of a Volume of Neocortex. Cell 162, 648-661.

Kawakami, K. (2004). Transgenesis and gene trap methods in zebrafish by using the Tol2 transposable element. Methods Cell Biol 77, 201-222.

Kay, J.N., Chu, M.W., and Sanes, J.R. (2012). MEGF10 and MEGF11 mediate homotypic interactions required for mosaic spacing of retinal neurons. Nature 483, 465-469.

Kay, J.N., Finger-Baier, K.C., Roeser, T., Staub, W., and Baier, H. (2001). Retinal Ganglion Cell Genesis Requires lakritz, a Zebrafish atonal Homolog. Neuron 30, 725-736.

Kay, J.N., Link, B.A., and Baier, H. (2005). Staggered cell-intrinsic timing of ath5 expression underlies the wave of ganglion cell neurogenesis in the zebrafish retina. Development 132, 2573-2585.

Kechad, A., Jolicoeur, C., Tufford, A., Mattar, P., Chow, R.W., Harris, W.A., and Cayouette, M. (2012). Numb is required for the production of terminal asymmetric cell divisions in the developing mouse retina. J Neurosci 32, 17197-17210.

Keller, P.J. (2013). Imaging Morphogenesis: Technological Advances and Biological Insights. Science 340.

Keller, P.J., Schmidt, A.D., Wittbrodt, J., and Stelzer, E.H. (2008). Reconstruction of zebrafish early embryonic development by scanned light sheet microscopy. Science 322, 1065-1069.

Kerschensteiner, M., Reuter, M.S., Lichtman, J.W., and Misgeld, T. (2008). Ex vivo imaging of motor axon dynamics in murine triangularis sterni explants. Nat Protocols 3, 1645-1653.

Kimmel, C.B., Ballard, W.W., Kimmel, S.R., Ullmann, B., and Schilling, T.F. (1995). Stages of embryonic development of the zebrafish. Dev Dyn 203, 253-310.

Kimura, Y., Okamura, Y., and Higashijima, S. (2006). alx, a zebrafish homolog of Chx10, marks ipsilateral descending excitatory interneurons that participate in the regulation of spinal locomotor circuits. J Neurosci 26, 5684-5697.

Kimura, Y., Satou, C., and Higashijima, S. (2008). V2a and V2b neurons are generated by the final divisions of pair-producing progenitors in the zebrafish spinal cord. Development 135, 3001-3005.

Kohwi, M., and Doe, C.Q. (2013). Temporal fate specification and neural progenitor competence during development. Nat Rev Neurosci 14, 823-838.

Kokel, D., Bryan, J., Laggner, C., White, R., Cheung, C.Y.J., Mateus, R., Healey, D., Kim, S., Werdich, A.A., Haggarty, S.J., *et al.* (2010). Rapid behavior-based identification of neuroactive small molecules in the zebrafish. Nat Chem Biol 6, 231-237.

Kokel, D., Dunn, T.W., Ahrens, M.B., Alshut, R., Cheung, C.Y., Saint-Amant, L., Bruni, G., Mateus, R., van Ham, T.J., Shiraki, T., *et al.* (2013). Identification of nonvisual photomotor response cells in the vertebrate hindbrain. J Neurosci 33, 3834-3843.

Kosodo, Y., Suetsugu, T., Suda, M., Mimori-Kiyosue, Y., Toida, K., Baba, S.A., Kimura, A., and Matsuzaki, F. (2011). Regulation of interkinetic nuclear migration by cell cycle-coupled active and passive mechanisms in the developing brain. EMBO J 30, 1690-1704.

Koster, R.W., and Fraser, S.E. (2001). Tracing transgene expression in living zebrafish embryos. Dev Biol 233, 329-346.

Krishnaswamy, A., Yamagata, M., Duan, X., Hong, Y.K., and Sanes, J.R. (2015). Sidekick 2 directs formation of a retinal circuit that detects differential motion. Nature 524, 466-470.

Kwan, K.M., Fujimoto, E., Grabher, C., Mangum, B.D., Hardy, M.E., Campbell, D.S., Parant, J.M., Yost, H.J., Kanki, J.P., and Chien, C.B. (2007). The Tol2kit: a multisite gateway-based construction kit for Tol2 transposon transgenesis constructs. Dev Dyn 236, 3088-3099.

La Vail, M.M., Rapaport, D.H., and Rakic, P. (1991). Cytogenesis in the monkey retina. J Comp Neurol 309, 86-114.

Lardelli, M., Williams, R., Mitsiadis, T., and Lendahl, U. (1996). Expression of the Notch 3 intracellular domain in mouse central nervous system progenitor cells is lethal and leads to disturbed neural tube development. Mechanisms of Development 59, 177-190.

Leonhardt, H., Rahn, H.P., Weinzierl, P., Sporbert, A., Cremer, T., Zink, D., and Cardoso, M.C. (2000). Dynamics of DNA replication factories in living cells. The Journal of cell biology 149, 271-280.

Leung, L., Klopper, A.V., Grill, S.W., Harris, W.A., and Norden, C. (2011). Apical migration of nuclei during G2 is a prerequisite for all nuclear motion in zebrafish neuroepithelia. Development 138, 5003-5013.

Lewis, T.L., Courchet, J., and Polleux, F. (2013). Cellular and molecular mechanisms underlying axon formation, growth, and branching. The Journal of Cell Biology 202, 837-848.

Li, Y., Lu, H., Cheng, P.L., Ge, S., Xu, H., Shi, S.H., and Dan, Y. (2012a). Clonally related visual cortical neurons show similar stimulus feature selectivity. Nature 486, 118-121.

Li, Y.N., Tsujimura, T., Kawamura, S., and Dowling, J.E. (2012b). Bipolar cell-photoreceptor connectivity in the zebrafish (Danio rerio) retina. J Comp Neurol 520, 3786-3802.

Liu, W., Mo, Z., and Xiang, M. (2001a). The Ath5 proneural genes function upstream of Brn3 POU domain transcription factor genes to promote retinal ganglion cell development. Proceedings of the National Academy of Sciences 98, 1649-1654.

Liu, Y., Shen, Y., Rest, J.S., Raymond, P.A., and Zack, D.J. (2001b). Isolation and characterization of a zebrafish homologue of the cone rod homeobox gene. Investigative ophthalmology & visual science 42, 481-487.

Livesey, F.J., Young, T.L., and Cepko, C.L. (2004). An analysis of the gene expression program of mammalian neural progenitor cells. Proc Natl Acad Sci U S A 101, 1374-1379.

MacDonald, R.B., Randlett, O., Oswald, J., Yoshimatsu, T., Franze, K., and Harris, W.A. (2015). Muller glia provide essential tensile strength to the developing retina. J Cell Biol 210, 1075-1083.

Marro, S., Pang, Z.P., Yang, N., Tsai, M.C., Qu, K., Chang, H.Y., Sudhof, T.C., and Wernig, M. (2011). Direct lineage conversion of terminally differentiated hepatocytes to functional neurons. Cell Stem Cell 9, 374-382.

Masai, I., Yamaguchi, M., Tonou-Fujimori, N., Komori, A., and Okamoto, H. (2005). The hedgehog-PKA pathway regulates two distinct steps of the differentiation of retinal ganglion cells: the cell-cycle exit of retinoblasts and their neuronal maturation. Development 132, 1539-1553.

Masland, R.H. (2012). The tasks of amacrine cells. Vis Neurosci 29, 3-9.

Mason, L., Scott, E.K., Staub, W., Finger-Baier, K., and Baier, H. (2009). Expression patterns from GAL4 enhancer trap screen. ZFIN Direct Data Submission (http://zfin.org).

Matos-Cruz, V., Blasic, J., Nickle, B., Robinson, P.R., Hattar, S., and Halpern, M.E. (2011). Unexpected diversity and photoperiod dependence of the zebrafish melanopsin system. PLoS One 6, e25111.

Maurer, K.A., Riesenberg, A.N., and Brown, N.L. (2014). Notch signaling differentially regulates Atoh7 and Neurog2 in the distal mouse retina. Development 141, 3243-3254.

Memberg, S.P., and Hall, A.K. (1995). Dividing neuron precursors express neuron-specific tubulin. J Neurobiol 27, 26-43.

Miyata, T., Kawaguchi, A., Saito, K., Kawano, M., Muto, T., and Ogawa, M. (2004). Asymmetric production of surface-dividing and non-surface-dividing cortical progenitor cells. Development 131, 3133-3145.

Mizeracka, K., DeMaso, C.R., and Cepko, C.L. (2013). Notch1 is required in newly postmitotic cells to inhibit the rod photoreceptor fate. Development 140, 3188-3197.

Mizuguchi, R., Kriks, S., Cordes, R., Gossler, A., Ma, Q., and Goulding, M. (2006). Ascl1 and Gsh1/2 control inhibitory and excitatory cell fate in spinal sensory interneurons. Nat Neurosci 9, 770-778.

Morgan, J.L., Dhingra, A., Vardi, N., and Wong, R.O. (2006). Axons and dendrites originate from neuroepithelial-like processes of retinal bipolar cells. Nat Neurosci 9, 85-92.

Morrison, S.J., Perez, S.E., Qiao, Z., Verdi, J.M., Hicks, C., Weinmaster, G., and Anderson, D.J. (2000). Transient Notch activation initiates an irreversible switch from neurogenesis to gliogenesis by neural crest stem cells. Cell 101, 499-510.

Mueller, T., and Wullimann, M.E. (2015). Atlas of Early Zebrafish Brain Development, 2nd edn.

Mullins, M.C., Hammerschmidt, M., Haffter, P., and Nusslein-Volhard, C. (1994). Large-scale mutagenesis in the zebrafish: in search of genes controlling development in a vertebrate. Curr Biol 4, 189-202.

Mumm, J.S., Godinho, L., Morgan, J.L., Oakley, D.M., Schroeter, E.H., and Wong, R.O. (2005). Laminar circuit formation in the vertebrate retina. Prog Brain Res 147, 155-169.

Mumm, J.S., Williams, P.R., Godinho, L., Koerber, A., Pittman, A.J., Roeser, T., Chien, C.B., Baier, H., and Wong, R.O. (2006). In vivo imaging reveals dendritic targeting of laminated afferents by zebrafish retinal ganglion cells. Neuron 52, 609-621.

Nakashima, K., Umeshima, H., and Kengaku, M. (2015). Cerebellar granule cells are predominantly generated by terminal symmetric divisions of granule cell precursors. Dev Dyn 244, 748-758.

Nakhai, H., Sel, S., Favor, J., Mendoza-Torres, L., Paulsen, F., Duncker, G.I., and Schmid, R.M. (2007). Ptf1a is essential for the differentiation of GABAergic and glycinergic amacrine cells and horizontal cells in the mouse retina. Development 134, 1151-1160.

Neumann, C.J., and Nuesslein-Volhard, C. (2000). Patterning of the zebrafish retina by a wave of sonic hedgehog activity. Science 289, 2137-2139.

Nikolaou, N., and Meyer, M.P. (2015). Lamination Speeds the Functional Development of Visual Circuits. Neuron 88, 999-1013.

Noctor, S.C., Martinez-Cerdeno, V., Ivic, L., and Kriegstein, A.R. (2004). Cortical neurons arise in symmetric and asymmetric division zones and migrate through specific phases. Nat Neurosci 7, 136-144.

Norden, C., Young, S., Link, B.A., and Harris, W.A. (2009). Actomyosin is the main driver of interkinetic nuclear migration in the retina. Cell 138, 1195-1208.

Nusslein-Volhard, C. (2012). The zebrafish issue of Development. Development 139, 4099-4103.

Nye, J.S., Kopan, R., and Axel, R. (1994). An activated Notch suppresses neurogenesis and myogenesis but not gliogenesis in mammalian cells. Development 120, 2421-2430.

Odermatt, B., Nikolaev, A., and Lagnado, L. (2012). Encoding of luminance and contrast by linear and nonlinear synapses in the retina. Neuron 73, 758-773.

Pang, Z.P., Yang, N., Vierbuchen, T., Ostermeier, A., Fuentes, D.R., Yang, T.Q., Citri, A., Sebastiano, V., Marro, S., Sudhof, T.C., and Wernig, M. (2011). Induction of human neuronal cells by defined transcription factors. Nature 476, 220-223.

Parsons, M.J., Pisharath, H., Yusuff, S., Moore, J.C., Siekmann, A.F., Lawson, N., and Leach, S.D. (2009). Notch-responsive cells initiate the secondary transition in larval zebrafish pancreas. Mechanisms of development 126, 898-912.

Passini, M.A., Levine, E.M., Canger, A.K., Raymond, P.A., and Schechter, N. (1997). Vsx-1 and Vsx-2: differential expression of two paired-like homeobox genes during zebrafish and goldfish retinogenesis. J Comp Neurol 388, 495-505.

Peng, C.Y., Yajima, H., Burns, C.E., Zon, L.I., Sisodia, S.S., Pfaff, S.L., and Sharma, K. (2007). Notch and MAML signaling drives Scl-dependent interneuron diversity in the spinal cord. Neuron 53, 813-827.

Poggi, L., Vitorino, M., Masai, I., and Harris, W.A. (2005). Influences on neural lineage and mode of division in the zebrafish retina in vivo. J Cell Biol 171, 991-999.

Prasov, L., and Glaser, T. (2012). Dynamic expression of ganglion cell markers in retinal progenitors during the terminal cell cycle. Mol Cell Neurosci 50, 160-168.

Quesada, A., Prada, F., Armengol, J.A., and Genis-Galvez, J.M. (1981). Early morphological differentiation of the bipolar neurons in the chick retina. A Golgi analysis. Anat Histol Embryol 10, 328-341.

Quillien, A., Blanco-Sanchez, B., Halluin, C., Moore, J.C., Lawson, N.D., Blader, P., and Cau, E. (2011). BMP signaling orchestrates photoreceptor specification in the zebrafish pineal gland in collaboration with Notch. Development 138, 2293-2302.

Randlett, O., MacDonald, R.B., Yoshimatsu, T., Almeida, A.D., Suzuki, S.C., Wong, R.O., and Harris, W.A. (2013). Cellular requirements for building a retinal neuropil. Cell Rep 3, 282-290.

Randlett, O., Poggi, L., Zolessi, F.R., and Harris, W.A. (2011). The oriented emergence of axons from retinal ganglion cells is directed by laminin contact in vivo. Neuron 70, 266-280.

Rapaport, D.H., and Stone, J. (1983). The topography of cytogenesis in the developing retina of the cat. J Neurosci 3, 1824-1834.

Rapaport, D.H., Wong, L.L., Wood, E.D., Yasumura, D., and LaVail, M.M. (2004). Timing and topography of cell genesis in the rat retina. J Comp Neurol 474, 304-324.

Reese, B.E., and Galli-Resta, L. (2002). The role of tangential dispersion in retinal mosaic formation. Prog Retin Eye Res 21, 153-168.

Remak, R. (1852). Ueber extracellulare Entstehung thierischer Zellen und über die Vermehrung derselben durch Theilung. Archiv für Anatomie, Physiologie und wissenschaftliche Medicin, 47-57.

Ren, J.Q., McCarthy, W.R., Zhang, H., Adolph, A.R., and Li, L. (2002). Behavioral visual responses of wild-type and hypopigmented zebrafish. Vision Res 42, 293-299.

Rhyu, M.S., Jan, L.Y., and Jan, Y.N. (1994). Asymmetric distribution of numb protein during division of the sensory organ precursor cell confers distinct fates to daughter cells. Cell 76, 477-491.

Robles, E., Laurell, E., and Baier, H. (2014). The retinal projectome reveals brain-area-specific visual representations generated by ganglion cell diversity. Curr Biol 24, 2085-2096.

Rohrer, H., and Thoenen, H. (1987). Relationship between differentiation and terminal mitosis: chick sensory and ciliary neurons differentiate after terminal mitosis of precursor cells, whereas sympathetic neurons continue to divide after differentiation. J Neurosci 7, 3739-3748.

Rothman, T.P., Specht, L.A., Gershon, M.D., Joh, T.H., Teitelman, G., Pickel, V.M., and Reis, D.J. (1980). Catecholamine biosynthetic enzymes are expressed in replicating cells of the peripheral but not the central nervous system. Proc Natl Acad Sci U S A 77, 6221-6225.

Rouaux, C., and Arlotta, P. (2013). Direct lineage reprogramming of post-mitotic callosal neurons into corticofugal neurons in vivo. Nat Cell Biol 15, 214-221.

Sauer, F.C. (1935). Mitosis in the neural tube. J Comp Neurol 62, 377-405.

Scheer, N., and Campos-Ortega, J.A. (1999). Use of the Gal4-UAS technique for targeted gene expression in the zebrafish. Mechanisms of Development 80, 153-158.

Scheer, N., Groth, A., Hans, S., and Campos-Ortega, J.A. (2001). An instructive function for Notch in promoting gliogenesis in the zebrafish retina. Development 128, 1099-1107.

Scheer, N., Riedl, I., Warren, J.T., Kuwada, J.Y., and Campos-Ortega, J.A. (2002). A quantitative analysis of the kinetics of Gal4 activator and effector gene expression in the zebrafish. Mech Dev 112, 9-14.

Schmitt, E.A., and Dowling, J.E. (1994). Early eye morphogenesis in the zebrafish, Brachydanio rerio. J Comp Neurol 344, 532-542.

Scott, E.K., Mason, L., Arrenberg, A.B., Ziv, L., Gosse, N.J., Xiao, T., Chi, N.C., Asakawa, K., Kawakami, K., and Baier, H. (2007). Targeting neural circuitry in zebrafish using GAL4 enhancer trapping. Nat Meth 4, 323-326.

Semmelhack, J.L., Donovan, J.C., Thiele, T.R., Kuehn, E., Laurell, E., and Baier, H. (2014). A dedicated visual pathway for prey detection in larval zebrafish. Elife 3.

Šestan, N., Artavanis-Tsakonas, S., and Rakic, P. (1999). Contact-Dependent Inhibition of Cortical Neurite Growth Mediated by Notch Signaling. Science 286, 741-746.

Sethuramanujam, S., McLaughlin, A.J., deRosenroll, G., Hoggarth, A., Schwab, David J., and Awatramani, Gautam B. (2016). A Central Role for Mixed Acetylcholine/GABA Transmission in Direction Coding in the Retina. Neuron.

Seung, H.S., and Sumbul, U. (2014). Neuronal cell types and connectivity: lessons from the retina. Neuron 83, 1262-1272.

Shelly, M., Cancedda, L., Heilshorn, S., Sumbre, G., and Poo, M.-m. (2007). LKB1/STRAD Promotes Axon Initiation During Neuronal Polarization. Cell 129, 565-577.

Shelly, M., Cancedda, L., Lim, B.K., Popescu, A.T., Cheng, P.L., Gao, H., and Poo, M.M. (2011). Semaphorin3A regulates neuronal polarization by suppressing axon formation and promoting dendrite growth. Neuron 71, 433-446.

Shen, Q., Zhong, W., Jan, Y.N., and Temple, S. (2002). Asymmetric Numb distribution is critical for asymmetric cell division of mouse cerebral cortical stem cells and neuroblasts. Development 129, 4843-4853.

Shen, Y.C., and Raymond, P.A. (2004). Zebrafish cone-rod (crx) homeobox gene promotes retinogenesis. Developmental biology 269, 237-251.

Shi, Z., Trenholm, S., Zhu, M., Buddingh, S., Star, E.N., Awatramani, G.B., and Chow, R.L. (2011). Vsx1 regulates terminal differentiation of type 7 ON bipolar cells. J Neurosci 31, 13118-13127.

Shin, J., Poling, J., Park, H.C., and Appel, B. (2007). Notch signaling regulates neural precursor allocation and binary neuronal fate decisions in zebrafish. Development 134, 1911-1920.

Siller, K.H., and Doe, C.Q. (2009). Spindle orientation during asymmetric cell division. Nat Cell Biol 11, 365-374.

Song, P.I., Matsui, J.I., and Dowling, J.E. (2008). Morphological types and connectivity of horizontal cells found in the adult zebrafish (Danio rerio) retina. J Comp Neurol 506, 328-338.

Spitzer, N.C. (2012). Activity-dependent neurotransmitter respecification. Nat Rev Neurosci 13, 94-106.

Suzuki, S.C., Bleckert, A., Williams, P.R., Takechi, M., Kawamura, S., and Wong, R.O. (2013). Cone photoreceptor types in zebrafish are generated by symmetric terminal divisions of dedicated precursors. Proc Natl Acad Sci U S A 110, 15109-15114.

Taylor, M.K., Yeager, K., and Morrison, S.J. (2007). Physiological Notch signaling promotes gliogenesis in the developing peripheral and central nervous systems. Development 134, 2435-2447.

Telley, L., Govindan, S., Prados, J., Stevant, I., Nef, S., Dermitzakis, E., Dayer, A., and Jabaudon, D. (2016). Sequential transcriptional waves direct the differentiation of newborn neurons in the mouse neocortex. Science 351, 1443-1446.

Temizer, I., Donovan, J.C., Baier, H., and Semmelhack, J.L. (2015). A Visual Pathway for Looming-Evoked Escape in Larval Zebrafish. Curr Biol 25, 1823-1834.

Tian, N. (2008). Synaptic activity, visual experience and the maturation of retinal synaptic circuitry. J Physiol 586, 4347-4355.

Trimarchi, J.M., Stadler, M.B., and Cepko, C.L. (2008). Individual retinal progenitor cells display extensive heterogeneity of gene expression. PLoS One 3, e1588.

Turner, D.L., and Cepko, C.L. (1987). A common progenitor for neurons and glia persists in rat retina late in development. Nature 328, 131-136.

Turner, D.L., Snyder, E.Y., and Cepko, C.L. (1990). Lineage-independent determination of cell type in the embryonic mouse retina. Neuron 4, 833-845.

Vierbuchen, T., Ostermeier, A., Pang, Z.P., Kokubu, Y., Sudhof, T.C., and Wernig, M. (2010). Direct conversion of fibroblasts to functional neurons by defined factors. Nature 463, 1035-1041.

Vihtelic, T.S., Doro, C.J., and Hyde, D.R. (1999). Cloning and characterization of six zebrafish photoreceptor opsin cDNAs and immunolocalization of their corresponding proteins. Vis Neurosci 16, 571-585.

Virchow, R. (1855). Cellular-Pathologie. Virchows Arch, 3-39.

Vitorino, M., Jusuf, P.R., Maurus, D., Kimura, Y., Higashijima, S., and Harris, W.A. (2009). Vsx2 in the zebrafish retina: restricted lineages through derepression. Neural Dev 4, 14.

Walsh, M.K., and Lichtman, J.W. (2003). In Vivo Time-Lapse Imaging of Synaptic Takeover Associated with Naturally Occurring Synapse Elimination. Neuron 37, 67-73.

Wan, L., Almers, W., and Chen, W. (2005). Two ribeye genes in teleosts: the role of Ribeye in ribbon formation and bipolar cell development. The Journal of neuroscience : the official journal of the Society for Neuroscience 25, 941-949.

Wang, L., Hou, S., and Han, Y.-G. (2016). Hedgehog signaling promotes basal progenitor expansion and the growth and folding of the neocortex. Nat Neurosci advance online publication.

Weber, I.P., Ramos, A.P., Strzyz, P.J., Leung, L.C., Young, S., and Norden, C. (2014). Mitotic position and morphology of committed precursor cells in the zebrafish retina adapt to architectural changes upon tissue maturation. Cell Rep 7, 386-397.

Wetts, R., and Fraser, S.E. (1988). Multipotent precursors can give rise to all major cell types of the frog retina. Science 239, 1142-1145.

Wettstein, D.A., Turner, D.L., and Kintner, C. (1997). The Xenopus homolog of Drosophila Suppressor of Hairless mediates Notch signaling during primary neurogenesis. Development 124, 693-702.

Whitford, K.L., Dijkhuizen, P., Polleux, F., and Ghosh, A. (2002). Molecular control of cortical dendrite development. Annu Rev Neurosci 25, 127-149.

Williams, P.R., Suzuki, S.C., Yoshimatsu, T., Lawrence, O.T., Waldron, S.J., Parsons, M.J., Nonet, M.L., and Wong, R.O. (2010). In vivo development of outer retinal synapses in the absence of glial contact. J Neurosci 30, 11951-11961.

Wilsch-Bräuninger, M., Florio, M., and Huttner, W.B. (2016). Neocortex expansion in development and evolution — from cell biology to single genes. Current Opinion in Neurobiology 39, 122-132.

Wong, L.L., and Rapaport, D.H. (2009). Defining retinal progenitor cell competence in Xenopus laevis by clonal analysis. Development 136, 1707-1715.

Wong, R.O. (2012). Introduction - from eye-field to eyesight. In Retinal Development, E. Sernagor, S.J. Eglen, W.A. Harris, and R.O.L. Wong, eds. (Cambridge University Press), pp. 1-8.

Wright, M.A., Mo, W., Nicolson, T., and Ribera, A.B. (2010). In vivo evidence for transdifferentiation of peripheral neurons. Development 137, 3047-3056.

Yamagata, M., and Sanes, J.R. (2008). Dscam and Sidekick proteins direct lamina-specific synaptic connections in vertebrate retina. Nature 451, 465-469.

Yamagata, M., Weiner, J.A., and Sanes, J.R. (2002). Sidekicks: synaptic adhesion molecules that promote lamina-specific connectivity in the retina. Cell 110, 649-660.

Yang, Z., Ding, K., Pan, L., Deng, M., and Gan, L. (2003). Math5 determines the competence state of retinal ganglion cell progenitors. Dev Biol 264, 240-254.

Yeo, W., and Gautier, J. (2004). Early neural cell death: dying to become neurons. Developmental Biology 274, 233-244.

Yonehara, K., Balint, K., Noda, M., Nagel, G., Bamberg, E., and Roska, B. (2011). Spatially asymmetric reorganization of inhibition establishes a motion-sensitive circuit. Nature 469, 407-410.

Yoshida, K., Watanabe, D., Ishikane, H., Tachibana, M., Pastan, I., and Nakanishi, S. (2001). A key role of starburst amacrine cells in originating retinal directional selectivity and optokinetic eye movement. Neuron 30, 771-780.

Yoshimatsu, T., D'Orazi, F.D., Gamlin, C.R., Suzuki, S.C., Suli, A., Kimelman, D., Raible, D.W., and Wong, R.O. (2016). Presynaptic partner selection during retinal circuit reassembly varies with timing of neuronal regeneration in vivo. Nat Commun 7, 10590.

Yoshimatsu, T., Williams, P.R., D'Orazi, F.D., Suzuki, S.C., Fadool, J.M., Allison, W.T., Raymond, P.A., and Wong, R.O. (2014). Transmission from the dominant input shapes the stereotypic ratio of photoreceptor inputs onto horizontal cells. Nat Commun 5, 3699.

Young, R.W. (1985a). Cell differentiation in the retina of the mouse. Anat Rec 212, 199-205.

Young, R.W. (1985b). Cell proliferation during postnatal development of the retina in the mouse. Brain Res 353, 229-239.

Yu, Y.C., Bultje, R.S., Wang, X., and Shi, S.H. (2009). Specific synapses develop preferentially among sister excitatory neurons in the neocortex. Nature 458, 501-504.

Yu, Y.C., He, S., Chen, S., Fu, Y., Brown, K.N., Yao, X.H., Ma, J., Gao, K.P., Sosinsky, G.E., Huang, K., and Shi, S.H. (2012). Preferential electrical coupling regulates neocortical lineage-dependent microcircuit assembly. Nature 486, 113-117.

Zolessi, F.R., Poggi, L., Wilkinson, C.J., Chien, C.B., and Harris, W.A. (2006). Polarization and orientation of retinal ganglion cells in vivo. Neural Dev 1, 2.

Zuber, M., and Harris, W.A. (2012). Formation of the eye field. In Retinal Development, E. Sernagor, S.J. Eglen, W.A. Harris, and R.O.L. Wong, eds. (Cambridge University Press), pp. 8-29.